La collana della Scuola di Alta Formazione Dottorale accoglie le migliori tesi di dottorato dell'Università degli Studi di Bergamo, insignite della dignità di stampa e sottoposte a procedura di *blind peer review*.

A deep and systematic intervention on the built environment must be undertaken to foster environmental, economic, and social sustainability; this research contributes to the scientific debate, focusing on holistic renovation from outside of reinforced concrete buildings by embracing a life cycle perspective. Within such a new perspective the diagrid structures as an innovative strengthening technique from outside are investigated.

Simone Labò received his doctorate in Engineering and Applied sciences (XXXI cycle) from the University of Bergamo where he is currently a research fellow in structural engineering. His research interest is focused on the holistic renovation of existing reinforced concrete buildings targeting energy efficiency, seismic safety, and resilience. He has been working on integrated retrofit solutions carried out on the outside of the building and conceived by addressing Performance-Based and Life Cycle Thinking approaches.

ISBN: 978-88-97413-45-5
DOI: 10.6092/978-88-97413-45-5

Simone Labò DIAGRID EXOSKELETONS FOR THE RETROFIT OF RC BUILDINGS

19

Collana della Scuola di Alta Formazione Dottorale
- 19 -

Simone Labò

DIAGRID EXOSKELETONS FOR THE RETROFIT OF RC BUILDINGS
Holistic sustainable solutions to renovate post world war II RC buildings in a Life-Cycle Perspective

UNIVERSITÀ DEGLI STUDI DI BERGAMO

2021

Collana della Scuola di Alta Formazione Dottorale

Diretta da Paolo Cesaretti

Ogni volume è sottoposto a *blind peer review*.

ISSN: 2611-9927

Sito web: https://aisberg.unibg.it/handle/10446/130100

Simone Labò

DIAGRID EXOSKELETONS FOR THE RETROFIT OF RC BUILDINGS
Holistic sustainable solutions to renovate post world war II RC buildings in a Life-Cycle Perspective

Università degli Studi di Bergamo

2021

Diagrid Exoskeletons for the Retrofit of RC Buildings. Holistic sustainable solutions to renovate post world war II RC buildings in a Life-Cycle Perspective / Simone Labò. – Bergamo :
Università degli Studi di Bergamo, 2021.
(Collana della Scuola di Alta Formazione Dottorale; 19)

ISBN: 978-88-97413-45-5
DOI: 10.6092/978-88-97413-45-5

Progetto grafico: Servizi Editoriali – Università degli Studi di Bergamo
© 2018 Università degli Studi di Bergamo
via Salvecchio, 19
24129 Bergamo
Cod. Fiscale 80004350163
P. IVA 01612800167

https://aisberg.unibg.it/handle/10446/175166

Acknowledgments

I wish to thank the professors who supported me in this dissertation, as supervisors – Prof. Alessandra Marini and Prof. Paolo Riva – and as co-supervisor – Prof. Andrea Belleri.
I wish to thank Professor Benson Shing who welcomed me at the University of California San Diego.
I am especially grateful to my family, to my colleagues and friends for accompanying me on this journey.

Table of contents

Introduction 1

Chapter 1. Research motivation 3

1.1 Problem Statement 3

1.1.1 Current practice in the renovation 5

1.1.2 Need for holistic solutions based on a LCT approach 6

1.1.3 Structural renovation strategies under a LC perspective lens 8

1.1.4 Aim and scope and content of the research work 11

1.2 State of the art of Diagrid structures 12

1.3 Use of Diagrid exoskeleton in the renovation of existing buildings 16

1.3.1 Challenges when adopting diagrid exoskeletons in the renovation of the existing building 17

Chapter 2. Diagrid structure: new performance objectives and structural design 20

2.1 Structural design for high-rise buildings: generalities 20

2.1.1. Optimal module of the diagrid 20

2.1.2 Diagrid global stiffness 23

2.1.3 Internal actions in diagrid structures 25

2.2 Renovation of the existing building with a diagrid exoskeleton: design criteria 28

2.2.1 Existing Reinforced concrete buildings 28

2.2.2 New performance objectives under a LCT perspective 29

2.3 Elastic, dissipative and responsive diagrid structure: an overview 31

2.3.1 Structural design of diagrid structures 33

2.3.1.1 Architectural and formal constraint 33

2.3.2 Elastic diagrid 34

2.3.2.1 Stiffness constraint 34

2.3.2.2 Strength constraint 36

2.3.3 Passive-Responsive Diagrid: principles and structural behavior 37

Chapter 3: Sensitivity analysis of the structural response of the retrofitted system 40

3.1 Simplified model of the retrofitted structure 40

3.2 Equations of motion 45

3.3 Elastic retrofit solution: simplification to a SDOF system and parametric analyses 47

3.3.1 Parametric analyses on the Elastic SDOF system 52

3.4 Non-Linear retrofit solution: Sensitivity analyses 59

3.5 From SDOF system to MDOF system 75

Chapter 4: Application of the diagrid for the strengthening of a reference building 77

4.1 General overview 77

4.1.1 Architectural and structural features of the reference building 78

4.1.2 Qualitative preliminary structural considerations 82

4.2 Numerical analysis of the structural response 83

4.2.1 Non-linear static Pushover analyses and seismic vulnerability assessment of the reference building 86

4.3 Diagrid structure design 91

4.3.1 Structural design of the retrofit solution 91

4.3.1.1 Architectural aspects 92

4.3.1.2 Preliminary proportioning of the exoskeleton: stiffness constraint and equivalent minimum stiffness 94

4.3.1.3 Strength constraint 96

4.3.1.4 Evaluation of the connection properties 98

4.3.2 Non-linear analyses and result discussion 99

4.3.2.1 Non-linear static Pushover analysis of the retrofitted building 99

4.3.2.2 Non-linear Time History analyses 101

4.3.3 Adaptive-Responsive Diagrid 106

Concluding remarks 109

Table of contents

Appendices 113

Appendix 1 114

Appendix 2 119

Appendix 3 121

Appendix 4 131

Appendix 5 132

Appendix 6 134

Appendix 7 136

References 137

List of figures 143

List of tables 151

Glossary 153

Introduction

Enormous resources are being invested in Europe to foster environmental, economic, and social sustainability; however, such relevant effort to reach ambitious targets may be a missed chance, unless a deep and systematic intervention on the built environment is undertaken to target sustainability, safety, and resilience at the same time.

This thesis contributes to the scientific debate, focusing on holistic renovation from outside of reinforced concrete building by embracing a life cycle perspective. Effectiveness of such an approach to the renovation with respect to traditional retrofit actions emerges both in the construction time when addressing the barriers to the renovation such as the inhabitant relocation and the existing building disruption, and when broadening the time frame of the analyses, shifting from the construction time to a life cycle perspective. In this second case, the potential of the holistic approach becomes clear in reducing costs, impacts on the inhabitants, and impacts on the environment over the building life cycle. The results of this new approach is a retrofit solution based on a Life Cycle Thinking, which not only entails the use of recyclable/reusable materials, but also encourages interventions carried out from the outside the buildings, and implies the adoption of reparable, easily maintainable, adaptable and fully demountable solutions with prefabricated components, thus guaranteeing, at the end-of-life, the selective dismantling and reuse or recycle of the components to reduce construction waste. The described solutions, which couples structural retrofit in the renovation action, stem as an enhancement of past pioneering “camouflage” interventions, such as double-skin solutions entailing in many benefits such as the protection of human lives, resilience and the lengthening of the existing buildings service life, the repairing costs and building downtime reduction, reduction of the environmental impact associated with seismic risk over the building life cycle and long-term protection of the investment (Marini, et al., 2018).

Within such a new perspective, new technology options are needed to innovatively combine structural retrofit, architectural restyling, and energy efficiency measures; in this work, an effective retrofit solution is proposed. Among the possible retrofit solutions, the diagrid structures as an innovative strengthening technique from outside are investigated.

In the first part of this thesis, the state of the art of diagrid design is reported. New criteria for the design of retrofit solutions are set, and a design procedure for elastic diagrid is proposed. In the third chapter, a parametric evaluation of the retrofitted system through a simplified 2

DOF system is conducted, and a set of design spectra are defined in order to simplify the design procedure and derive the optimal retrofit parameter for RC buildings. Finally, a reference case study representative of the typical RC building is developed in the fifth chapter of this work to assess and validate the procedure.

Chapter 1. Research motivation

1.1Problem Statement

The urgent need to foster sustainability in our society has led to the definition of international policies to be applied to any economic sector. In Europe, Roadmap 2050 envisions a society where greenhouse gas (GHG) emissions are cut by 80-95% compared with the 1990 levels but maintaining the actual levels of wellbeing and prosperity (COM, 2011). To comply with such a demanding Roadmap, the construction sector should undertake some significant corrective actions to reduce its dramatic impacts on the environment (Figure 1), corresponding to 36% of CO2 emissions, 40% of energy consumption, and 35% of raw material depletion (Marini, et al., 2014). So far, the new solution sets aimed at reducing the environmental footprint of new and existing buildings often disregard some major aspects. Indeed, when considering sustainability in the construction sector, two main issues must be taken into account: the construction rate of new buildings and the multiple deficiencies of the existing ones.

Regarding the former, the actual average European construction rate is low (about 1% according to (BPIE, 2011)); therefore the sole construction of new high-performance buildings will not enable meeting the ambitious European targets. Sustainability in the construction sector can only be pursued by substantially renovating the existing building stock, which is obsolete, massively energy consuming, and vulnerable to natural and man-induced hazards (Passoni, et al., 2018; Marini, et al., 2018). An integrated deep renovation of the existing building stock fostering safety, resilience, and sustainability should always be preferred (Casprini, et al., 2018), overcoming the multiple deficiencies of the existing building, particularly those connected to the structural vulnerability that may result in additional impacts on the environment connected to possible damage or even collapse of the building in the case of a natural disaster. Sustainability must account for the hazard risks reduction, considering that the building may be exposed to extreme conditions, and that, from a structural point of view, 40% of European buildings have already exhausted their nominal service life (typically 50 years). Indeed, these structures were generally designed without any seismic regulation thus resulting, in the case of an earthquake, unsafe and responsible for a significant impact on the environment in terms of waste production and CO2 emission (Belleri & Marini, 2016).

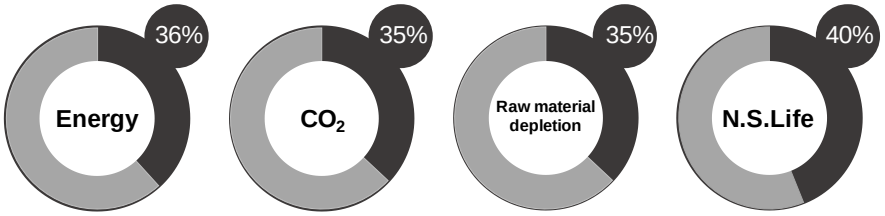

Figure 1: Existing building stock impacts on the environment (data from BPIE, 2011; Marini, et al., 2014).

Although this scenario could be extended to the whole existing building stock, this work focuses on the Post-World War II Reinforced Concrete (RC) heritage representing about 50% of the European building stock.

RC buildings, that are generally clustered in degraded suburbs and characterized by anonymous architectural features and living discomfort (Figure 2), are responsible for a considerable amount of energy consumption throughout Europe due to the low efficiency and the high structural vulnerability of this significant portion of the existing building stock, which makes the EU targets unreachable unless a massive retrofit intervention is carried out.

They are characterized by severe impacts on the environment, especially regarding energy consumption and waste production. In 2009, the average heating consumption, obtained by energy evaluations of these buildings sorted by climatic area, show that the post-world War II buildings are particularly energy-demanding with respect to the targets imposed by the current regulations; more precisely, the average annual energy consumption of these buildings is higher than 200 kWh/MQ (Marini, et al., 2014).

Figure 2: Typical residential district built after the WWII in European city peripheries (from: Feroldi 2014).

Moreover, having been built before the 1970s, most of these buildings were conceived to withstand only the static loads thus resulting, inherently vulnerable with respect to seismic action. They were designed before any seismic regulation code and, therefore, about 30-40% of the existing RC building does not respect minimum safety level targets, thus contributing to a non-resilient and unsustainable society.

Despite this severe scenario, nowadays, the average European renovation rate of the reinforced concrete building stock is only 1.5% (BPIE, 2011). To effectively meet the European targets, it is primarily needed to boost such a renovation rate by understanding and removing the barriers that affect the current practice in the renovation. The European "Building Performance" Observatory (BPIE) identified, as major barriers to the renovation of the existing building, the need to relocate the inhabitants, the extended downtime required during the construction works, the high cost of the interventions and the lack of adequate business models fostering the renovation (Krimgold, et al., 2004; La Greca & Margani, 2018).

1.1.1 Current practice in the renovation

Over the years, the only attempt to improve the conditions of buildings requiring renovation has been pursuit through either demolition and reconstruction interventions, or through episodic, non-integrated retrofit actions, usually aimed at solving a single problem at a time, such as the energy efficiency upgrade or the structural retrofit. Both these approaches are highly inefficient from many points of view.

The demolition and reconstruction approach, unless required from a structural point of view, has high economic and environmental costs and, of course, it affects the building functionality and requires the inhabitants' relocation. Moreover, from a sustainable point of view, when considering rebuilding it is necessary to account for some aspects. First, the construction of new buildings may require the production of new materials, thereby increasing impacts associated with material depletion and CO_2 emissions, among others. Second, the disposal of existing construction materials represents a critical issue nowadays.

On the other hand, the uncoupled approach, despite being often financially subsidized and fully compliant with the most updated codes and regulations, fails to foster either sustainability and resilience. The concept of uncoupled renovation is not viable since it is not sustainable under an economic, social, and environmental point of view. In the worst scenario of strong earthquakes, the sole energy upgrading intervention on an unsafe structure may lead to the collapse of the building, with a consequent loss of the investment, a high impact on the

environment, and, most importantly, to human losses. On the other hand, the sole seismic retrofit may lead to very poor aesthetic and functional results (Figure 3), while leaving the building still energy intensive.

Figure 3: Traditional uncoupled retrofit approach. Sole energy retrofit industrial warehouse after the Emilia-Romagna earthquake (2012) (*left*). Sole structural retrofit (*right*) (from http://www.studiomapi.it/).

Moreover, in the current practice, the structural retrofit is often carried out only in emergency situations and it is conceived and designed mainly to avoid human losses. Its application may result in safe and resilient but rather unsustainable interventions. For example, damage control, and reparability after an earthquake are not mandatory parts of the retrofit design thus resulting in severe restoration measures on the building after a seismic event.
Sustainability and resilience cannot be pursued independently and therefore, the sectorial code approach should give place to an integrated approach. Such an approach shall be adopted also considering safety as a cornerstone of sustainable intervention (Marini, et al., 2017).

1.1.2 Need for holistic solutions based on a LCT approach

To overcome the major drawbacks of the uncoupled approach, the concept **of a holistic and integrated** renovation was recently introduced (Feroldi, 2014; Marini, et al., 2014; Passoni, 2016; Vitiello, et al., 2016) among others. The term holistic renovation refers to an approach that concurrently tackles all building deficiencies, increases the structural service life while pursuing safety, sustainability, and resilience. Moreover, such an envisioned renovation strategy requires a new paradigm to be fully effective: sustainability, resilience, and safety can be achieved only by embracing a Life Cycle Perspective (Marini, et al., 2017; Marini, et al.,

2018). The effectiveness of such an approach compared to traditional retrofit actions emerges when broadening the time frame of the analyses, shifting from the construction time to a life cycle perspective. In this case, the potential of the holistic approach becomes clear in reducing costs, impacts on the inhabitants, and the environment over the whole building life. More precisely, it entails a substantial shift in the design perspective: from a design satisfying sectorial building code requirements at the construction time to a design considering the whole building performances under a Life Cycle perspective (Marini, et al., 2017; Marini, et al., 2018).

Considering this new approach, new awareness on the actual multifaceted building needs and new technology options are needed to combine structural retrofit, architectural restyling, and energy efficiency measures; thus, a synergistic and cooperative work of researchers, design professionals, and all the stakeholders in the construction sector is required.

When extending the reference time frame to the entire life cycle of the building, the concept of building retrofit design should be re-conceived embracing new principles and standards, linking the seismic retrofit to the energy and architectural retrofit and addressing sustainability issues. In particular, the concept of Life Cycle Thinking (LCT) can be addressed and applied to the entire construction to guarantee safety, resilience, minimum cost, nearly zero energy consumption, and nearly zero construction waste production.

Focusing on the structural design of the retrofit solution, besides ensuring the performance targets at the damage, life safety, and collapse limit states, a LCT approach consists of a careful selection of technologies and materials aimed at the reduction of the environmental footprint and costs of the retrofit solution. According to this approach, as already mentioned above, the design of the retrofit should consider its impacts over the whole life cycle of the structure; therefore, it should be conceived to be fully demountable and recyclable, made of sustainable materials (Thormark, 2006), and to be easily repairable after an extreme event. In case of earthquakes, the damage should be preferably lumped into “fuse” elements to avoid extended damage to the existing building. This would lead to a reduction of the building downtime, repair costs, and would avoid the inhabitants’ relocation: indeed, the damage reduction on the existing non-structural elements considerably reduces the indirect losses which are significantly higher than the direct ones.

Finally, to ensure easy assemblage and demountability of the components, pre-fabrication and dry techniques should be adopted. These characteristics make the system adaptable to possible future and innovative technologies, to future building needs and to possible incremental

rehabilitation strategies[1]. Considering the end of life of the intervention, the additional structural system may still have good performances, so, if it is conceived as dry assembled and demountable, it could be disassembled and reused or recycled, with a substantial reduction of demolition waste and need for disposal (Marini, et al., 2017).

To summarize, dry solutions, standardized elements and connections, micro-prefabrication, and off-site production of the components may become fundamental features of possible innovative strategies. In this context, it is worth noting that these features could be easily adapted for a retrofit solution from outside. When addressing building renovation barriers, working from outside the building may avoid the relocation of the inhabitants and the damage on the inside finishing. In this way, we can increase the feasibility of the intervention while reducing the indirect costs of the renovation (Figure 4).

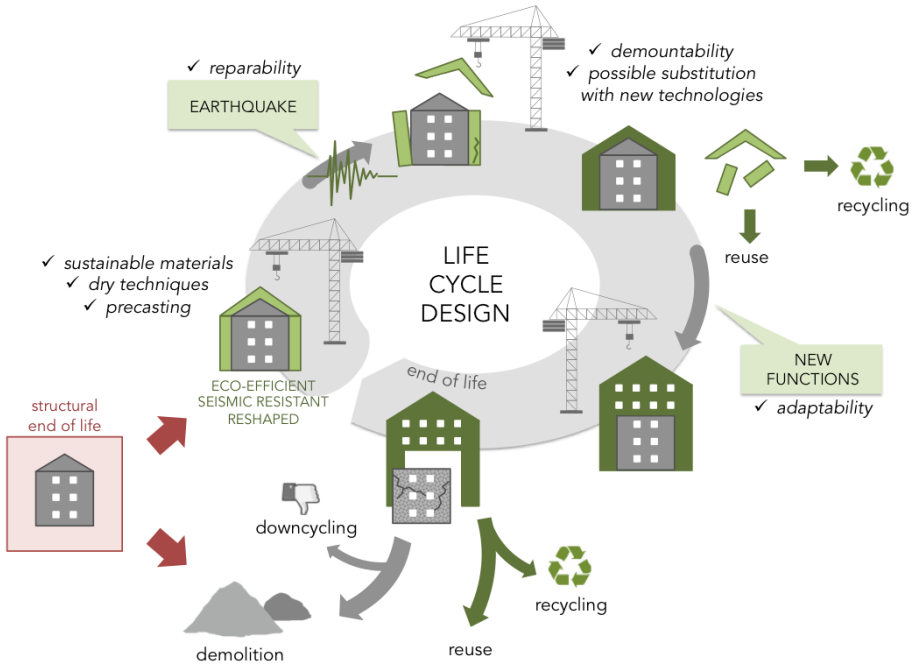

Figure 4: Life Cycle Design for sustainability and resilience (Marini et al. 2017).

1.1.3 Structural renovation strategies under a LC perspective lens

The LC perspective and the holistic approach to the renovation would establish the new qualitative multiple criteria and quantitative metrics to be addressed to assess the effectiveness and actual sustainability of existing and new solutions. Common practices may be found as unsustainable and might require redesign or enhancements; dismissal of some techniques could

[1] See Appendix 1

be envisioned in favor of new solution sets. As an example, the common seismic retrofit of RC frames, obtained through either strengthening of selective frame bays, or strengthening of the frame nodes may pose some problems related to the impairment of the finishing, while also requiring relocation of the inhabitants and long duration of the retrofit works, besides being non-compliant with the reparability and demountability requirements. On the other hand, by introducing fast assemblage and easy disassembly, along with sustainability, among the mandatory targets of the retrofit, the development of new off-site light prefabricated components, could become critical to increase the cost-effectiveness, the quality and timing of the construction project. Dry-assembly on site could also reduce waste and improve the health and safety of the construction site. Standardized connection and modularity would facilitate selective dismantling and reuse of the retrofit components at the end of life; while favoring substitution/reparability after a seismic event, thus reducing downtime and waste.

In the last year, to facilitate reparability, lumping the damage into sacrificial and easily replaceable elements was proposed. Some distinguished examples are braced frames with controlled rocking and energy dissipating fuses (Deierlein, et al., 2011; Gioiella, et al., 2016), hinged walls with dissipative elements at the base (Belleri & Marini, 2016; Qu, et al., 2012), shear links for eccentrically braced steel frames (Mansour, et al., 2011).

However, to effectively reduce the impacts during the operation phase and overcome two of the major barriers to the renovation, solutions carried out from outside, that combine energy and structural upgrade, should be introduced (Takeuchi, et al., 2009; Marini, et al., 2017). Exoskeleton applied as an energy-structural second skin in adherence or close to the existing building were recently proposed. Different technical solutions were proposed for RC buildings, featuring (a, b) shear walls, or (c, d) shell structures (Figure 5). In the shear wall solution, strength and stiffness, as well as seismic actions, are lumped into a few elements. Such elements must be encased in the exoskeleton, which in turn may become quite massive and resistant, and require new foundations (Figure 5 (a)). Both traditional steel-braced frames or RC walls (Riva, et al., 2011) and innovative rocking, post-tensioned, or hinged walls could be adapted. With this solution, energy efficiency upgrading is guaranteed by the finishing curtain walls or by the envelope attached to the exoskeleton. In this case, the two structure-energy systems work in parallel.

In the shell solution, the new façades are exploited to enforce a box-structural behavior (Giuriani & Marini, 2008; Giuriani, et al., 2015), resulting in a substantial reduction of the size of each structural component and a reduced foundation overload (Figure 5 (c)).

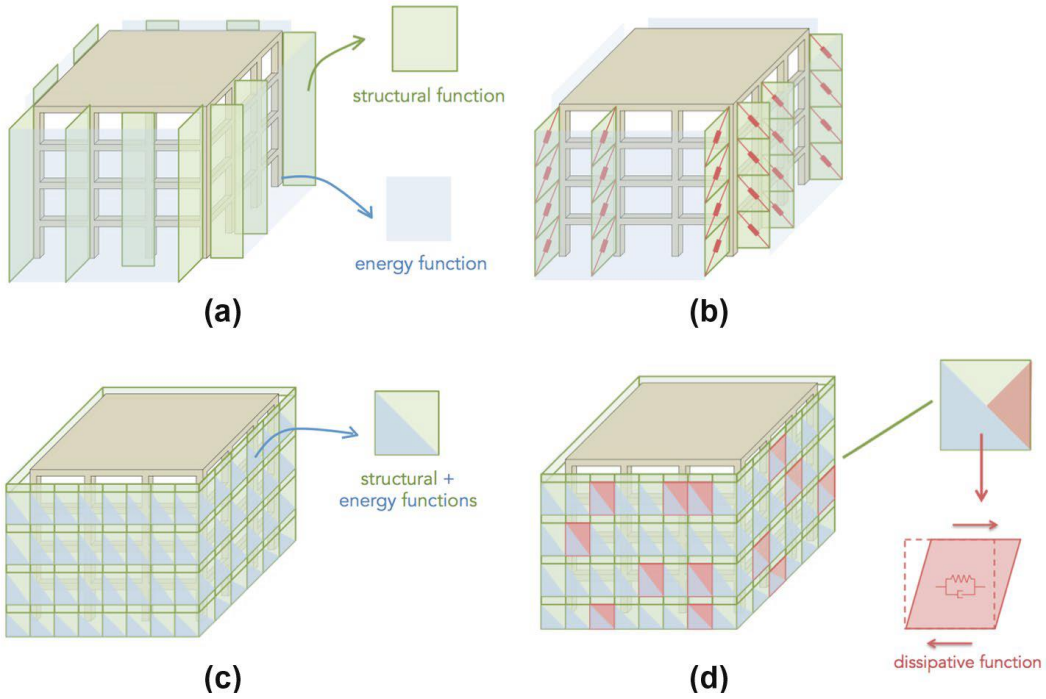

Figure 5: Retrofit solutions: (a) non-dissipative or (b) dissipative shear walls embedded in the external exoskeleton, (c) non-dissipative, or (d) dissipative shell structure with twofold use of the same encasing components (adapted from Marini et al., 2016).

The energy efficiency upgrade and structural safety could be achieved through a dual-use of the same elements: for instance, the thermo-insulating envelope could be used also as an in-plane seismic resisting structure. Within this category, diagrid structures are investigated (Labò, et al., 2016; Labò, et al., 2017; Labò, et al., 2018; Misawa, et al., 2015).

Diagrids are shell structures in which the shell behavior is ensured by a lattice structure. The term diagrid derives from the match between "diagonal" and "grid" (Yadav & Garg, 2015) and refers to a structural system made of horizontal and diagonal elements arranged in order to gain structural integrity through triangular modules composed by 2 diagonal elements of length L_d and inclination Ψ, and 1 horizontal element (Figure 6). Horizontal and vertical loads are transferred to the foundation system through a lattice structure made of trusses undergoing axial forces.

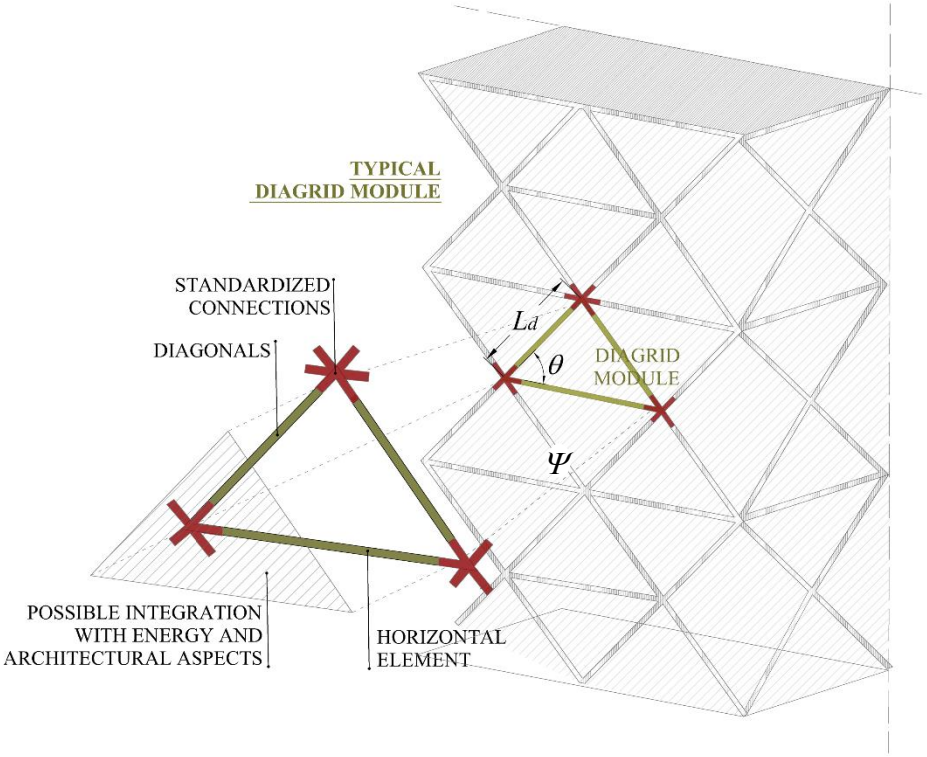

Figure 6: Diagrid structure: definition of diagrid module, node, and horizontal and diagonal elements.

1.1.4 Aim and scope and content of the research work

Enormous resources are being invested in Europe to foster environmental, economic, and social sustainability; however, such relevant effort to reach ambitious targets may be a missed chance, unless a deep and systematic intervention on the built environment is undertaken to target sustainability, safety, and resilience at the same time. This thesis provides a contribution to the scientific debate, focusing on holistic renovation from outside of reinforced concrete building by embracing a life cycle perspective. Effectiveness of such an approach to the renovation with respect to traditional retrofit actions emerges both in the construction time when addressing the barriers to the renovation such as the inhabitant relocation and the existing building disruption, and when broadening the time frame of the analyses, shifting from the construction time to a life cycle perspective. In this second case, the potential of the holistic approach becomes clear in reducing costs, impacts on the inhabitants, and impacts on the environment over the building life cycle. The results of this new approach is a retrofit solution based on a Life Cycle Thinking, which not only entails the use of recyclable/reusable materials, but also encourages interventions carried out from the outside the buildings, and implies the adoption of reparable,

easily maintainable, adaptable and fully demountable solutions with prefabricated components, thus guaranteeing, at the end-of-life, the selective dismantling and reuse or recycle of the components to reduce construction waste. The described solutions, which couples structural retrofit in the renovation action, stem as an enhancement of past pioneering "camouflage" interventions, such as double-skin solutions entailing in many benefits such as the protection of human lives, resilience and the lengthening of the existing buildings service life, the repairing costs and building downtime reduction, reduction of the environmental impact associated with seismic risk over the building life cycle and long-term protection of the investment (Marini et al. 2018). Within such a new perspective, new technology options are needed to innovatively combine structural retrofit, architectural restyling, and energy efficiency measures; in this work, an effective retrofit solution is proposed. Among the possible retrofit solutions, the diagrid structures as an innovative strengthening technique from outside are investigated. In the first part of this thesis, the state of the art of diagrid design is reported. New criteria for the design of retrofit solutions are set, and a design procedure for elastic diagrid is proposed. In the third chapter, a parametric evaluation of the retrofitted system through a simplified 2 DOF system is conducted, and a set of design spectra are defined in order to simplify the design procedure and derive the optimal retrofit parameter for RC buildings. Finally, a reference case study representative of the typical RC building is developed in the fifth chapter of this work to assess and validate the procedure.

1.2 State of the art of Diagrid structures

Diagrid structures are not new. Diagrid structures have been widely developed in the last years as an innovative structural system of new tall and complex buildings because of their high architectural potential and adaptability. The idea of diagrid as new construction typology lies at the intersection between the engineering and the architecture fields; in the following, some distinguished examples of diagrid structures together with some considerations about the structural design of diagrid structures for high-rise buildings are presented.

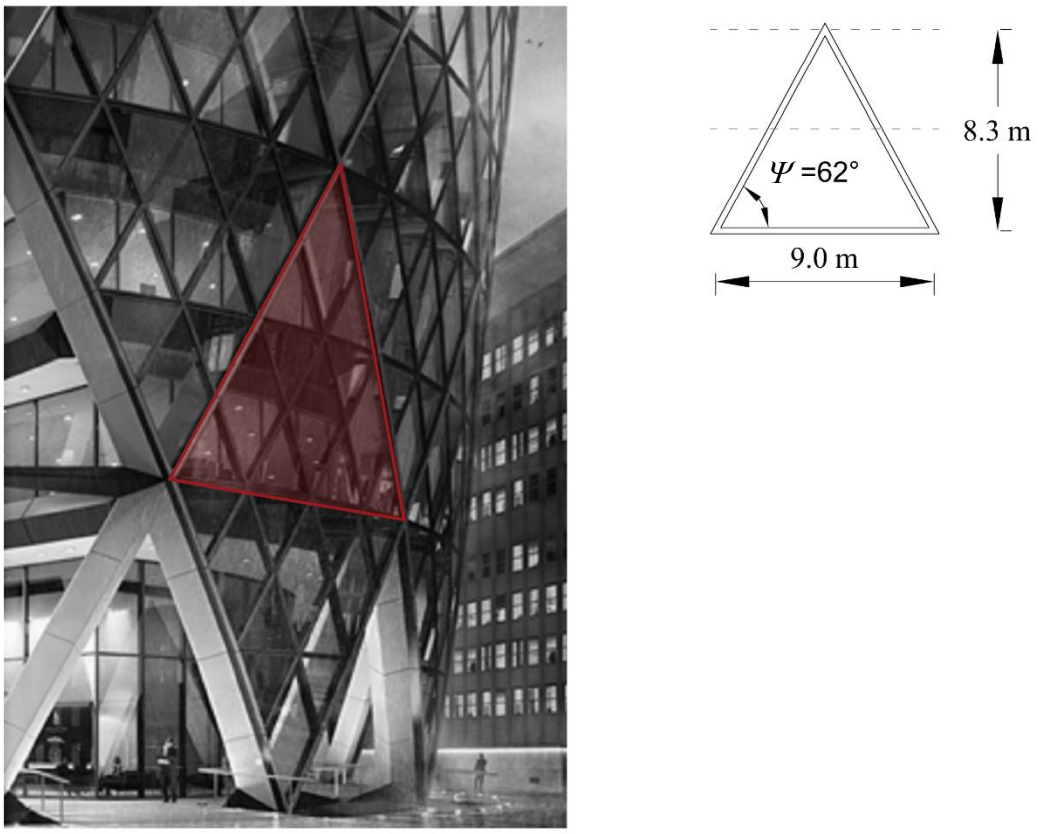

Figure 7: SWISS RE TOWER, Location: London, England, Architect: Foster & Partners, Engineer: Arup, Year: 2004.

The Swiss Re Tower was built in London between the year 2000 and 2004 and was designed by the architects Foster and partners and by the structural and wind engineers Arup and RWDI. The Swiss Re Tower was the first significative example for which the collaborative teamwork between engineers, architects, and steel contractors was needed. This application of the diagrid exoskeleton had an important influence on the diffusion of diagrid for new tall buildings in later years.

The structure is a 40-story building, with typical inter-story height equal to 4.15m, for a total height of 180 m. The Swiss Re Tower has a circular plan with variable diameter along with the height and it reaches its widest point, with a diameter equal to 56 m, at the 20th story.

The height of the triangular module is equal to the 2-story height (8.3m) and is 9 m wide; the diagonals are circular hollow section members, with the cross-section diameter varying between 508 mm (s^2=40 mm) at the lowest floors and 273 mm (s=12.5 mm) at the top.

[2] s = thickness

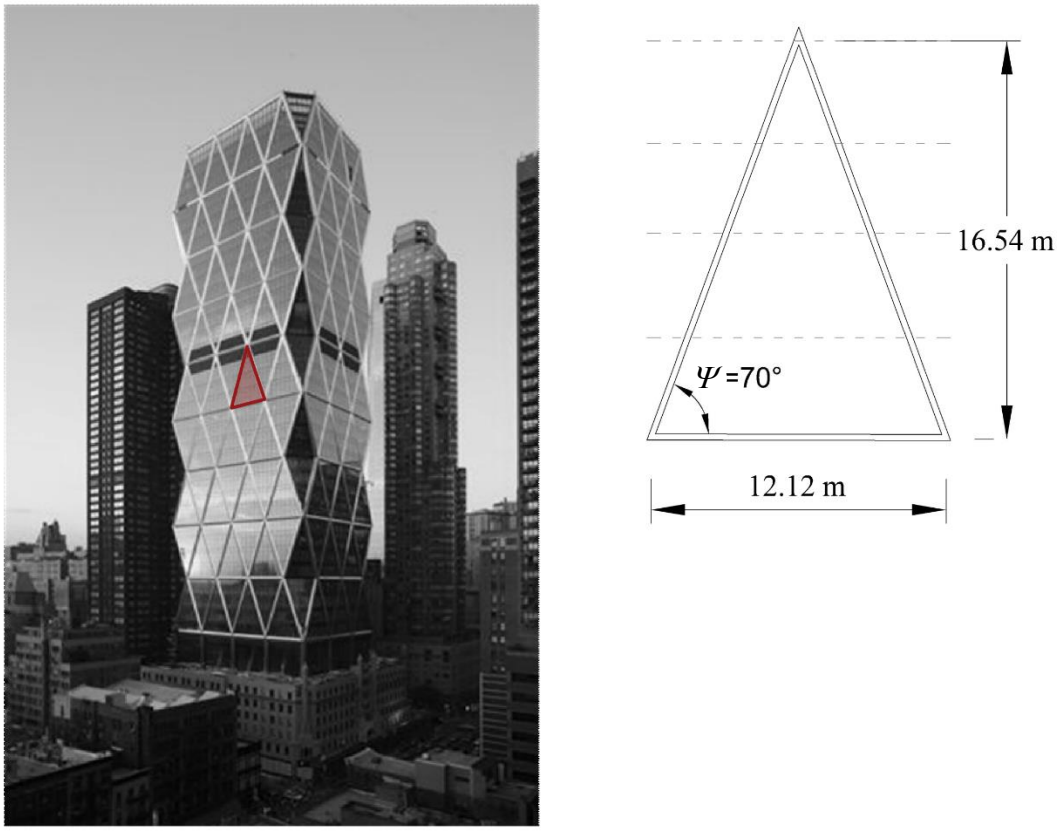

Figure 8: HEARST MAGAZINE TOWER, Location: New York City, USA, Architect: Foster & Partners, Engineer: WSP Cantor Seniuk, Year: 2006.

The Hearst Magazine Tower in New York was designed by Foster with the structural engineer firm WSP Cantor Seinuk. The structure was completed in 2006 and was the first skyscraper built in New York City after 09/11. The structure was built on an existent historic 6-story building thus creating a remarkable contrast in style, while the diagrid, was used as structural system from the 10th to the 44th floor. The result is a 46-story building, 183 m tall, with a rectangular plan of 48x37 m.

The triangular module has 4-story high (16.54 m) and 12.25 m wide; the diagonal cross-sections are I shaped with variable geometry: W14x370 is the maximum size at the base of the diagrid structure (10th floor), while W14x132 is the minimum size at the top.

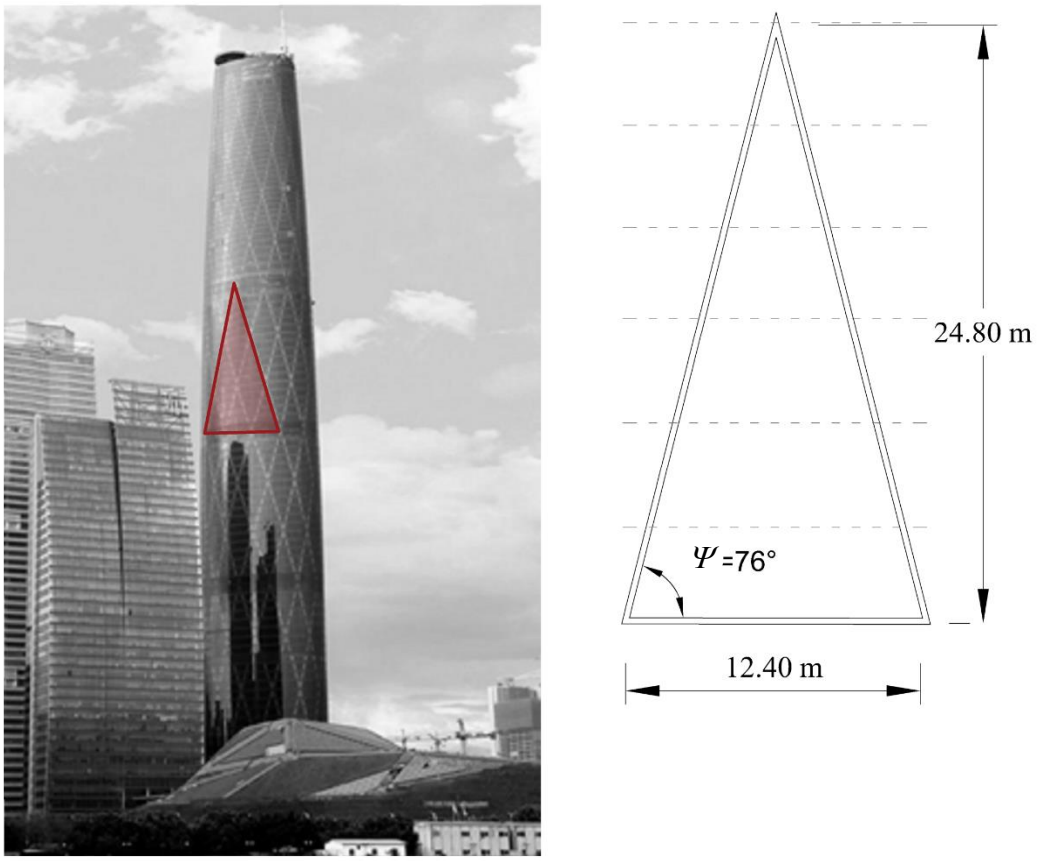

Figure 9: GUANGZHOU WEST TOWER, Location: Guangzhou, (CHINA), Architect: Wilkinson Eyre Architects, Engineer: Arup, Year: 2010.

The Guangzhou West Tower in the Central Business District of Guangzhou was built in 2010 and designed by Wilkinson Eyre architects and by the Arup structural engineer Craig Gibbons. The structure is a 103-story building, 440 m tall; to date, it is the tallest building in China and one of the 10 tallest in the world. The building has a triangular plan; in particular, the floor plate is an equilateral triangle with round corners, with each side 60m at the base, increasing to a maximum value of 66m at approximately 1/3 of the building height, at which point the side begins to reduce, up to 43.5 m, at the top.

The triangular module of the diagrid has 6-story high (24.8 m); the diagonals are steel tubular members filled with high strength concrete, with variable diameter: 1080 mm (s= 55 mm) at the first floor and 700 mm (s= 20 mm) at the top).

In this case, however, the diagrid structure is flanked to a central triangular concrete core that fully participates in the lateral resistance up to the 70th floor.

1.3 Use of Diagrid exoskeleton in the renovation of existing buildings

In this thesis, diagrids are innovatively proposed for the retrofit of existing buildings. The application of diagrid structures, particularly if conceived in agreement with the life cycle thinking principles and criteria, could represent a new solution set for a next generation of retrofit strategy. The adoption of an exoskeleton serving as seismic, energy and architectural retrofit measure does neither require the demolition of the finishing nor the inhabitants' relocation, thus entailing the reduction of costs, waste, while increasing the feasibility of the retrofit. Moreover, through an accurate selection of material and technologies, the intervention can be conceived as to allow maximum adaptability, reparability, and demountability in order to achieve all the life cycle thinking principles and targets.

The effectiveness of diagrid structures as strengthening solution could be easily highlighted through the comparative evaluation of this technique respect to the traditional ones under a LC perspective. Figure 10 shows a schematic comparison between two different retrofit techniques and it emphasizes how diagrid exoskeletons can represent a quite effective choice under a life cycle perspective. Diagrids can be designed to be integrated with energy efficiency measures, and by adopting sustainable materials. The possible pre-fabrication of the components enables off-site production of the retrofit components and speeds their assembly while reducing the construction time; they can be conceived as to enable total demountability and possible selective dismantling of the retrofit system, thus reducing waste, down-cycling or landfill disposal, while fostering reuse and recyclability of the retrofit components at the end of life. Diagrids represent a very promising solution for a deep and sustainable renovation of the existing building stock. Given the high adaptability and flexibility of diagrids compared with other solutions, when the initial cost of the retrofit is too demanding or to minimize the existing building disruption, these structures can be easily adapted in an incremental rehabilitation plan[3]. Incremental rehabilitation is an innovative approach to the seismic renovation of the existing building that integrates an ordered series of discrete rehabilitation over an extended period of time.

[3] See Appendix 1

	RC walls	Steel walls
Construction and Use Phase		
Construction time	medium	low (prefabricated solution)
Construction costs	medium-low	medium-high
Need of inhabitants' relocation	no (from outside)	no (from outside)
Fast assembling and disassembling	no	yes
Adaptability to building functions during its life cycle	no	yes
Need of maintenance	low	low
Post earthquake phase		
Repair costs	high (demolition may be required)	low (damage is lumped in the diagonals or in sacrificial elements)
Impacts connected to the repair operations	high (demolition may be required)	low (damage is lumped in the diagonals or in sacrificial elements)
Building downtime	low (from outside)	low (from outside)
End-of-Life		
Recyclability	no	yes
Reusability	no	yes

Figure 10: Comparison of different techniques under a life cycle perspective. Under a LC perspective, the differences between the traditional solution (R.C. Walls) and the Diagrid are immediately apparent.

1.3.1 Challenges when adopting diagrid exoskeletons in the renovation of the existing building

In order to adopt diagrid exoskeletons in the renovation of existing buildings, some critical issues must be tackled. Working from outside poses some major challenges, which may hinder its feasibility.

- **Stiff infills, partition walls and stairwell**

The diagrid design could be affected by the presence of stiff elements such as infills or staircase walls. These elements significantly affect the existing building stiffness and response in the case of a seismic event. The assessment of the real stiffness of the existing building is an essential point in order to correctly determine the structural properties of the retrofitting structures. Stiff stairwells, for example, can collect a significant share of the seismic action on the existing buildings, and may fail before the activation of the new retrofit system. In this context, it is fundamental to point out that, also if the retrofit guarantees the satisfaction of the life safety displacement demand, the solution cannot be considered as acceptable. The stairwell

is the critical safe egress of the inhabitants in the case of an emergency, and damage on this fundamental element must be avoided.

In order to overcome these issues, recent work (Cavalli, et al., 2017) has thoroughly analyzed the effect of the infill panels and the staircase walls on the behavior of reinforced concrete buildings. The presence of infill panels and staircase walls significantly affects the response of the existing building and the proportioning of the retrofit solution. In order to increase the effectiveness of the retrofit solution and preserve the safety of stairwell and the infill panels, it is essential to increase the stiffness of the retrofit solution k_2 way beyond those values ($k_2=2k_1$-$3k_1$ in Feroldi (2014)) adopted to guarantee the sole Life Safety Limit State (LSLS). Some preliminary interventions may as well be carried out to reduce the initial stiffness and thus the seismic action acting on the existing building. Whit this aim, for example, the adoption of vertical sliding joints into the infill panels can increase the displacement capacity of the existing infilled frame, thus reducing the damages and the frame-panels interaction (Preti & Bettini, 2012).

- **Lack of floor diaphragms**

Finally, it is worth noting that the feasibility of retrofit solution from outside relies on the floor diaphragm action. Diaphragms are fundamental to transfer the floor inertia forces to the vertical elements; however, especially in the case of RC buildings, the capacity of the existing floors is frequently disregarded. Noteworthy, floor in-plane failure is rarely observed in the aftermath of an earthquake, but it may become an issue after the retrofit, especially with non-dissipative solutions, since larger seismic actions might be transferred across the floor as a result of increased stiffness and since the seismic actions must be transferred, in the case of the diagrid, across the longitudinal length of the existing building. The need of strengthening the existing floors to trigger in-plane diaphragm action may require internal works, thus missing the target to operate from outside the building and may hinder the whole renovation process.

The results of recent research (Feroldi, 2014), based on a preliminary numerical and experimental evaluation, showed that, in low to medium seismicity zones, the existing composite brick-RC slabs perform like in-plane rigid diaphragms by developing an arch-and-tie system within the thickness of the floor, which collects and transfers the seismic action to the seismic resisting walls. The main failure mechanisms governing the in-plane ultimate response of the beam and block floor systems were analyzed, and the strength of the brick-to-RC joist interface was acknowledged as the critical property determining the floor capacity.

Based on these results, existing floor strengthening may only be required at the upper levels of buildings located in high seismicity zones. When floor in-plane strengthening is needed, ‘dry solutions’ such as intrados diaphragms made of steel truss work connected to the floor intrados, concealed at the sight with false ceilings, were proposed (Feroldi, et al., 2019). As an alternative solution, new diaphragms can be assembled in the floors of the external gallery bridging the retrofit solutions; this solution minimizes disruptions to the inhabitants and meets the target to operate from the outside.

In the latter case, the connection of the external diaphragm to the existing frame can be guaranteed through post-tensioned tendons and deep anchorages to transfer tensile actions and either studs or specific devices to be appositely designed to transfer shear forces. The same connections can be adopted to fix the existing building to the new seismic retrofit at the floor level (Marini, et al., 2017).

Chapter 2. Diagrid structure: new performance objectives and structural design

2.1Structural design for high-rise buildings: generalities

2.1.1. Optimal module of the diagrid

The structural performances of diagrids are strongly dependent on the geometry and the characteristic of the modules (Maqhareh, 2014); the diagonal length (L_d), the inclination angle (ψ), and the module height (h) are the parameters to be defined in the diagrid design.

The optimal module geometry is a trade-off between the architectural and aesthetic needs and the envisioned structural performances and response. While the diagrid architectural layout can vary as a function of the building features (window size and location, as well as the building final use itself), different researchers worked on the definition of the optimal module that guarantees the maximum structural performance of the diagrid. The most significant results were obtained by Kyoung Sun Moon at Yale University (Moon, et al., 2007; Moon, 2008) who showed that high inclination angle is optimal as to ensure maximum flexural stiffness (90° would be the optimal angle, yet considering triangular modules this angle cannot be applied), and 35° to provide maximum shear stiffness. As concern with the shear stiffness, Moon et al. derived the optimal angle by using a simple braced frame model subjected to bending moment (M) and shear (V) (Figure 11). The axial force (F_d) in the diagonal element is equal to:

$$F_d = \frac{V}{2\cos(\psi)}$$ **Equation 1**

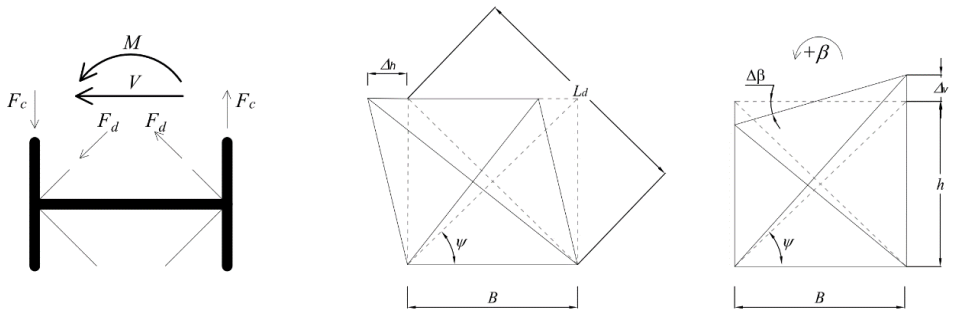

Figure 11: Braced frame model (Moon et al. 2007).

Assuming an elastic behavior it yields,

$$F_d = A_d \sigma_d = A_d E_d \varepsilon_d \qquad \textbf{Equation 2}$$

where A_d and E_d are the cross-section and the elastic modulus of the diagonal element, respectively; ε_d is the elastic strain related to the elongation of the diagonal (e_d) due to the lateral motion:

$$\varepsilon_d = \frac{e_d}{L_d} = \frac{\Delta_h \cos(\psi)}{h/\sin(\psi)} = \frac{\Delta_h \cos(\psi)\sin(\psi)}{h} \qquad \textbf{Equation 3}$$

Therefore, by considering the shear deformation (ξ) only (neglecting $\Delta\beta$ being the angle related to the negligible elongation of the column of the braced frame model) Moon et al. obtained the following approximation for the total elongation strain (ε_d)

$$\varepsilon_d \approx \xi \cos(\psi)\sin(\psi) \approx \frac{\xi \sin(2\psi)}{2} \qquad \textbf{Equation 4}$$

Combining the Equation 1 and Equation 4, it yields:

$$V = (A_d E_d \sin(2\psi)\cos(\psi))\xi \qquad \textbf{Equation 5}$$

By defining the shear stiffness as $D_T = V/\xi$, it yields:

$$D_T = V = A_d E_d \sin(2\psi)\cos(\psi) \qquad \textbf{Equation 6}$$

Figure 13 shows the shear stiffness as a function of the angle ψ. the maximum shear stiffness is obtained for a diagonal angle equal to 35° (Figure 12).

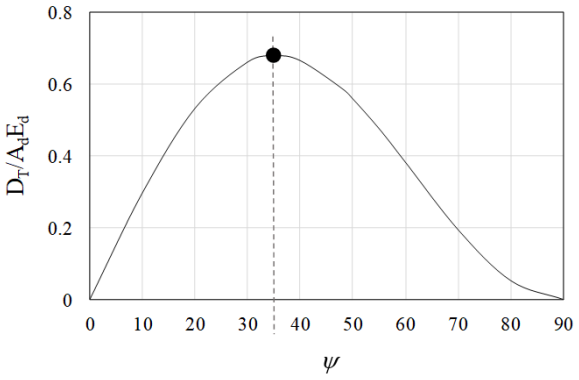

Figure 12: Normalized shear stiffness as a function of the inclination angle (Moon et al. 2007).

It is worth noting that in the braced frame in Figure 11 the bending moment is carried by the vertical columns; however, since diagrid structures differ from conventional braced frames because of the absence of vertical columns, the bending action must be endured by the diagonal

elements. Considering that the conventional optimal angle for bending stiffness is 90°, and the optimal angle for shear stiffness is 35°, it is expected that the optimal angle of the diagonal elements of a diagrid structure will range between those two values and it will depend on the height and shape of the building. In order to validate this assumption, Moon et al. studied the behavior of a 60-story building by varying the diagrid angle as shown in Figure 13. The results reported in Figure 14 confirmed the assumption, showing that the optimal angle of the diagonal member for the considered 60-story building is almost equal to 70°.

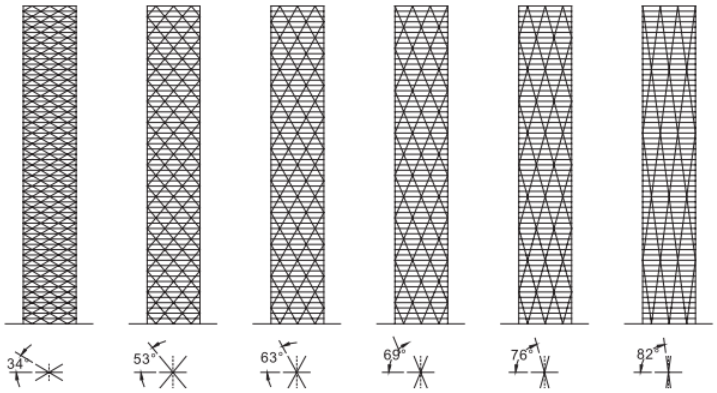

Figure 13: 60-story diagrid with different diagonal angle (Adapted from Moon et al. 2007).

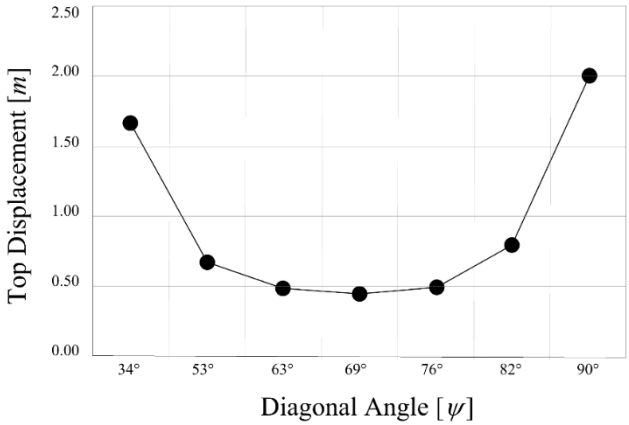

Figure 14: Top displacement of the diagrid as a function of the diagonal angle (Moon et al. 2007).

To corroborate the assumption, Moon et al. (2007) investigate the optimal angle through a parametric analysis by varying the number of building floors (42- and 20-story buildings). The results highlighted that the optimal angle could vary between 35° and 90°, and it decreases with decreasing the building height, as the shear deformation becomes dominant.

In all those configurations, the stresses in the diagonal elements were checked with respect to compliance with the current code considering that the design of the diagrid, must account for the strength limit of the diagonal elements. About this aspect, other papers that investigate the behavior of diagrid structures for tall buildings considering both stiffness and strength requirements (Mele, et al., 2012; Montuori, et al., 2013), demonstrated that for lower values of diagonal angles the strength requirement is often the governing criteria in the diagrid design. For this reason, in the design procedure, both the stiffness of the whole system and the stress level in the diagonals to avoid the overstress of these elements must be attentively considered.

2.1.2 Diagrid global stiffness

To evaluate the global stiffness of the diagrid exoskeletons, recent studies (Baker, 2013; Montuori, et al., 2015) have demonstrated that the whole system could be modeled as a cantilever beam, albeit taking into account the discrete nature of the diagrid. Since a deep beam is introduced to represent the whole building, the shear deformation became significant and, the Timoshenko theory has to be addressed while the Euler-Bernoulli beam theory would be inaccurate for such beams. In this work, the procedure, introduced by Baker (2013), and analyzed by Mele et al. (2016) for tall diagrids is addressed and adapted considering the seismic loads instead of the wind actions and by taking into account both linear and mass proportional modal shapes (Figure 15a, b).

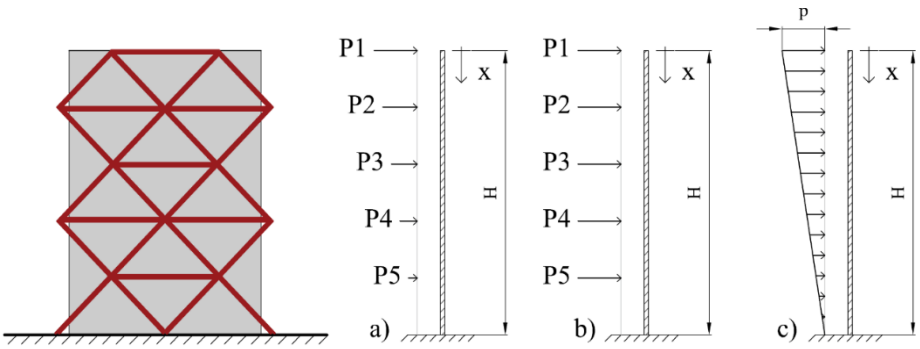

Figure 15: Different configurations of the Timoshenko beam for the simplified representation of the retrofitted system (existing building-diagrid): a) distributed triangular load proportional to the first mode shape, b) nodal point load with mass proportional distribution; c) analytic simplification of the case a) with a triangular distributed load.

The Timoshenko beam theory is then developed through the equations of the second derivative of the elastic curve as follows:

1) definition of the bending moment (*M(x)*) and the shear force (*V(x)*) in the *N* integration intervals of the Timoshenko beam; considering *N* the number of nodal forces.
2) from the beam theory, one can relate the bending moment to the beam deflection $M = -EI\frac{d\varphi}{dx}$. Defining *E* and *I* as the elastic and area inertia moduli, respectively, it yields:

$$\varphi_1 = -\frac{1}{EI}\int M_1(x)dx + C_1$$
$$\ldots$$
$$\varphi_N = -\frac{1}{EI}\int M_N(x)dx + C_N$$

Equation 7

where C_i are the constants of integration.

3) the constants of integration are determined by enforcing the following boundary conditions:

$$\varphi_1\left(\frac{H}{N}\right) = \varphi_2\left(\frac{H}{N}\right)$$
$$\ldots$$
$$\varphi_i\left(\frac{i\cdot H}{N}\right) = \varphi_{i+1}\left(\frac{i\cdot H}{N}\right)$$
$$\ldots$$
$$\varphi_N\left(H\right) = 0$$

Equation 8

4) Assuming *k* as the Timoshenko shear coefficient, *A* the cross-section of the beam, *G* the shear modulus, and *H* the beam height, from the beam theory it yields

$$V = -kAG\left(-\varphi + \frac{dy}{dx}\right)$$

Equation 9

and, therefore:

$$y_1 = -\frac{V_1}{kAG} - \int -\varphi_1(x)dx + C_{N+1}$$
$$\ldots$$
$$y_N = -\frac{V_N}{kAG} - \int -\varphi_N(x)dx + C_{N+N}$$

Equation 10

5) By enforcing the boundary conditions in Equation 10, the equations of the Timoshenko beam can be obtained:

$$y_1\left(\frac{H}{N}\right) = y_2\left(\frac{H}{N}\right)$$

Equation 11

...

$$y_i\left(\frac{i \cdot H}{N}\right) = y_{i+1}\left(\frac{i \cdot H}{N}\right)$$

...

$$y_N\left(H\right) = 0$$

Finally, to consider the discrete nature of the diagrid system, according to (Montuori, et al., 2015) the cross-section of the Timoshenko beam and the inertia stiffness must be considered as follow:

$$\begin{cases} A = 2 \cdot n_w A_{d,w} \cos(\vartheta) \\ I = n_w A_{d,f} \sin(\vartheta) \cdot l^2 \end{cases}$$

Equation 12

where, n_w is the number of diagonals on the "web" façade (defined as the parallel façade to the seismic action); n_f is the number of diagonals on the "flange" façade (defined as that orthogonal to the seismic action direction); $A_{d,f}$ and $A_{d,w}$ are the cross-section area of the diagonal elements on the "flange" and "web" facades, respectively; l is the plan direction of the building parallel to the considered horizontal loads' direction (Figure 16).

2.1.3 Internal actions in diagrid structures

In the design of the diagrid exoskeleton also the state of stress of the diagonal elements has to be carefully considered. When considering elastic diagrids, vertical and horizontal loads can be analyzed separately (Moon, et al., 2007; Montuori, et al., 2013; Mele, et al., 2012). In particular, by representing the gravity loads by vertical forces at each node of the diagrid, and by assuming that the bending moment is resisted by the diagrid "flange" façades, whilst the shear force is counteracted by the diagrid "web" façades, the diagrid internal forces can be evaluated as shown in Figure 16, where $F_{p,k}$, $F_{m,k}$, and $F_{v,k}$ are the forces in the *k-th* module due to vertical loads, overturning moment and shear force, respectively; and $N_{p,k}$, $N_{m,k}$ and $N_{v,k}$ are the correspondent internal actions.

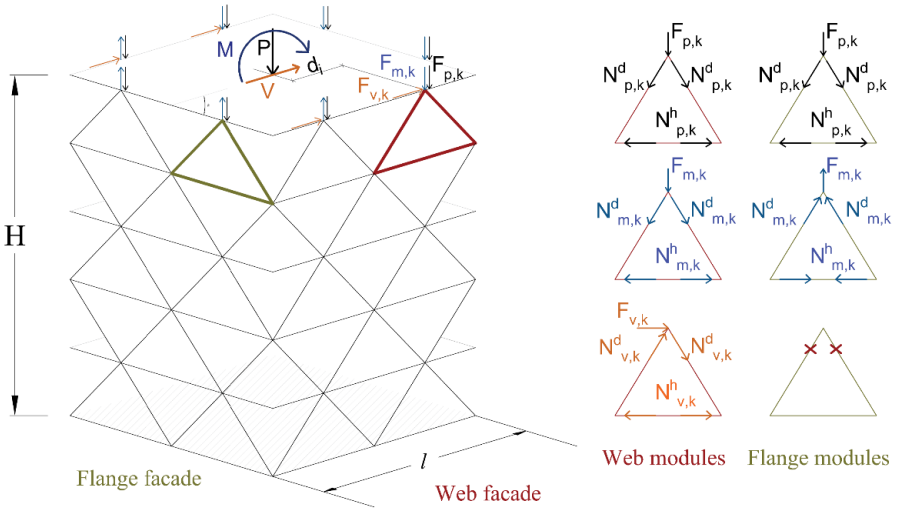

Figure 16: Internal actions in the diagrid structure due to gravity and later loads. After Montuori et al. (2013).

The gravity loads generate compressive loads ($N^{d}_{p,k}$) in the diagonal members and traction in the horizontal one ($N^{h}_{p,k}$). These forces can be calculated as reported in the following.

$$N^{d}_{p,k} = \frac{F_{p,k}}{2 \cdot \cos(90 - \psi)}$$
$$N^{h}_{p,k} = \frac{F_{p,k}}{2} \cdot \tan(90 - \psi)$$

Equation 13

The horizontal loads generate bending moment and shear forces on the diagrid structure. Assuming that the bending moment is resisted by the flange and the shear by the web, the contributions N_{mk} and N_{vk} can be obtained.

The contribution given by the bending moment is:

$$N^{d}_{m,k} = \frac{F_{m,k}}{2 \cdot \cos(90 - \psi)}$$
$$N^{h}_{m,k} = \frac{F_{m,k}}{2} \cdot \tan(90 - \psi)$$

Equation 14

and, the contribution due to the shear action is equal to:

$$N^{d}_{v,k} = \frac{F_{v,k}}{2 \cdot \sin(90 - \psi)}$$
$$N^{h}_{v,k} = \frac{F_{v,k}}{2}$$

Equation 15

where,

$$F_{m,k} = \pm \frac{M_m d_k}{\sum_{i=1}^{n_k} d_i^2}$$ **Equation 16**

and

$$F_{v,k} = \pm \frac{V_m \cos(\alpha)_k}{\sum_{i=1}^{n_k} \cos(\alpha)_i}$$ **Equation 17**

When the diagrid is subject to gravity and seismic loads, the axial force in the diagonal elements of the *k-th* module at the m-th floor can be calculated as follows:

$$N_k = N_{p,k} + N_{m,k} + N_{v,k} = \frac{F_{p,k}}{2 \cdot \sin(\psi)} \pm \frac{M_m d_k}{\sum_{i=1}^{n_k} d_i^2} \cdot \frac{1}{2 \cdot \sin(\psi)} \pm \frac{V_m \cos(\alpha)_k}{\sum_{i=1}^{n_k} \cos(\alpha)_i} \cdot \frac{1}{2 \cdot \cos(\psi)}$$ **Eq. 18**

where *d* is the distance of the *i-th* module from the whole diagrid centroid axis (Figure 16) and n_k is the total number of the modules in the whole diagrid.

It is important to note that this is true when the diagrid module spans one floor of the building, and it is composed of trusses only; i.e. the actions are transferred through the main nodes and axial forces. In the case of tall buildings, the module can be developed over several floors, and in these cases, the internal actions in the diagonals may change (Figure 17). Isostatic triangular module made of trusses cannot be further considered but a beam system subjected to bending moment and shear actions have to be addressed; consequently, additional consideration to Eq. 18 must be made.

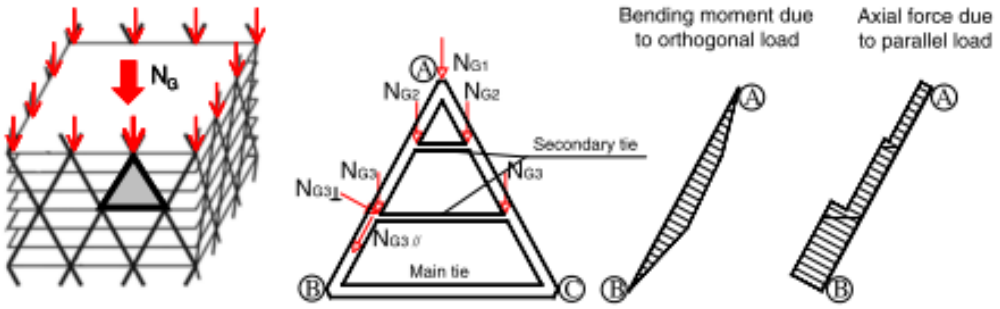

Figure 17: Internal actions in the diagonal elements due to the gravity loads in the case of module higher than one floor of the building. (Mele, et al., 2012).

2.2 Renovation of the existing building with a diagrid exoskeleton: design criteria

The structural design of diagrids as a retrofit solution for existing building is a complex process, in which different aspects have to be taken into account particularly when addressing LCT (Section 1.1.3), such as the structural interactions between the existing building and the additional retrofit structure, the use of eco-compatible materials and demountable technology, among others. In this section, a set of design targets is defined to have an effective retrofit solution, and a design method for linear elastic diagrids is proposed considering both the existing building and the diagrid features.

2.2.1 Existing Reinforced concrete buildings

When designing diagrid structures as a strengthening exoskeleton for reinforced concrete buildings, it is fundamental to correctly consider the interaction between the retrofitting structure and the existing building. With this aim, a brief introduction about the behavior and structural features of typical RC existing buildings is made.

Post-World War II RC buildings are typically made of one direction masonry infilled frames (one-way frames) and are characterized by low-ductility structural details. Floors are usually made of one-way RC beam and brick block systems, often lacking RC topping. All these features highly contribute to the seismic vulnerability of these constructions but, mostly, seismic vulnerabilities are triggered by in plan and vertical irregularities that often characterize these buildings.

Plan irregularities mainly consist of irregular shapes of the existing buildings (Figure 18a), the asymmetric position of the structural frames, or eccentric position of stiff elements such as the staircase or the elevator cores. A plan irregularity can lead to a concentration of the seismic actions into few localized elements that, in the case of post-world War II buildings, are not designed to withstand horizontal loads leading to a partial or global collapse of those elements.

Vertical irregularities are often the results of the irregular distribution of the masonry infill walls along with the existing building height (Shing & Mehrabi, 2002; Klingner & Bertero, 1978; Fardis & Panagiotakos, 1997) (Figure 18b). This type of irregularities is the result of the static design before the seismic regulation codes for which masonry infills were considered as non-structural elements and, therefore, only as additional dead loads in the design phase without any consideration about the interaction with the structural frame under horizontal loads. Nowadays, however, it is widely acknowledged that, even though they are considered

non-structural elements, they interact with the frame when the structure is subjected to earthquake loads. Such interaction may or may not be beneficial to the performance of the structure. An irregular distribution along the existing building height of the infill panels can lead to a displacement concentration and the consequent collapse of the structure. For example, the absence of the infill panels at the ground floor of the existing building (pilotis), or a partially infilled bay or ribbon windows in the basement lead to the on-set soft-story failure mechanisms because of the shear failure of the columns.

In the evaluation of the structural behavior, stiff elements with low ductility such as infills, or staircase walls must be considered; these elements often characterize RC buildings and significantly affect their structural response.

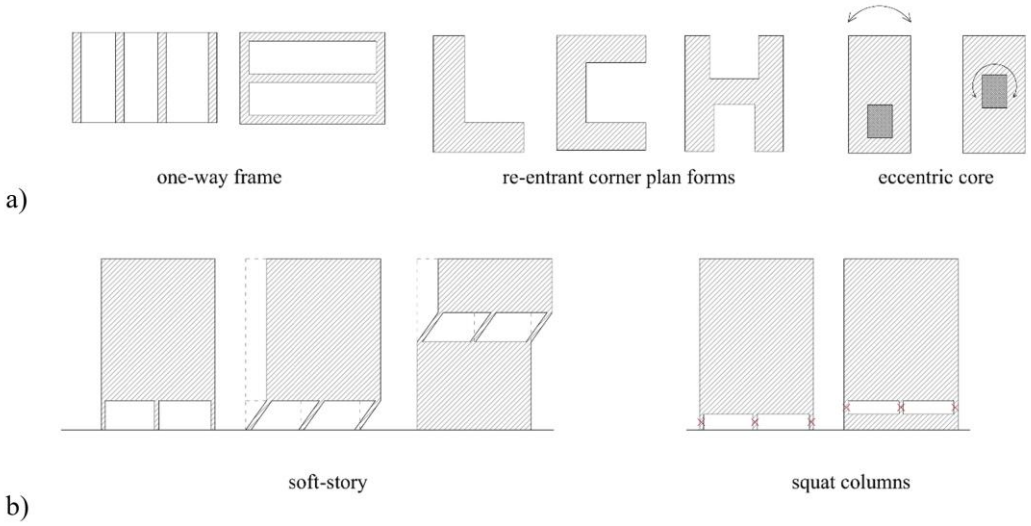

Figure 18: Main seismic vulnerabilities in RC frames: a) Plan irregularities, and b) vertical irregularities.

2.2.2 New performance objectives under a LCT perspective

The design of the diagrid as a retrofit measure is based on a new multi-criteria performance-based design, initially proposed by (Passoni, et al., 2018), in which the conventional design performance objectives are reset, and new design targets are introduced. Accounting for criteria based on new structural targets, environmental sustainability, and social-economic sustainability of the retrofit, the new approach results in a revisited Performance-Based Design (PBD) for resilient, sustainable, and feasible solutions.

- New criteria for the structural retrofit

The renovation of existing buildings requires additional design parameters with respect to new buildings. The sole control of the total drift or the base shear is indeed insufficient to guarantee

the safety and to optimize the performances of the structure after the seismic upgrade. Some other important criteria should thus be considered, which are usually disregarded.

Very often, for example, diaphragms and foundations are not addressed in the new seismic-resistant system. When the seismic action exceeds the floor capacity, the diaphragm should be retrofitted. Similarly, the capacity of the existing foundations should be checked for the additional forces induced by earthquakes and, when not verified, should be upgraded. The capacity of the existing floors and foundations represent thus additional targets that should be controlled in the design of the seismic retrofit interventions.

Another important criterion that should be observed in the performance-based design of a structural retrofit is the protection of the egress path; however, the actions in the staircase walls are usually never controlled, especially if they are masonry infill walls. In general, the staircase wells should always be verified to the seismic loads and protected through the retrofit intervention.

Finally, a Performance-Based Design (PBD) should also be able to reduce the damage after natural disasters to both structural and nonstructural elements to facilitate the rescue operations in the post-earthquake emergency, reduce the reconstruction costs, and reduce the waste. It has been observed that about 50-70% of the total direct losses due to earthquakes are connected to non-structural elements (Whittaker & Soong, 2003). A fair calibration of the structural design targets may thus allow controlling damages and reduce Life Cycle costs.

- New criteria fostering environmental sustainability

Basing on the necessity to adopt a holistic solution based on a LCT approach to the renovation, all the principles described in paragraph 1.1.2 can be considered as additional criteria for the new multi-criteria PBD in order to foster the environmental sustainability of the renovation process. Together with the LCT, the new PBD allows controlling additional parameters to minimize the environmental impact of the intervention and the retrofitted building, the overall cost of the intervention, and the operating costs in terms of CO_2 during the whole life cycle.

- New criteria fostering social-economic sustainability

To foster the social-economic sustainability of the seismic retrofit interventions, two main criteria should be pursuit: adopting holistic solutions and avoiding the relocation of inhabitants by applying the intervention from outside the building.

The design of those solutions implies the definition of additional structural requirements. For example, additional diaphragms cannot be realized at the extrados of the floors, but a gallery should be added outside the building and its floor could be conceived as an external floor

diaphragm. Moreover, new foundations may be required for the additional exterior elements, but this may avoid the retrofit of the existing foundation system, which is usually an expensive and time-consuming operation.

All these new criteria transform the traditional PBD approach into a new multi-criteria approach, which also includes the principles of Life Cycle Thinking to account for environmental and social-economic sustainability (Passoni, et al., 2018). Besides considering new structural targets to control the seismic response of retrofitted existing buildings, to protect the escape route, to reduce the damage to structural and nonstructural elements, and to allow the feasibility of the retrofit intervention from outside (floor diaphragms and foundation system), the principles of LCT are considered to compare different holistic interventions with similar energy and structural performances (Figure 19).

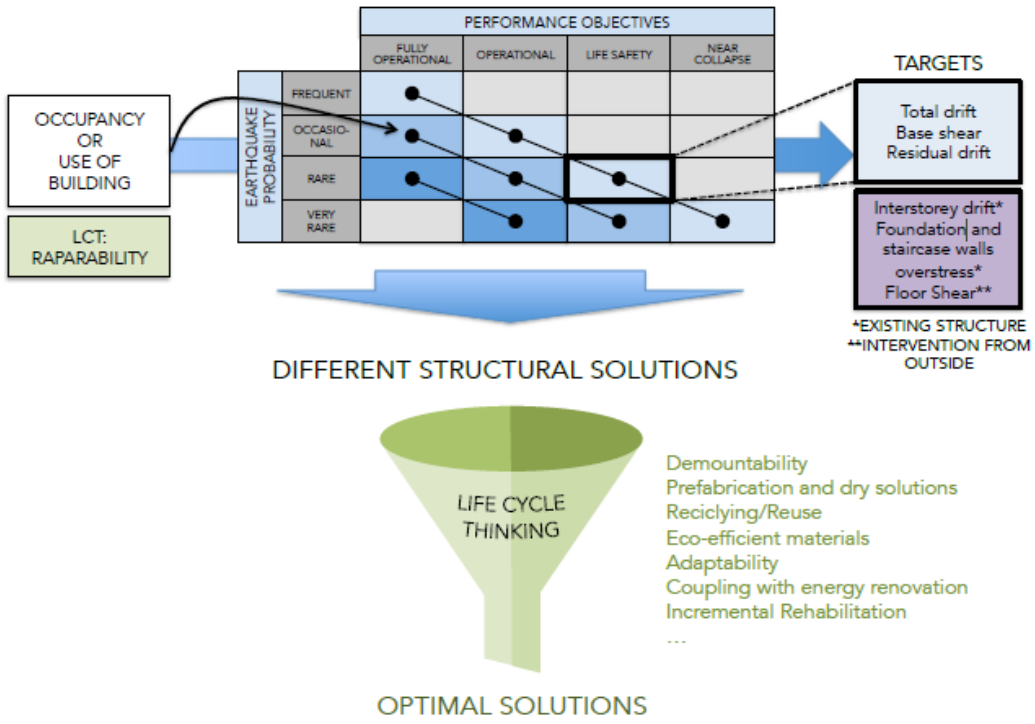

Figure 19: Conceptual scheme of the new multi-criteria performance-based design approach (From Passoni et al. 2018).

2.3 Elastic, dissipative and responsive diagrid structure: an overview

Diagrid as strengthening solution can be developed as (1) an over-resistant elastic exoskeleton, that meets the required targets by adding a stiff and over-resistant external exoskeleton limiting the displacements of the existing structure thus avoiding any possible damage on the retrofitted building; (2) a dissipative structure which controls the seismic response of the existing building

by dissipating seismic energy into new devices, which may be either façade components or localized dampers (either hysteretic, viscoelastic, or viscous, etc.); (3) a passive-responsive structure which adapts its response by changing its static scheme as a function of the seismic event. Usually, this kind of behavior, known as 'smart behavior', is provided with controllers and actuators actively inducing the envisioned property change (Morales-Beltran & Teuffel, 2013) yet, in this case, the system is conceived as 'passively' adapting to variable load condition by adopting localized sacrificial elements that break as a fuse for the structure and that can be easily replaced at the end of the earthquake.

Considering the first 2 solutions, both have advantages and drawbacks. By damping the system, dissipative solutions often allow reducing the cross-section of the structural components, thus optimizing the material consumption and localizing the damage into a few replaceable elements. On the other hand, the devices can be expensive, the design process may be quite difficult, and the need for larger deformation capacity of the existing structure may require additional preliminary interventions triggering larger ductility in the structural nodes. Moreover, unless carefully designed, dissipative solutions may be ineffective since displacement-activated dampers may not reach yielding and remain inactive while the infill walls may reach their ultimate resistance for displacements of few millimeters (Uva, et al., 2012).

When over-resistant structures are considered, stiff façades are added to existing structures, and the existing building can remain elastic; however, in case of extraordinary strong seismic events (such as those reaching values beyond the spectrum), the high building stiffness may lead to a substantial increment of seismic actions, resulting in a remarkable overload of floor diaphragms and foundations. In this scenario, 'passive-responsive' structures can be proposed (Labò, et al., 2017; Antonini, et al., 2017).

Thanks to non-linear responsive elements, these structures may be designed to act as stiff systems (elastic) up to the Damage Limit State (DLS), and as dissipative systems at the Life Safety Limit State (LSLS), therefore avoiding the damage for low-intensity earthquakes but enabling yielding and thus ductile behavior in case of strong earthquakes thus introducing a cap on the loads transferred to the floor diaphragms and the foundations but still guaranteeing a ductile behavior.

2.3.1 Structural design of diagrid structures

In the design of diagrid structures as strengthening solutions for RC buildings focus must be made on 1) the geometry of the diagrid itself, which must meet architectural and aesthetic needs and constraints; subsequently, specific constraints that depend on the strengthening solution adopted must be considered.

As far as the elastic diagrid is concerned, the additional constraints that must be considered are 2) the minimum stiffness of the diagrid, which guarantees the damage control in the existing building, and 3) the maximum axial force in the diagrid's diagonal members as to avoid their buckling. In the case of passive-responsive diagrids, it has to be considered also 4) the non-linear responsive elements features.

2.3.1.1 Architectural and formal constraint

The optimal diagrid geometry is influenced by several parameters related to the existing building layout and features and diagrid performances. As far as the existing building is concerned, the retrofitting diagrid has to comply with architectural and aesthetic needs (location of openings, inter-story height, etc...), as well as its plan layout has to enable possible living spaces expansion. The retrofitting diagrid could be built either, in close proximity or as an enlargement of the existing building (Figure 20b), and in the second case, new living spaces and double façade systems could be developed thus increasing the potential value of the project.

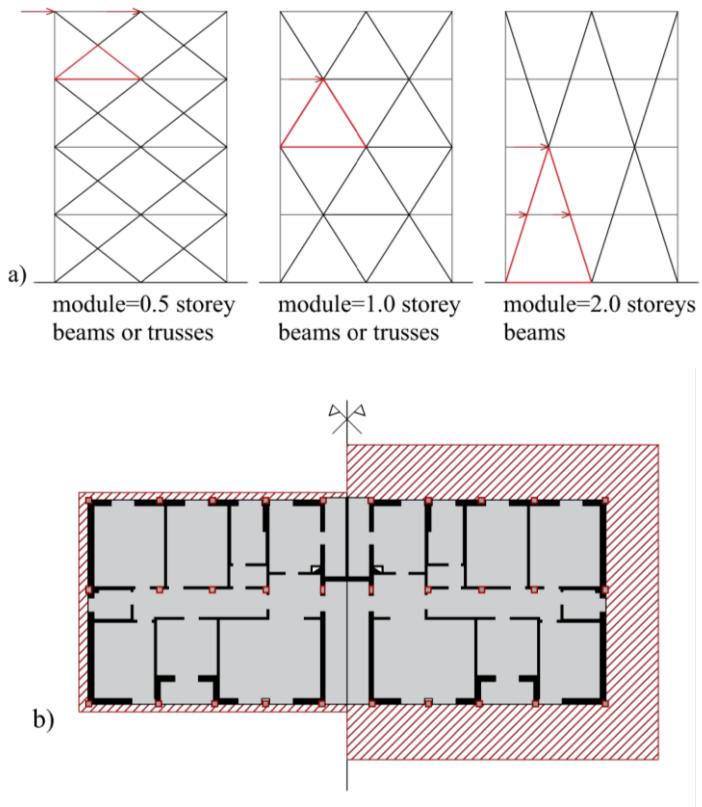

Figure 20: Different possible configurations of the diagrid: a) By varying the module geometry. b) The horizontal projection of the retrofitted structure in the case of diagrid in adhesion and as an enlargement of an existing building.

Another parameter that significantly affects the architectural design but also the structural performance of the diagrids is the module's geometry (Maqhareh, 2014). Considering the remarks made in paragraph 2.1.1, for the integrated retrofit of low-medium rise buildings, an optimal reference angle of 35° should be considered, while also accounting for the geometry and the characteristics of the reference building. However, among the alternative formal possibilities, the optimal solutions should be derived by combining, in an integrated way, all these aspects.

2.3.2 Elastic diagrid

2.3.2.1 Stiffness constraint

The objective of the stiffness constraint is to limit and control the displacement of the existing structure when subjected to the design earthquake thus avoiding excessive damage, and, consequently, the long-term disruption of the building activities, the relocation of its inhabitants, and minimizing the costs after a seismic event.

In order to set the stiffness constraint, the target maximum top displacement d_{TOP} of the existing building is identified (in the case of post-world war II RC building, for example, this target can be derived from the limit inter-story drift δ allowed by the infill panels). Through this constraint, therefore, the cross-section area of the diagonal elements of the diagrid that satisfy the displacement target is derived.

With this aim, as described in paragraph 2.1.2, the whole system could be modeled as a Timoshenko beam. It is worth noting that for ordinary post-world war RC structures, a triangular distributed load p (Figure 15c) can be introduced to considerably simplify the analytical procedure and easily generalize the equation of the Timoshenko beam. This load distribution does not introduce significant errors in the diagrid design. Concerning an average stiffness and geometry of existing RC buildings, it has been demonstrated that the top displacement obtained with the continuous triangular load distribution, only slightly under-estimate the top displacement obtained with the nodal point loads along with the building height. For a cantilever beam higher than 12.60 m (that corresponds to 4 floors for an average height of 3.15 m), the error is less than 15%. Vice versa, for buildings shorter than 9 m, the nodal point load configuration should be preferred.

Introducing this simplification and following the steps reported in paragraph 2.1.2, it follows:

$$M(x) = -\left(\frac{px^2}{2} - \frac{px^3}{6H}\right)$$
$$V(x) = -\left(px - \frac{px^2}{2H}\right)$$

Equation 19

therefore, the beam deflection is equal to

$$\varphi = -\frac{1}{EI}\int -\left(\frac{px^2}{2} - \frac{px^3}{6H}\right)dx + C_1$$
$$\varphi = -\frac{1}{EI}\left[\frac{px^3}{6} - \frac{px^4}{24H}\right] + C_1$$

Equation 20

by enforcing the boundary condition at the base of the Timoshenko beam ($\varphi(H) = 0$)

$$C_1 = -\frac{pH^3}{8EI}$$
$$\varphi = \frac{1}{EI}\left[\frac{px^3}{6} - \frac{px^4}{24H} - \frac{pH^3}{8}\right]$$

Equation 21

according to Equation 9, the derivative of the Timoshenko beam can be obtained:

$$\frac{dy}{dx} = \frac{-px + px^2/2H}{kAG} + \frac{1}{EI}\left[\frac{px^3}{6} - \frac{px^4}{24H} - \frac{pH^3}{8}\right] \qquad \textbf{Equation 22}$$

By integrating and imposing the boundary condition at the base of the Timoshenko beam (*y(H)=0*), the equation of the elastic curve of the Timoshenko beam with a triangular distributed load is obtained.

Since this constraint aims to control the displacement at the top of the existing building, the displacement of the Timoshenko beam in *x* equal to *0* (Figure 15c), is evaluated:

$$y(0) = \frac{8pH^2}{24A_sGk} + \frac{11pH^4}{120EI} \qquad \textbf{Equation 23}$$

where *p* is the distributed triangular load on the cantilever beam; *E*, *I*, and A_s are the elastic modulus, the area moment of inertia, and the cross-section area of the diagonal elements, respectively; *k* is the Timoshenko shear coefficient, and *H* is the building height. As reported in Equation 12 the discrete nature of the diagrid has to be considered by assuming:

$$\begin{cases} A_s = 2n_W A_{d,W1}\cos(\vartheta) \\ I = n_f A_{d,f1}\sin(\vartheta) l^2 \end{cases}$$

where, n_W and n_f are the number of diagonals on the web façade and the flange façade, respectively. $A_{d,W1,}$ and $A_{d,f1}$ are the area of the diagonal elements on the web and flange façade; *l* is the plan dimension of the building parallel to the considered seismic direction (Figure 16). By imposing the maximum displacement *y(0)* equal to the limit top displacement (d_{TOP}), the minimum cross-section areas ($A_{d,W,}$ and $A_{d,f}$) that satisfy the stiffness target can be obtained.

2.3.2.2 Strength constraint

In the design of diagrid structures, attention has to be also paid to the maximum axial force in the diagonal elements. To avoid buckling, the maximum axial compression action N_k of each structural member must be smaller than its nominal buckling capacity N_k^{LIM} (EC8, CEN 2005). In particular, it yields:

$$N_k \le N_k^{LIM} = \chi \frac{A_d \cdot f_{yk}}{\gamma_{M0}} \qquad \textbf{Equation 24}$$

where A_d is the cross-section area of the diagonal element, f_{yk} is the maximum allowed axial stress allowed, γ_{M0} is the material safety factor, and the coefficient χ is a function of the profile slenderness.

The choice of the material, the cross-section, the boundary condition of the diagrid modules, and, consequently, the effective length of the diagonal elements plays a critical role in this step of the design procedure to reduce diagrid weight and cost. For this reason, different configurations of diagrid structures must be analyzed for each case and critically compared.

2.3.3 Passive-Responsive Diagrid: principles and structural behavior

In the case of responsive diagrid, the responsive behavior is attained by changing boundary conditions at the diagrid's base supports as a function of the earthquake intensity, while the diagrid lattice structure remains elastic.

At the Damage Limit State, the diagrid elements are designed as hinged at the base, whereas for very high earthquakes, beyond a target base shear, hinges are conceived to downgrade into non-linear supports allowing for the controlled sliding of the diagrid's base. Activation of these supports significantly reduces the stiffness of the structure, thus increasing its fundamental period; as a result, seismic loads decrease, and building displacements increase.

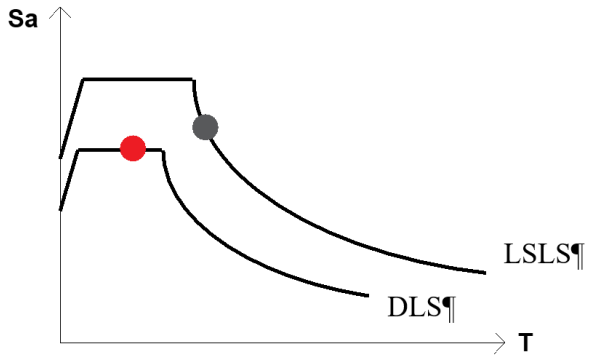

Figure 21: Responsive structure behavior.

The design of these special non-linear supports can be made through an iterative procedure in order to calibrate the optimal properties of the new sliding supports. In particular, the new support is initially rigid and behaves as an elastoplastic system beyond a target base shear flow (that for example could represent the limit base shear to avoid damage in the existing floors, or the overstress of the existing foundation system). In addition, excessive horizontal displacement and second-order effects are avoided by limiting the maximum displacement of the supports with a bumper at the end of the gap.

It is worth noting that it has been demonstrated that responsive diagrids require preliminary interventions at the existing building ground floor to reduce the damage following the onset of

the diagrid sliding (Labò, et al., 2017). Such interventions are for instance the disengagement of the infills from the RC frame at the ground floor (Preti & Bettini, 2012) and the local increase of the column ends ductility (Antonopoulos & Triantafillou, 2003). The mechanism requires large displacement ductility of the first-floor columns, which can be attained by deliberately triggering and controlling (through the diagrid) a soft-story configuration and by increasing the columns' rotational capacity (providing confinement, as using fiber reinforced polymer wrapping or HPFRC Jacketing). The retrofitted building behaves as an isolated structure with the isolation concentrated at the ground floor to avoid extensive damage to the upper floors of the existing structure. This preliminary intervention allows us to accommodate the displacements induced by the sliding system. Moreover, the controlled soft-story behavior will dominate the deformed shape of the building during the earthquake overcoming all the uncertainties that characterized the finite element models of reinforced concrete buildings (infill panel behavior among others). Indeed, the performance evaluation of a retrofit solution is affected by the non-structural elements modeling. The proposed retrofit scheme overcomes all the uncertainties related to the infill models thanks to the controlled soft-story behavior that will dominate the inelastic deformed shape of the structure.

Thanks to the preliminary interventions, the maximum allowable inter-story drift at the first level represents the main design parameter considered in the retrofit. A sketch of the retrofitted building and the hysteresis shape of the diagrid base restraints are shown in Figure 22.

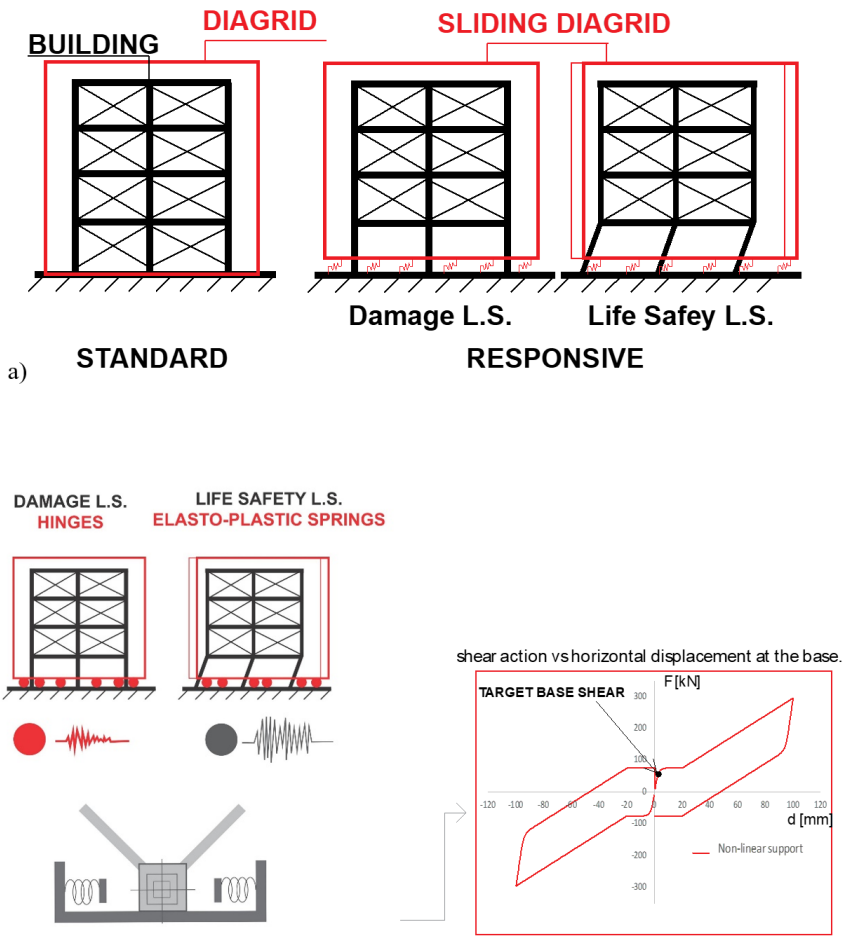

Figure 22:a) Sketch of the retrofitted building equipped with special sliding supports; b) hysteretic cycle of the innovative support, which is the sum of traditional elastoplastic support (*dashed line*) and a gap system (*dotted line*).

Chapter 3: Sensitivity analysis of the structural response of the retrofitted system

The interaction between the diagrid and existing building is here evaluated through parametric analyses using a simplified 2 Degrees of Freedom (2DOF) model. In particular, the objective of this section is to identify the parameters governing the structural response as well as the optimal retrofit parameters to avoid or control the damage to the existing building. It is worth noting that the results of this sensitivity analyses can be extended for the analysis of the response of any retrofit solution carried out from outside.

3.1 Simplified model of the retrofitted structure

The 2DOF model representative of the retrofitted system is reported in Figure 23, in which the existing building and the diagrid structural response are described by the degree of freedom u_1 and u_2, respectively.

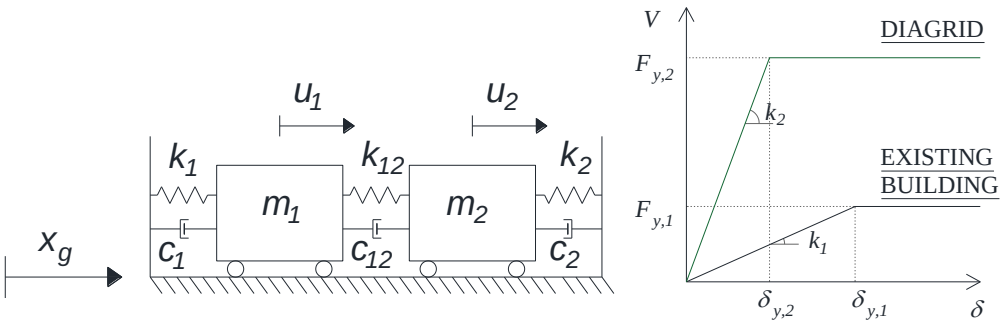

Figure 23: 2 degrees of freedom model. a) Simplified 2DOF system. u1 is the relative displacement of the existing building; u_2 is the relative displacement of the retrofitting exoskeleton; b) Response curve of the retrofitted structure with 2 degrees of freedom (2DOF) working in parallel.

The parameters needed to define the structural response of the existing building both in the elastic and plastic field are the fundamental period (T_1), the effective mass (m_1), the initial elastic stiffness (k_1), the damping coefficient (c_1), and the yielding force ($F_{y,1}$).

In general, these properties can be derived starting from the capacity curve of the existing building and through the usual procedure for the MDOF to SDOF conversion (Decanini, et al., 2001; Feroldi, 2014; Kuramoto, et al., 2000; Mehrabi & Shing, 2003).

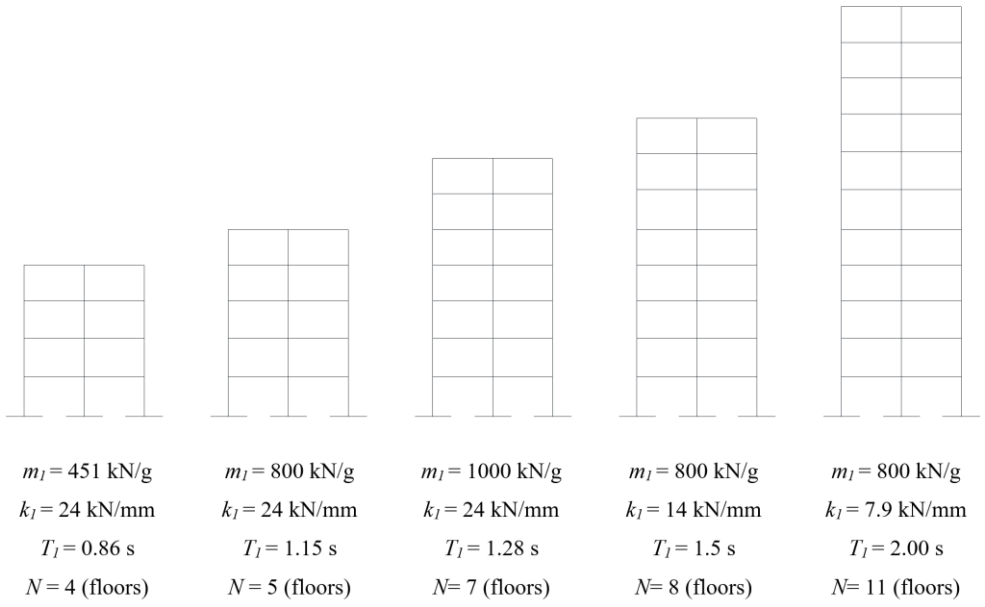

Figure 24: Reference geometry representative of ordinary Post World War RC buildings (Ref. Marini et al. (2014), Feroldi (2014)).

In this section, input parameters will be introduced to represent the ordinary post Second World War reinforced concrete buildings according to Marini et al. (2014). The elastic properties of the reference cases are summarized in Figure 24[1] with reference to typical post World War II (WWII) buildings featuring a different number of floors. As for the yielding force of the existing building, $F_{y,1}$ is defined as a percentage of the associated elastic seismic demand ($m_1 * S_a(T_1)$) through the parameter η (Equation 25). η represents the yielding strength of the existing building, adimensionalized with respect to the mass (m_1) multiplied by the ground acceleration $Sa(T_1)$. Different values of η are considered to represent weak (η=0.3), medium (η=0.5–0.6), and strong (η=0.85) buildings, respectively.

$$\eta = \frac{F_{y,1}}{[m_1 \cdot S_a(T_1)]} \qquad \textbf{Equation 25}$$

[1] The relation between the elastic period and the height of the existing building is introduced according to Verderame et al. (2007)

$$T_1 = 0.071 \cdot H^{0.96}$$

where H is the existing building height.

Given the elastic stiffness (k_1) and the yielding force ($F_{y,1}$), the yielding displacement ($\delta_{y,1}$) can be derived ($\delta_{y,1} = \frac{F_{y,1}}{k_1}$). Regarding the damping coefficient, a damping ratio (ζ) equal to 0.03 is considered.

For the DOF2, the elastic stiffness (k_2) is defined as a function of k_1. Feroldi (2014), demonstrated that the simplification of the whole system into a 2DOF is acceptable if the ratio between the elastic stiffness of the retrofitting exoskeleton (k_2) and the stiffness of the existing building (k_1) ranges between 0 and 12. The mass of the retrofit solution (m_2), is assumed in first approximation as equal to 1/10÷1/20 of the mass of the existing building (m_1) (Passoni, 2016). Also in this case, ζ is considered equal to 0.03.

As shown in Figure 23: 2 degrees of freedom model. a) Simplified 2DOF system. u1 is the relative displacement of the existing building; u_2 is the relative displacement of the retrofitting exoskeleton; b) Response curve of the retrofitted structure with 2 degrees of freedom (2DOF) working in parallel. the two masses are connected through a general link modelling the connection between the existing structure and the diagrid by the elastic stiffness (k_{12}), by the damping coefficient (c_{12}), and in the case of non-linear behavior, by the yielding displacement of the connections ($\delta_{y,12}$). The damping coefficient is supposed constant, while the other two parameters are investigated in this work.

As for the ground acceleration (X_g), 7 accelerograms compatible with the code spectrum were determined by adopting the software Rexel 2.2beta (Iervolino, et al., 2010). The structural system is supposed to be located in L'Aquila (Italy), on a flat surface made of deposit of sand or medium-dense sand gravel or stiff grave (soil category C and T1 topography) (NTC, 2018). A maximum scale factor equal to 2 and upper and lower tolerance equal to 10% and 15%, were imposed. It is worth noting that for the selected accelerograms the lower tolerance limit imposed by the Eurocode (EC8, CEN 2005) is not met. However, such a requirement is not always satisfied in the case of high seismicity areas; for this reason, a lower tolerance limit was obtained by increasing the Eurocode limit value (10%) by 5% until a compatible set was identified (Iervolino, et al., 2008) (Figure 25).

It is worth noting that the results of the sensitivity analysis will be normalized in order to remove the influence on the selected design spectra. Therefore, any values of the maximum ground acceleration could be adopted being the absolute value unnecessary considering the adimensionalization of the strength parameter η.

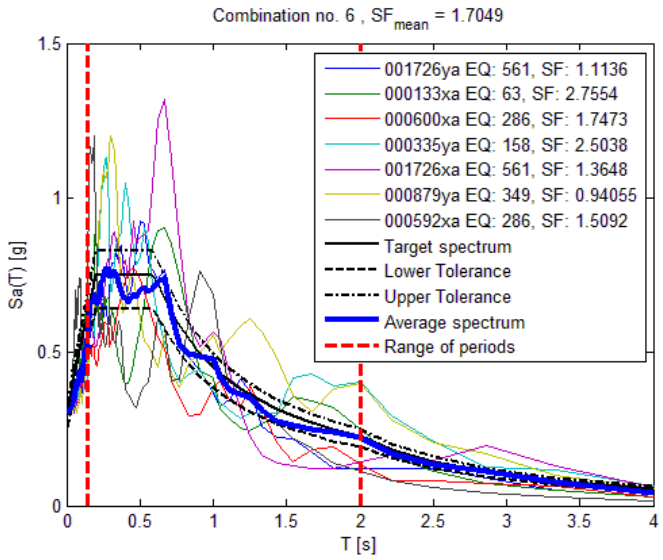

Figure 25: Selected combination of compatible accelerograms used for the time history analyses (Iervolino et al. 2010). All the 7 accelerograms are reported in Appendix 2.

The structural response is analyzed with reference to a set of parameters. The damage to the existing building is evaluated through the parameter μ that represents the "ductility demand" to the existing building after the retrofit. μ is defined as the ratio between the maximum displacement (δ_{MAX}) experienced by the DOF 1 during a seismic event (X_g) and the yielding displacement ($\delta_{y,1}$) of the DOF 1 (Figure 26b).

Equation 26

$$\mu = \frac{\delta_{MAX}}{\delta_{y,1}}$$

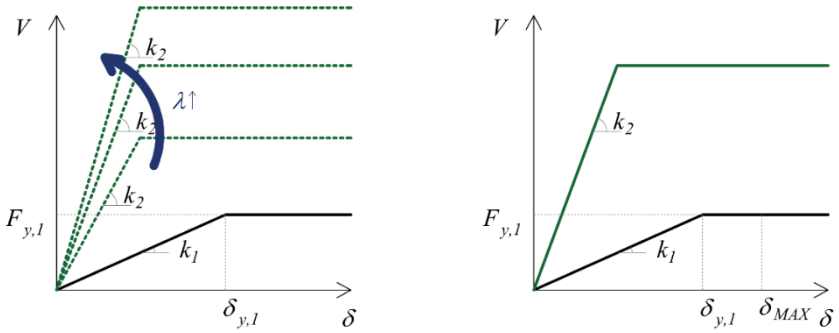

Figure 26: Representation of the parameter λ and μ on the response curve of the retrofitted structure with 2 degrees of freedom (2DOF) working in parallel.

Other fundamental parameters to derive the optimal retrofit solution are the stiffness parameters named λ and λ_{12}. λ represents the ratio between the elastic stiffness of the retrofit

(k_2) and the stiffness of the existing building (k_1) (Figure 26a), while, λ_{12} is the ratio between the elastic stiffness of the connection (k_{12}) and that of the existing building (k_1).

$$\text{a) } \lambda = \frac{k_2}{k_1}$$

$$\text{b) } \lambda_{12} = \frac{k_{12}}{k_1}$$

Equation 27

In the case of non-linear connection, the yielding displacement ratio β is introduced as the ratio between the connection yielding displacement ($\delta_{y,12}$) and the yielding displacement of the existing building ($\delta_{y,1}$).

$$\beta = \frac{\delta_{y,12}}{\delta_{y,1}}$$

Equation 28

Through the parameters μ, β, λ, λ_{12} one can determine the optimal properties for the effective design of the retrofit solution.

Finally, the output parameters will be evaluated considering three damage states of the existing building expressed as a function of the inter-story ratio (θ): DS1 (θ=0.2%÷0.4%) no damage or minor cracking in the non-structural components; DS2 (θ=0.4%÷0.6%) moderate cracking in the non-structural components; DS3 (θ=0.6%÷0.8%) severe cracking in the non-structural components and moderate-severe damage in the structural members (Figure 27).

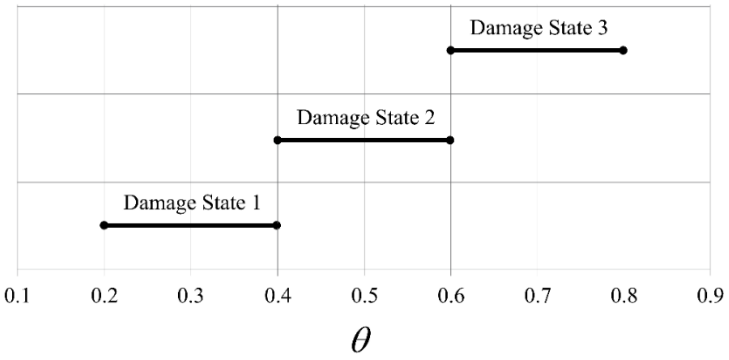

Figure 27: Damage states of the existing building. DS1: minor cracking; DS2: moderate cracking; DS3: Severe cracking.

In this section, θ=0.30%, θ=0.50% and θ=0.75% are adopted as reference values for the three damage states.

3.2 Equations of motion

The free-body model of the 2DOF system is represented in Figure 28. By enforcing balance to horizontal translation to DOF 1 and 2, it yields:

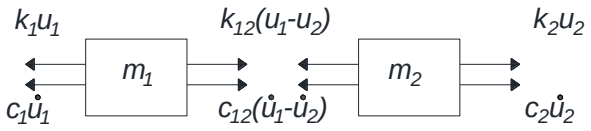

Figure 28: Free-body diagrams of the 2DOF system.

$$\begin{cases} \sum \vec{F}^{m_1} = 0 \\ m_1(\ddot{x}_G + \ddot{u}_1) + k_1 u_1 + c_1 \dot{u}_1 = k_{12}(u_2 - u_1) + c_{12}(\dot{u}_2 - \dot{u}_1) \\ \sum \vec{F}^{m_2} = 0 \\ m_2(\ddot{x}_G + \ddot{u}_2) + k_2 u_2 + c_2 \dot{u}_2 + k_{12}(u_2 - u_1) + c_{12}(\dot{u}_2 - \dot{u}_1) = 0 \end{cases} \qquad \textbf{Equation 29}$$

From which the equations of motion of the 2DOF can be derived:

$$\begin{cases} m_1(\ddot{x}_G + \ddot{u}_1) + k_1 u_1 + c_1 \dot{u}_1 = k_{12}(u_2 - u_1) + c_{12}(\dot{u}_2 - \dot{u}_1) \\ m_2(\ddot{x}_G + \ddot{u}_2) + k_2 u_2 + c_2 \dot{u}_2 + k_{12}(u_2 - u_1) + c_{12}(\dot{u}_2 - \dot{u}_1) = 0 \end{cases} \qquad \textbf{Equation 30}$$

In matrix form, the equations can be re-written as:

$$\begin{bmatrix} m_1 & 0 \\ 0 & m_2 \end{bmatrix} \begin{Bmatrix} \ddot{u}_1 \\ \ddot{u}_2 \end{Bmatrix} + \begin{bmatrix} c_1 + c_{12} & -c_{12} \\ -c_{12} & c_2 + c_{12} \end{bmatrix} \begin{Bmatrix} \dot{u}_1 \\ \dot{u}_2 \end{Bmatrix} + \begin{bmatrix} k_1 + k_{12} & -k_{12} \\ -k_{12} & k_2 + k_{12} \end{bmatrix} \begin{Bmatrix} u_1 \\ u_2 \end{Bmatrix} = \ddot{X}_g \begin{Bmatrix} m_1 \\ m_2 \end{Bmatrix} \qquad \textbf{Eq. 31}$$

and in a compact form:

$$\underline{M}\{\ddot{u}\} + \underline{C}\{\dot{u}\} + \underline{K}\{u\} = \{F\} \qquad \textbf{Equation 32}$$

in which, $\underline{M}$ is the mass matrix, $\underline{K}$ the stiffness matrix, $\underline{C}$ the damping matrix, and the vector $\{F\} = \{M\} \cdot \ddot{X}_g$ represents the seismic action on the simplified system.

When the connections are assumed non-linear, the inelastic behavior is described by the Bouc-Wen hysteresis law (Wen, 1976) (Figure 29: Hysteretic behavior of the connections according to Bouc-Wen law.). More precisely, the non-linear behavior of the connections is accounted for by substituting $k_{12}(u_2 - u_1)$ in Equation 30 with *P(t)* reported below:

$$P(t) = \alpha \cdot k_1 \cdot u_1 + (1-\alpha) \cdot k_1 \cdot \delta_{y,12} \cdot Z(t) \qquad \textbf{Equation 33}$$

where α is the post yielding stiffness ratio, and Z is an internal variable whose behavior is described by its derivative:

$$\frac{dZ}{dt} = \left(\frac{1}{\delta_{y,12}}\right) \cdot \left(\dot{u}_1 - \gamma \cdot \left|\dot{u}_1\right| \cdot Z(t) \cdot \left|z(t)\right|^{n-1} - \nu \cdot \dot{u}_1 \cdot \left|z(t)\right|^n\right) \qquad \textbf{Equation 34}$$

n, ν, and γ are dimensionless quantities; n governs the smoothness of the curve in the proximity of the yielding point, ν and γ control the size and the shape of the hysteretic loop ($|\nu|+|\gamma|=1$). Examples of hysteretic plots according to the Bouc–Wen hysteresis law are represented in Figure 29: Hysteretic behavior of the connections according to Bouc-Wen law.

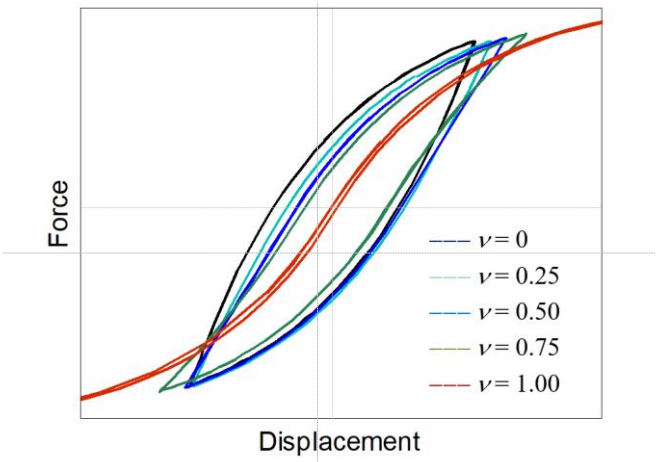

Figure 29: Hysteretic behavior of the connections according to Bouc-Wen law.

In this work, the equations of motion (Equation 30) are solved with the function Ode45 (The MathWorks, 2017). Ode45 is a versatile ordinary differential equation solver, and it adopts the Runge–Kutta method with variable time steps. The algorithm requires the conversion of the second-order differential equations into an equivalent system of first-order equations.

3.3 Elastic retrofit solution: simplification to a SDOF system and parametric analyses

In order to better understand the behavior of the whole elastic system, the in-frequency response of the two connected masses is investigated by using transfer functions[2].

In general, a transfer function is a mathematical function that gives the system outputs for every possible value of the input; it provides information which specifies the behavior of the component in a system. In the case of MDOF system, the transfer functions can be compacted into a transfer matrix $\underline{T}$ in which each component of the Transfer Matrix ($T(i,j)$) provides information about the response of the system at the i-DOF due to a unit force at the j-DOF. In order to evaluate the frequency response of the DOF1 the transfer functions of the 2DOF system represented in Figure 28 are developed.

Starting from the equations of motion (Equation 30), the transfer matrix ($\underline{T}(\omega)$) of the system described in Figure 28, is derived. The solution of the equations of motion, Equation 30, can be expressed as:

$$\begin{cases} \underline{u} = \underline{X} \cdot e^{i\omega\ t} \\ \dot{\underline{u}} = i\omega\, t \cdot \underline{X} \cdot e^{i\omega\ t} \\ \ddot{\underline{u}} = -\omega^2 \cdot \underline{X} \cdot e^{i\omega\ t} \end{cases} \qquad \textbf{Equation 35}$$

By substituting Equation 35 in Equation 32, it yields:

$$[-\omega^2 \underline{M} + i\omega\, \underline{C} + \underline{K}] \cdot \underline{X} \cdot e^{i\omega\ t} = \underline{F} \cdot e^{i\omega\ t} \qquad \textbf{Equation 36}$$

By defining the Impedance Matrix $Z(\omega)$ as:

$$\underline{Z}(\omega) = [-\omega^2 \underline{M} + i\omega\, \underline{C} + \underline{K}] \qquad \textbf{Equation 37}$$

and, combining Equation 37 and Equation 36, it yields:

[2] The term transfer function is also used in the frequency domain analysis of system using methods such as Laplace transform (where it means the amplitude of the output as a function of the frequency of the signal applied to the input) or, in the case of optical imaging devices, the Fourier Transform of the point spread function (spatial frequency). Moreover, transfer functions are widely used to solve vibrational problems such as, for example, to determine the features of additional masses introduced to minimize the vibration of the main mass of the system.

$$\underline{\underline{Z}}(\omega)\cdot \underline{X} = \underline{F} \qquad \textbf{Equation 38}$$

The transfer matrix is the inverse of the impedance matrix $\underline{\underline{Z}}(\omega)^{-1} = \underline{\underline{T}}(\omega)$,

$$Z^{-1} = \frac{\begin{bmatrix} Z_{22} & Z_{12} \\ Z_{21} & Z_{11} \end{bmatrix}}{\det|\underline{\underline{Z}}|} = \begin{bmatrix} t_{11} & t_{12} \\ t_{21} & t_{22} \end{bmatrix} \qquad \textbf{Equation 39}$$

where,

$$\det|\underline{\underline{Z}}| = Z_{11}Z_{22} - {Z_{12}}^2$$

The solution can be expressed as:

$$\begin{Bmatrix} x_1 \\ x_2 \end{Bmatrix} = \begin{bmatrix} t_{11} & t_{12} \\ t_{21} & t_{22} \end{bmatrix} \begin{Bmatrix} F_1 \\ F_2 \end{Bmatrix} \qquad \textbf{Equation 40}$$

or in the compact form:

$$\underline{X} = [\underline{\underline{Z}}(\omega)]^{-1}\underline{F} = \underline{\underline{T}}(\omega)\cdot\underline{F} \qquad \textbf{Equation 41}$$

where $\underline{\underline{T}}(\omega)$ is the transfer matrix and represents the behavior of the masses per unit input force as a function of the frequency.

By applying the described procedure to the reference system (Figure 23), one can evaluate the in-frequency response of the system when subjected to a harmonic load. The equations *T(i,j)* of the transfer functions that compose the transfer matrix $\underline{\underline{T}}(\omega)$ of the 2 DOF system are:

$$T(1,1) = \frac{k_2 + k_{12} + i\cdot(c_2 + c_{12})\cdot\omega - m_2\cdot\omega^2}{-(-k_{12} - i\cdot c_{12}\cdot\omega)^2 + (k_1 + k_{12} + i\cdot(c_1 + c_{12})\cdot\omega - m_1\omega^2)\cdot(k_2 + k_{12} + i\cdot(c_2 + c_{12})\cdot\omega - m_2\omega^2)} \qquad \textbf{Eq. 42}$$

$$T(1,2) = \frac{k_{12} + i\cdot c_{12}\cdot\omega}{-(-k_{12} - i\cdot c_{12}\cdot\omega)^2 + (k_1 + k_{12} + i\cdot(c_1 + c_{12})\cdot\omega - m_1\omega^2)\cdot(k_2 + k_{12} + i\cdot(c_2 + c_{12})\cdot\omega - m_2\omega^2)} \qquad \textbf{Eq. 43}$$

$$T(2,1) = \frac{k_{12} + i\cdot c_{12}\cdot\omega}{-(-k_{12} - i\cdot c_{12}\cdot\omega)^2 + (k_1 + k_{12} + i\cdot(c_1 + c_{12})\cdot\omega - m_1\omega^2)\cdot(k_2 + k_{12} + i\cdot(c_2 + c_{12})\cdot\omega - m_2\omega^2)} \qquad \textbf{Eq. 44}$$

$$T(2,2) = \frac{k_1 + k_{12} + i\cdot(c_1 + c_{12})\cdot\omega - m_1\cdot\omega^2}{-(-k_{12} - i\cdot c_{12}\cdot\omega)^2 + (k_1 + k_{12} + i\cdot(c_1 + c_{12})\cdot\omega - m_1\omega^2)\cdot(k_2 + k_{12} + i\cdot(c_2 + c_{12})\cdot\omega - m_2\omega^2)} \qquad \textbf{Eq. 45}$$

In this particular application, among all the transfer functions (*T(i,j)*) of the transfer matrix $\underline{T}(\omega)$, the component *T(1,1)* is the most significant to analyze, considering that it represents the response of the DOF1 due to a unit force in the DOF1.

Moreover, to better understand the behavior of the coupled system, a parametric evaluation of the transfer function *T(1,1)* is made. Figure 30 and Figure 31 represent the steady-state vibration amplitudes for the 2DOF system by varying the mass (m_2) and the stiffness (k_2) of the DOF2. More precisely, considering as reference values: m_1=800 kN/g and k_1=k_{12}=24 kN/mm, the properties of the second mass are varied within the following ranges of interest: m_2= [1/20, 1/8, 1/4, 1/2, 1]m_1, and k_2=[10, 8, 4, 2, 1]k_1, where: m_2=1/20m_1 and k_2=10k_1 are reasonable values of mass and stiffness of the retrofit system (Passoni, 2016), while m_2=m_1 and k_2=k_1 are introduced to emphasize the effect of the DOF2 on the response of the DOF1. It is important to note that: (a) the damping coefficients are assumed as constant, (b) negative amplitudes corresponding to some masses have been ignored, (c) as expected when the forcing frequency is close to one of the natural frequencies of the system, a resonance phenomenon occurs, (d) for comparable values of mass and stiffness of the 2 DOF, in the point of antiresonance, the amplitude of the vibration is equal to zero. This concept has been widely used in engineering applications to minimize the amplitude of oscillators when subjected to particular frequencies. In Figure 30 the stiffness k_2 is supposed equal to k_1; m_2, instead, decreases from m_1 to 0.05m_1.

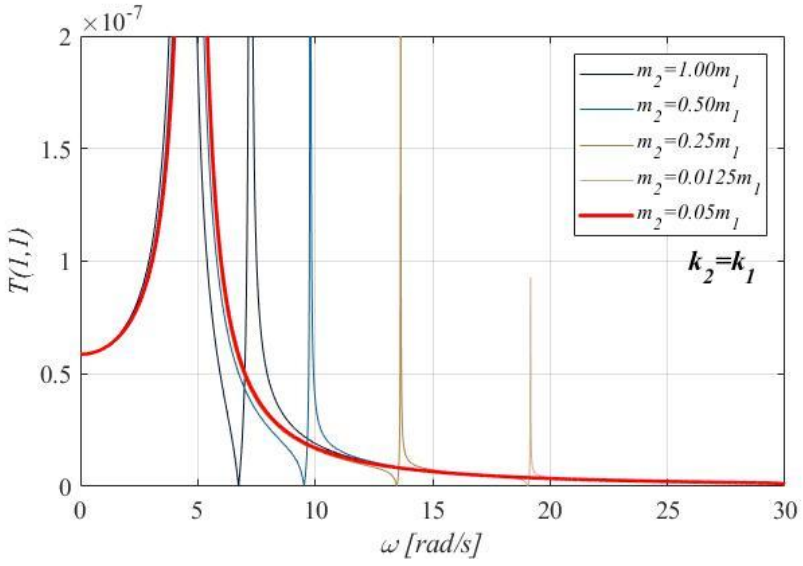

Figure 30: In-frequency response of the 2DOF system for k_2=k_1, for varying the mass (m_2) of the retrofit system.

In Figure 31, m_2 is assumed to be equal to m_1, while the stiffness of the DOF2 increases from k_1 to $10k_1$.

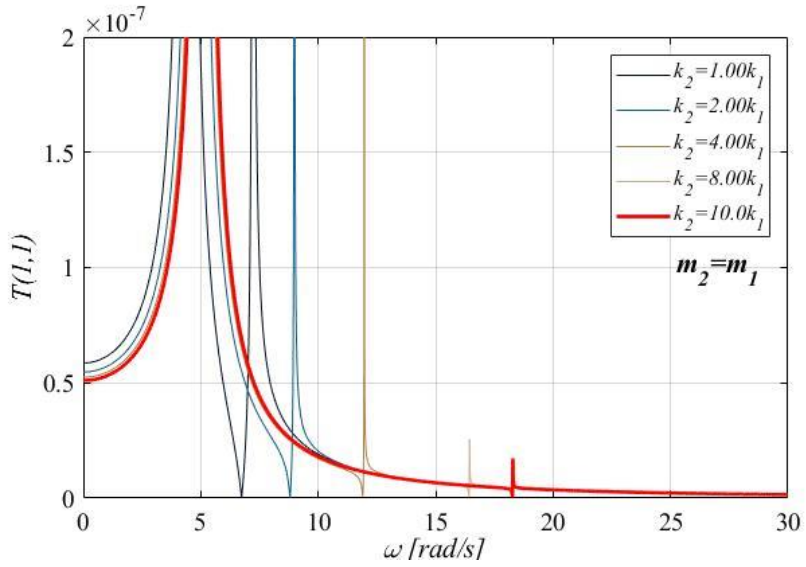

Figure 31: In-frequency response of the 2DOF system for $m_2=m_1$, for varying the retrofit stiffness k_2.

Some relevant conclusions can be drawn from these results: in a damped system, in which k_2 is significantly higher than k_1, and the mass ratio m_2/m_1 is lower than 1/10, the amplitude of the lowest resonance frequency is generally much greater than the higher frequency modes. For this reason, in these cases, it is often sufficient to consider only the lowest frequency mode in the design calculations.

Accordingly, in the application of elastic diagrid structures to retrofit existing buildings in which the mass of the diagrid can be considered negligible, while the stiffness is significantly higher than that of the existing building, the system can be idealized as just a Single DOF system (SDOF). It is worth noting that, to apply this simplification, the hypothesis of equal displacement of the 2 DOF becomes essential. Consequently, this simplification is considered acceptable only when elastic connections are considered; in the case of non-linear connections, other considerations have to be made.

The simplified model is reported in Figure 32a, in which the total mass $m=m_1+m_2$ is considered[3].

[3] Because of m_2 can be considered negligible, in many cases m can be considered equal to m_1.

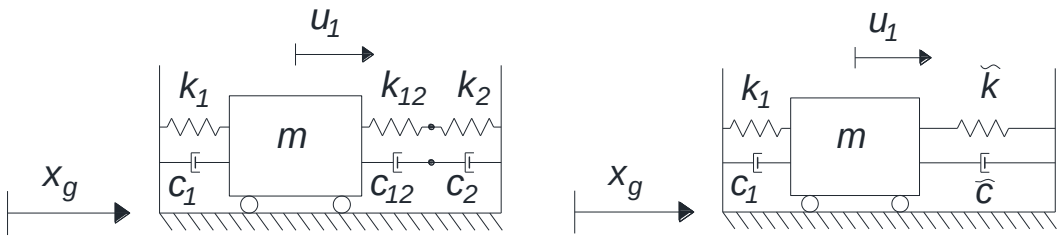

Figure 32: a) Simplified SDOF system; b) Simplified SDOF system with equivalent spring and damping.

In Figure 32b, the equivalent stiffness and damping of the retrofit solution are introduced, where:

$$\tilde{k} = \frac{k_2 k_{12}}{k_2 + k_{12}}$$

and, **Equation 46**

$$\tilde{c} = \frac{c_2 c_{12}}{c_2 + c_{12}}$$

The system can also be represented as shown in Figure 33, where, the total stiffness of the SDOF ($\hat{k}$) can be expressed as

$$\hat{k} = \tilde{k} + k_1$$ **Equation 47**

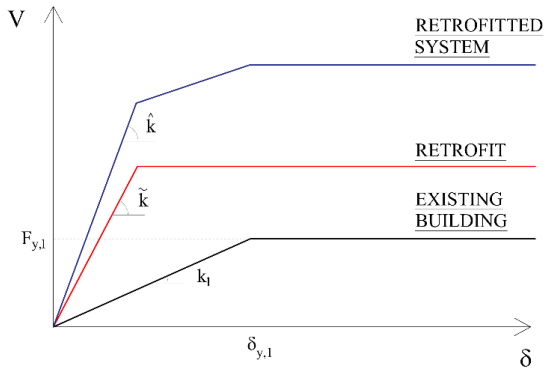

Figure 33: Response curve of the retrofitted structure with 2 degrees of freedom (2DOF) working in parallel.

It is worth noting that when considering the equivalent system in Figure 32b, the response parameters λ , and λ_{12} (Equation 27) must be re-defined as follows:

$$\tilde{\lambda} = \frac{\tilde{k}}{k_1} \qquad \textbf{Equation 48}$$

where $\tilde{\lambda}$ represents the ratio between the equivalent elastic stiffnesses of the retrofit ($\tilde{k}$) and the elastic stiffness of existing building (k_1).

3.3.1 Parametric analyses on the Elastic SDOF system

Sensitivity analyses for the evaluation of the retrofit properties were conducted. Given a target maximum displacement for the existing building (DOF1), the procedure for the determination of the elastic parameters of the retrofit is developed in two steps: considering the system in Figure 32b, the minimum equivalent stiffness ($\tilde{k}$) that satisfy the target is initially derived; then, the elastic properties of both, the connections and the DOF2 are separately investigated considering the system in Figure 32a.

The considered parameters and the range in which they are varied are summarized in Table 1. As far DOF1, the parameters of the reference cases described in Figure 24 are considered, while the equivalent stiffness of the retrofit $\tilde{k}$ is varied in the interval $0 \div 6k_1$, in which $\tilde{k}=0$ represents the As-Is condition (ante retrofit $\tilde{\lambda}=0$), and $\tilde{k}=6k_1$ is a reasonable value of equivalent retrofit stiffness (Feroldi, 2014).

DOF 1	**Symbol**	**Range**	**Unit**
Elastic Period	T_1	0.5-2.5	[s]
Effective mass	m_1	451-800-1000	[kN/g]
Elastic stiffness	k_1	7.5-13-24	[kN/mm]
Adim. yielding force	η	0.30-0.50-0.60-0.85	[-]
Retrofit			
Equivalent elastic stiffness	$\tilde{k}$	0-6	k_1
Target			
Inter-story drift target	θ	0.3-0.5-0.75	[%]

Table 1: Inputs used in the parametric evaluation of the elastic SDOF system.

- Minimum stiffness $\tilde{k}$:

By varying the adimensionalized yielding force of the DOF1 (η), the parametric curves in Figure 34 plot the required ductility (μ), as a function of the stiffness ratio ($\tilde{\lambda}$).

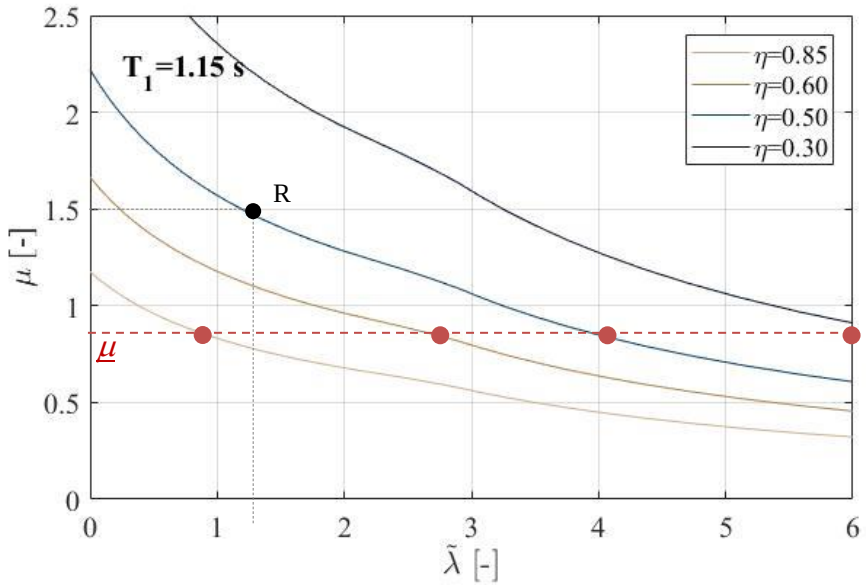

Figure 34: Evaluation of the ductility demand (μ) as a function of the retrofit stiffness ratio ($\tilde{\lambda}$) for varying adimensionalized yielding force of the existing building (η). R refers to the reference case in section 4.1.1.2. Red dotted line: the constant value of the ductility demand (μ).

As expected, the maximum damage on the DOF1, i.e. the maximum values of the demand parameter (μ), is obtained in the case of the existing building in the As-Is condition; for a fixed value of T_1, the ductility required in the existing structure decreases as the stiffness ratio increases, and the damage increases for a low value of η. This is reasonable considering that for weak building and low stiffness of the retrofit the ductility demand on the existing building will be higher. Also, the slopes of the curves show that for a given $\underline{\mu}$, the lower the strength of the existing building, the higher the required $\tilde{\lambda}$. In the following, to generalize the results, the plots of the parametric analyses for different periods of the existing building (T_1) are reported.

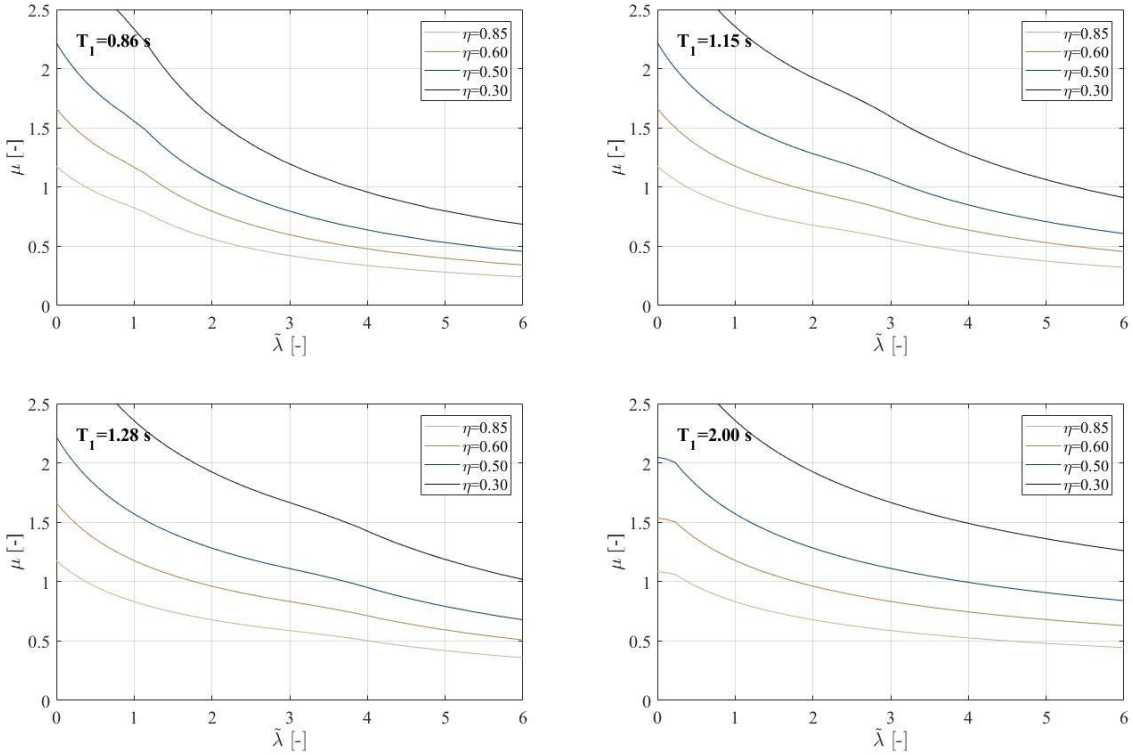

Figure 35: Evaluation of the ductility demand (μ) as a function of the retrofit stiffness ratio ($\tilde{\lambda}$) for varying adimensionalized yielding force of the existing building (η) and existing building fundamental period (T_1).

For a fixed value of the ductility demand parameter (μ), the higher the elastic period of the existing building (T_1), the higher the minimum required equivalent stiffness ($\tilde{k}$). These results can be reasonable considering that, higher values of T_1 correspond to lower values of k_1 which means, for a set target displacement of the DOF1, higher values of the minimum required equivalent stiffness ($\tilde{k}$). Furthermore, as expected, weaker buildings require a stiffer retrofit solution than the stronger ones.

In Figure 36, the ductility (μ) is expressed as a function of the existing building fundamental period (T_1) for varying the equivalent retrofit stiffness ($\tilde{k}$).

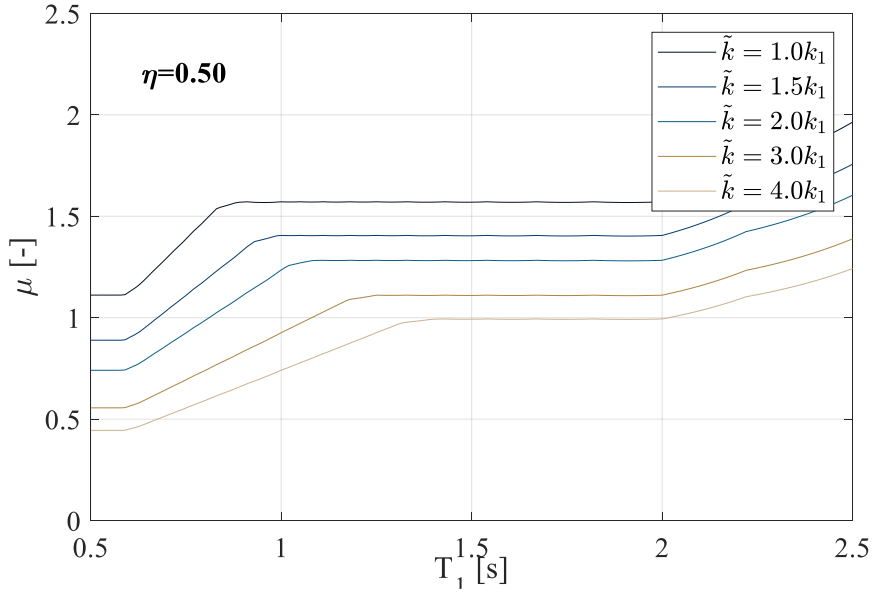

Figure 36: Evaluation of the ductility demand (μ) as a function of the existing building fundamental period (T_1) for varying the equivalent stiffness of the retrofit ($\tilde{k}$).

This plot could be used to derive the minimum equivalent stiffness of the retrofit ($\tilde{k}$) for a particular value of the ductility demand (μ) as a function of the period (T_1) and for a given value of the adimensionalized yielding force (η) of the existing building. Different values of η are considered in the following.

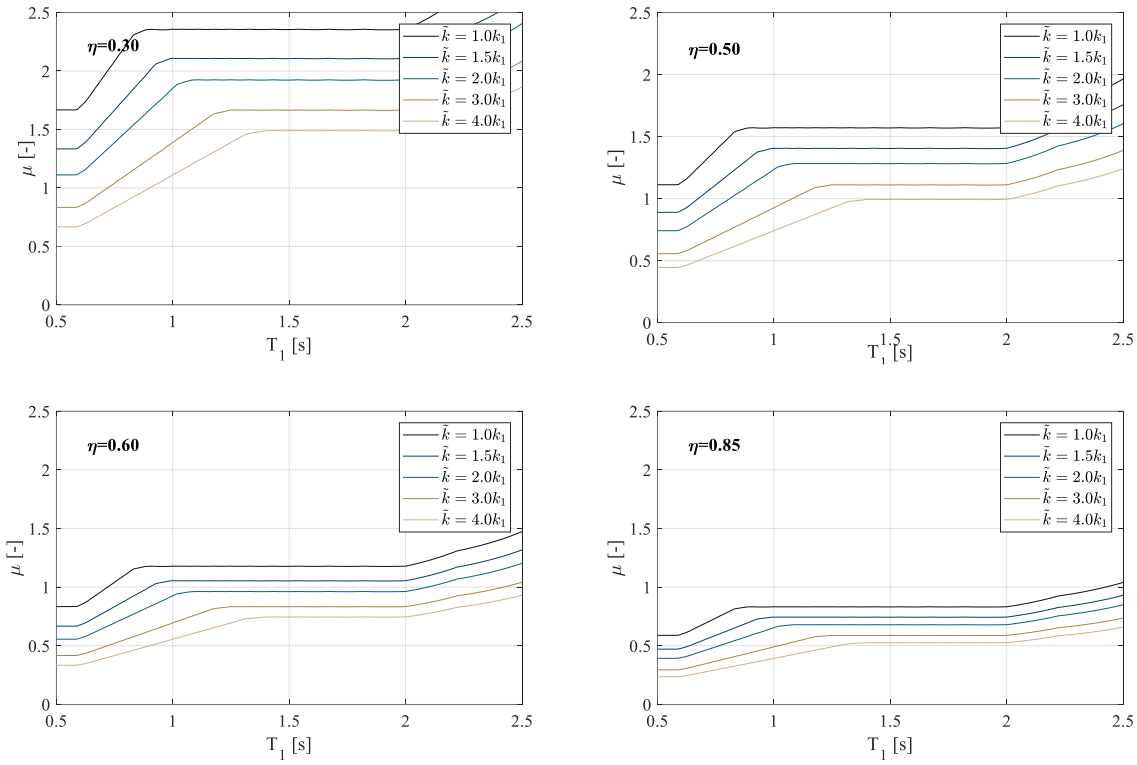

Figure 37: Evaluation of the ductility demand (μ) as a function of the existing building period (T_1) for varying retrofit stiffness ($\tilde{k}$) and adimensionalized yielding forces (η).

For a selected value of the ductility demand parameter (μ), the required equivalent stiffness ($\tilde{k}$) decreases for increasing the value of the adimensionalized yielding force (η). Moreover, for a selected value of fundamental period (T_1) and adimensionalized yielding force (η), the ductility demand (μ) decreases for increasing the equivalent stiffness of the retrofit solution ($\tilde{k}$).

- DOF2 and elastic connection properties (system in Figure 32a):

Once the equivalent stiffness of the retrofit solution ($\tilde{k}$) is defined, the elastic properties of connections and the DOF2 can be derived.

For a given $\tilde{k}$, considering the Equation 46a, one can derive the infinite pairs of (k_{12} ; k_2) that satisfy that Equation; a parametric study was conducted.

In Figure 38, the infinite pairs of (k_{12} ; k_2) are evaluated by varying the inter-story drift target (θ). In this case, among the ordinary RC building features presented in Figure 24, the 5-story reference case with m_1=800 kN/g, k_1=24 kN/mm, and an inter-story height equal to 3.15 [m] is considered.

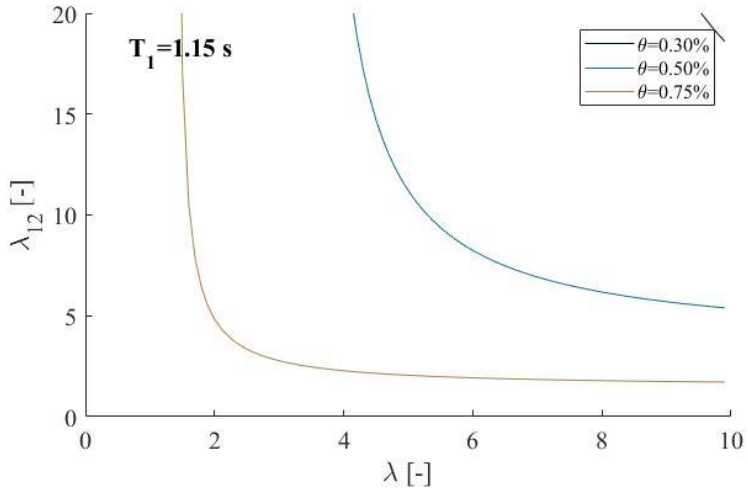

Figure 38: Evaluation of the series of pairs (k_{12}-k_2) obtained by varying the inter-story drift target of the existing building (θ).

By decreasing λ (i.e. decreasing k_2), the stiffness ratio of the connection (λ_{12}) increases exponentially and, as expected, by increasing the inter-story drift target (θ), both stiffness ratios decrease.

In Figure 39, the results are extended to the reference cases (Figure 24); however, the following results cannot be generalized for every building characterized by the same fundamental period (T_1), and subjected to every seismic event (X_g), being the curves obtained for specific values of $\tilde{k}$.

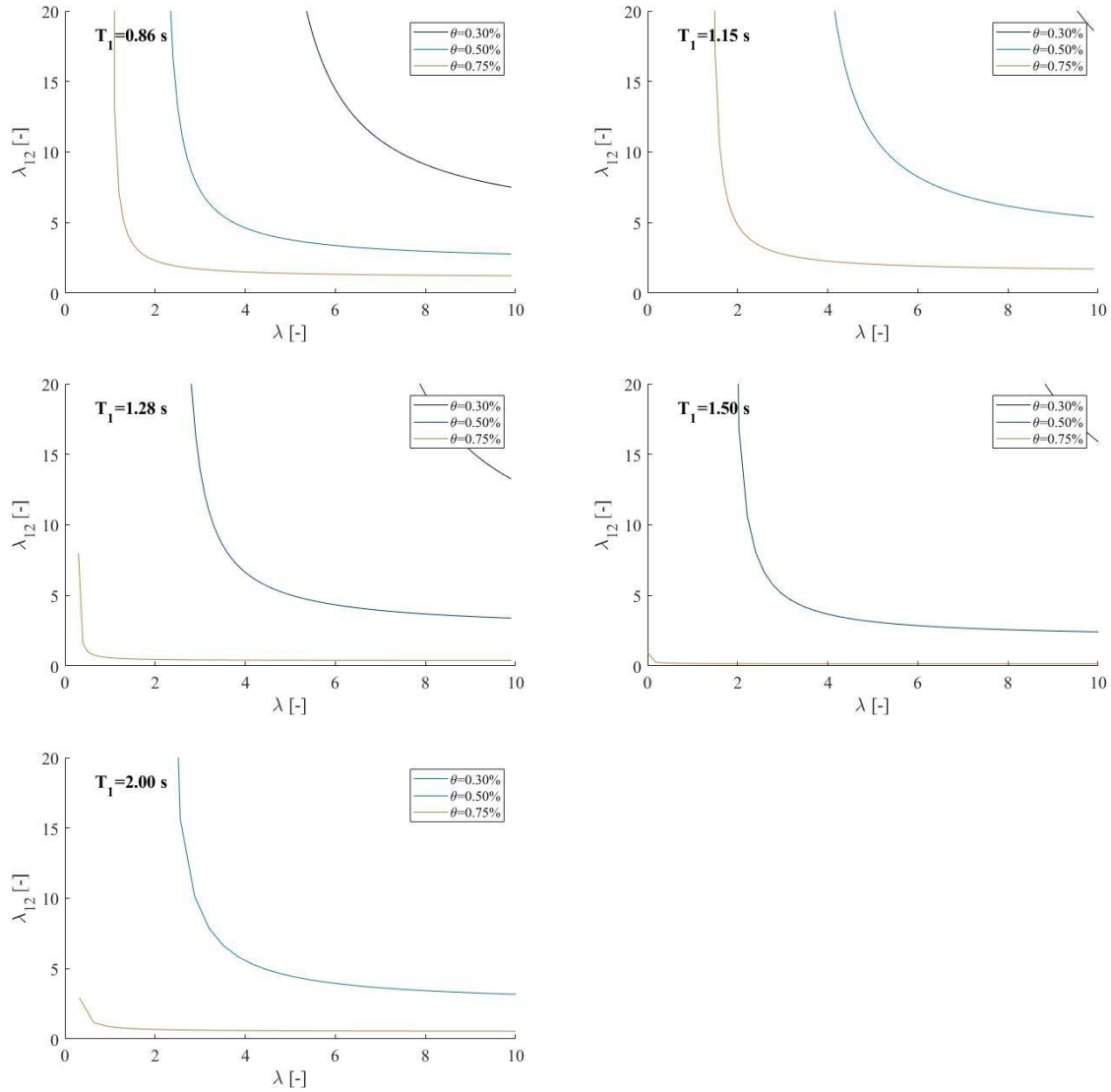

Figure 39: Parametric evaluation of the pairs of (k_{12}-k_2) for the reference existing buildings described in Figure 24 by varying the inter-story drift target (θ).

Comparing the results in Figure 39, it can be observed that, by increasing the natural period of the existing building (T_1), both the stiffness ratio of the connections and the stiffness ratio of the retrofit increase.

For acceptable values of the inter-story drift target (θ), there are infinite pairs of $(k_{12}; k_2)$ that satisfy the imposed target; however, the optimal combination of $(k_{12}; k_2)$ must be selected also addressing the technological limits of both connections and diagrid exoskeleton.

It is important to note that the connections play a fundamental role in the definition of the stiffness of the retrofit solution. Considering only the stiffness of the diagrid in the design of the structure may lead to significant underestimation of the retrofit stiffness, thus resulting in excessive and unacceptable damage to the existing structure in case of an earthquake. Only in

the theoretical case of $k_{12} \to \infty$ the equivalent stiffness can be considered as equal to the stiffness of the exoskeleton.

3.4 Non-Linear retrofit solution: Sensitivity analyses

In this section, a non-linear connection (k_{12}) between the two masses in the 2DOF system is introduced and parametric analyses are developed to identify the optimal properties of the connection. In the case of non-linear connection between DOF1 and the DOF2, the equal displacement hypothesis between the two degrees of freedom cannot be introduced and the structural system reported in Figure 23 must be considered.

As far as the existing building (DOF1) is concerned, the parameters described in the elastic analysis are considered.

Regarding the retrofit (DOF2), based on the results of recent studies focused on the design of retrofit structures for RC buildings (Feroldi, 2014; Passoni, 2016), the mass of the diagrid (DOF2) is varied in the range m_2=1/10÷1/20 m_1. The elastic stiffness of the diagrid (k_2), according to the procedure described in Section 3.2.2, varies within the range k_2 = [0÷12] k_1, in which k_2 =0 represents the As-Is condition, while k_2 =12 k_1 is an acceptable value for the stiffness of strengthening exoskeleton for RC building (Passoni, et al., 2018).

The elastic stiffness of the connections (k_{12}), instead, varies within the range k_{12} = [0÷24] k_1 in which $k_{12} = 0$ represents the As-Is condition (or no connection), while k_{12} =24 k_1 is selected based on the consideration drawn in Section 3.2.2 as well as to account for the technological limits of the connection. The non-linearity of the connections is described by the Bouc-Wen Model, (Equation 33, Equation 34), considering n=1, ν=γ=0.5, and α=0.001.

Sensitivity analyses are carried out to identify the optimal yielding displacement of the connection ($\delta_{y,12}$); $\delta_{y,12}$ is evaluated in the range $\delta_{y,12}$ = [0÷0.1] [m] in which $\delta_{y,12}$ =0 represents the As-Is condition, while $\delta_{y,12}$ =0.1 [m] is assumed to represent the elastic behavior of the connection[4]. In the sensitivity analysis the optimal $\delta_{y,12}$ is derived by evaluating the ductility demand (μ) as a function of the yielding displacement ratio (β). The considered parameters and their range of variation are summarized in Table 2.

[4] It means that, to have the connection yielding, a relative displacement higher than 10 cm between the diagrid and the existing building must occur; this relative displacement, for the considered cases, is very rare.

DOF 1	**Symbol**	**Range**	**Unit**
Elastic Period	T_1	0.5-2.5	[s]
Effective mass	m_1	451-800-1000	[kN/g]
Elastic stiffness	k_1	7.5-13-24	[kN/mm]
Adim. yielding force	η	0.30-0.50-0.60-0.85	[-]
DOF 2			
Elastic stiffness	k_2	0-12	k_1
Effective mass	m_2	1/10-1/20	m_1
Connections			
Elastic stiffness	k_{12}	0-24	k_1
Yielding displacement	$\delta_{y,12}$	0-0.1	[m]
Target			
Inter-story drift target	θ	0.3-0.5-0.75	[%]

Table 2: Input parameters and setting values adopted in the sensitivity evaluation of the non-linear 2 SDOF system.

The sensitivity analysis is carried out taking as reference the following parameters: m_1=800 [kN/g], k_1=24 [kN/mm], θ=0.5%. Moreover, to investigate the influence of the existing building features on the system response, the analysis is performed by changing one parameter of the DOF1 at a time.

- **Case 1. Varying the effective mass (m_1) of the DOF1**: the optimal yielding displacement of the connection ($\delta_{y,12}$) is investigated by evaluating the ductility demand (μ) as a function of the yielding displacement ratio (β) for varying the mass of the DOF1 (m_1). The influence of the parameter m_1 on the system response is then evaluated.
  In Figure 40 the ductility demand (μ) is plotted as a function of β for varying the mass of the DOF1 (m_1) and for fixed values of k_1, η and θ.

DOF 1	**Symbol**	**Range/Value**	**Unit**
Effective mass	m_1	451-800-1000	[kN/g]
Elastic stiffness	k_1	24	[kN/mm]
Adim. yielding force	η	0.85	[-]
Target displacement			
Inter-story drift target	θ	0.5	[%]

Table 3: Inputs of the non-linear 2 SDOF system used in case 1.

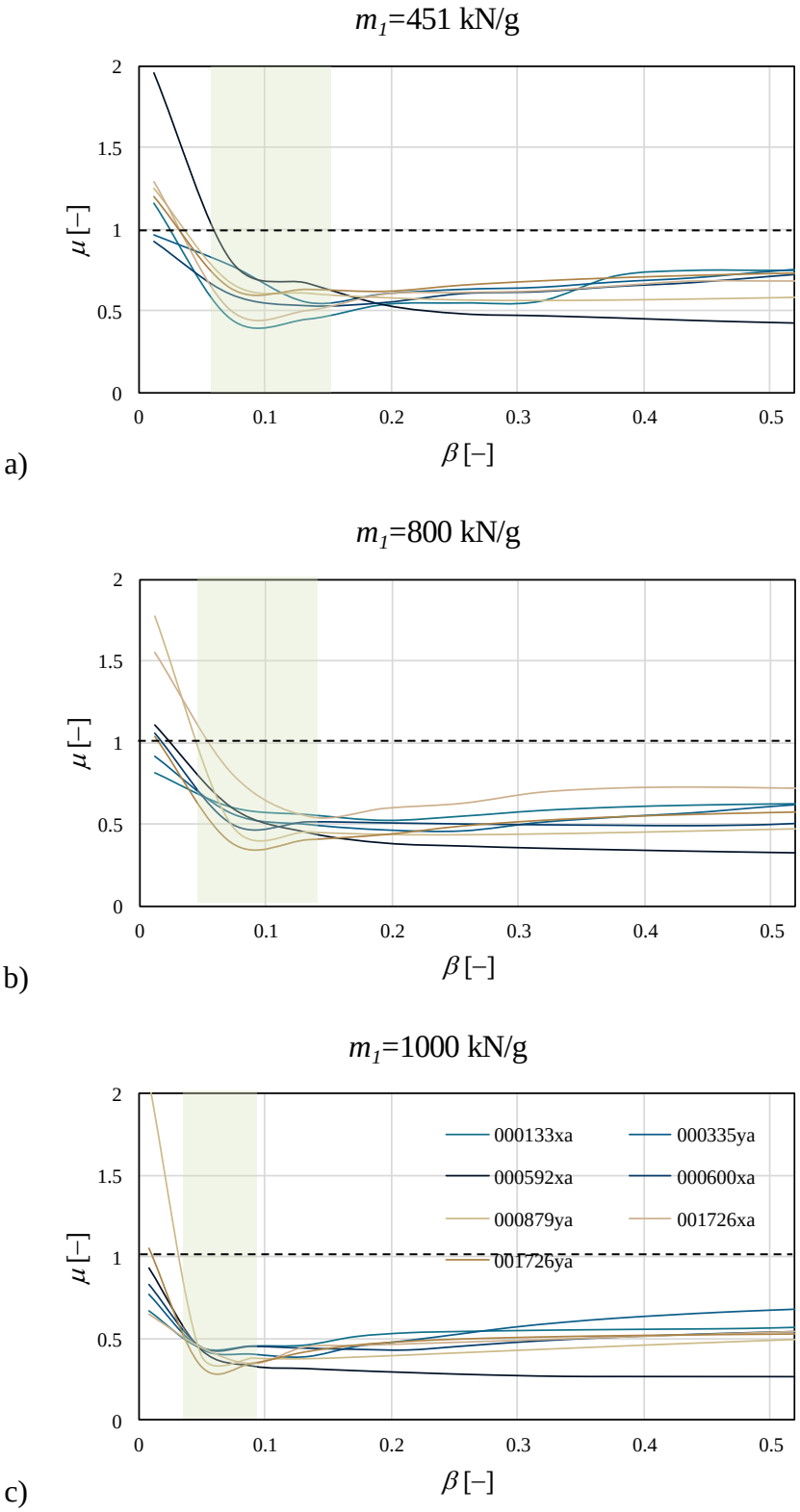

Figure 40: Ductility demand (μ) on the existing building (DOF1) as a function of yielding displacement ratio of the non-linear connections (β) in the cases of m_1=451-800-1000 [kN/g] (k_1=24 kN/mm, η=0.85, and θ=0.5%) for specific input accelerogram.

All curves show a stationary point (minimum). For specific values of β, the ductility demand on the existing building (DOF1) can be minimized; this entails minimum required displacement and minimum seismic action on the existing building. In Figure 40a and Figure 40b, the minimum ductility demand (μ) can be identified around β =0.1 [-] while, in the case m_1 is set equal to 1000 [kN/g] (Figure 40c) the minimum ductility demand (μ) can be identified around β=0.06 [-]. The design yielding displacement of the connections should be identified around these values.

It can be observed that the higher m_1, the smaller the yielding displacement ratio (β) of the connections. The results of these three analyses show that the minimum μ can be reached considering an optimal value of β ranging within the interval 0.05-0.15. In all the 3 cases, the minimum point of all the 7 curves can be visualized in close proximity of this range.

The curve related to the accelerogram 000592xa does not display a minimum point; the reason for this behavior is the low intensity of that seismic event that does not allow the connection to reach its yielding point. In the following other parameters of the system are investigated.

- **Case 2. Varying the elastic stiffness (k_1) of the DOF1**: the optimal yielding displacement of the connection ($\delta_{y,12}$) is investigated by evaluating the ductility demand (μ) as a function of the yielding displacement ratio (β) for varying the stiffness of the DOF1 (k_1). The influence of the parameter k_1 on the system response is then evaluated. In Figure 41 the ductility demand (μ) is plotted as a function of β for varying the stiffness of the DOF1 (k_1) and for fixed values of m_1, η and θ.

DOF 1	**Symbol**	**Range/Value**	**Unit**
Effective mass	m_1	800	[kN/g]
Elastic stiffness	k_1	7.9-14-24	[kN/mm]
Adim. yielding force	η	0.85	[-]
Target displacement			
Inter-story drift target	θ	0.5	[%]

Table 4: Inputs of the non-linear 2 SDOF system used in case 2.

a)

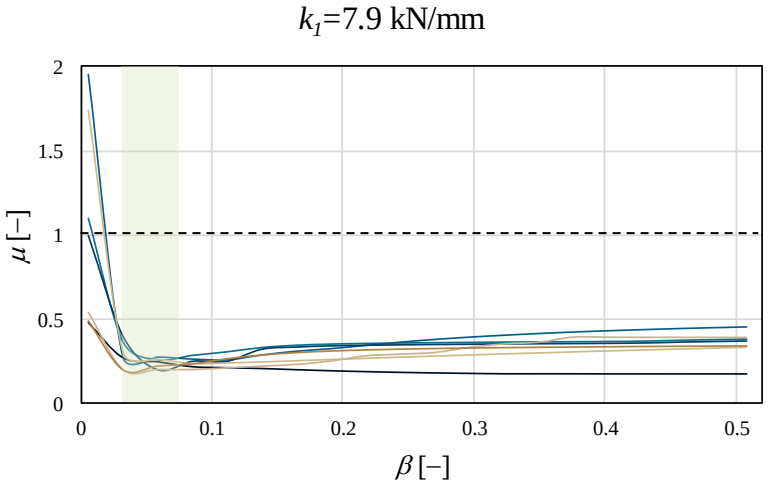

b)

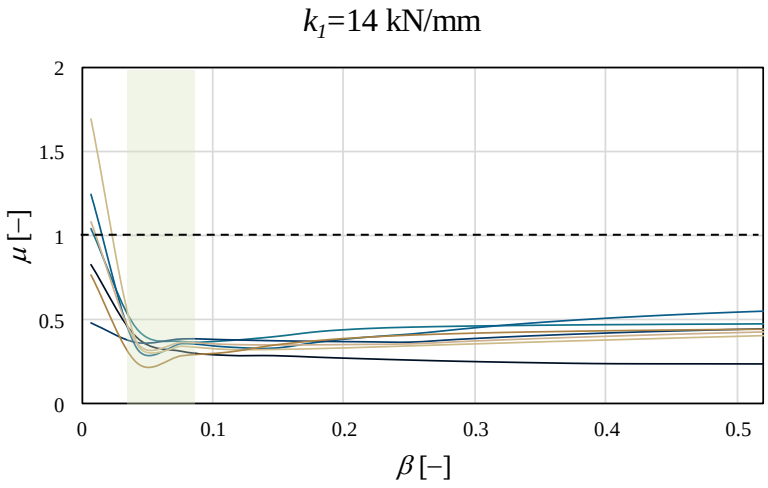

c)

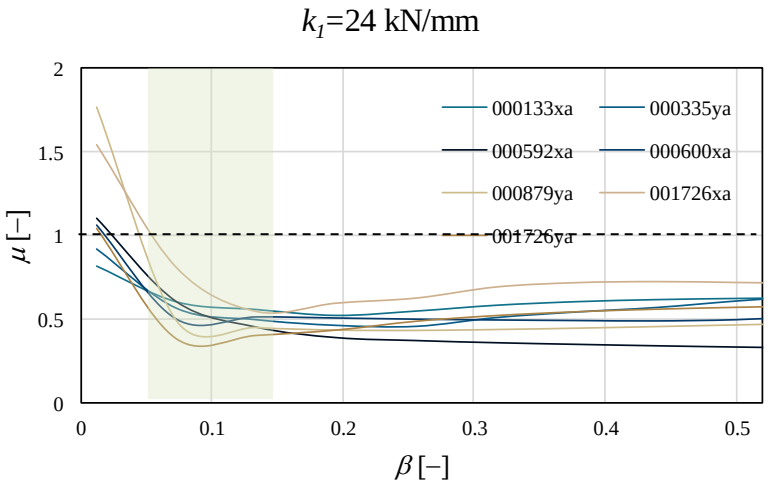

Figure 41: Ductility demand (μ) on the existing building (DOF1) as a function of yielding displacement ratio of the non-linear connections (β) in the cases of k_1=7.9-14-24 [kN/mm] (m_1=800 kN/mm, η=0.85, and θ=0.5%) for specific input accelerogram.

By varying the stiffness of the DOF1 (k_1), it can be observed that the smaller k_1, the smaller the yielding displacement ratio (β) of the connections; however, the stationary minimum point can be visualized in the same optimal range of the Case 1 (β=0.05-0.15).

Considering that the curves of the 7 accelerograms feature the same shape, in the following, the average curves are used to represent the global behaviors of the systems.

To evaluate how much this assumption can affect the response of the systems in the Cases 1 and 2, in Figure 42 the displacements of the DOF1 obtained solving the equations of motion with the optimal β for each accelerogram, are compared with the displacement of the DOF1 obtained introducing in the equations of motion only the optimal value of the average curve. The comparison is made by means the parameter μ; with this aim are introduced: μ_{Avg} on the x-axis, that represent μ obtained from the equations of motion considering the optimal β of the average curve, while in the y-axis is plotted μ_{opt} obtained with the optimal value for each accelerogram. Resulting in an average error smaller than 10%, the simplification introduced can be considered acceptable.

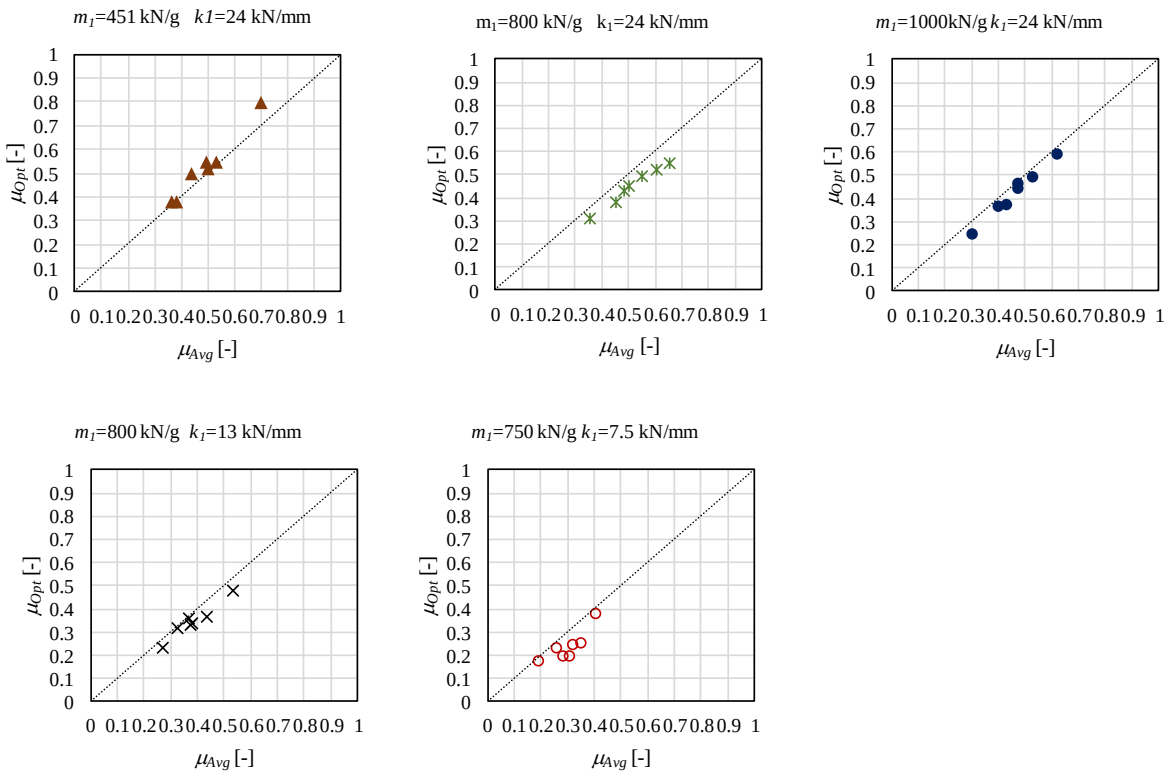

Figure 42: Comparison, in terms of ductility demand (μ), between the u1 obtained with the optimal value of each accelerogram and u_1 obtained with the optimal value of the average curve.

- **Case 3. Varying the inter-story drift target (θ):** the optimal yielding displacement of the connection ($\delta_{y,12}$) is investigated by evaluating the ductility demand (μ) as a function of the yielding displacement ratio (β) for varying the inter-story drift ratio (θ). To evaluate the influence of the parameter θ on the system response, all the previous values of mass (m_1) and stiffness (k_1) of the DOF1 are varied within the range of interest. The adimensonalized yielding displacement (η) is assumed equal to 0.85.

  In Figure 43÷Figure 45 the ductility demand (μ) is plotted as a function of β for varying the inter-story drift ratio (θ), and the stiffness (k_1) and the mass (m_1) of the DOF1.

DOF 1	**Symbol**	**Range/Value**	**Unit**
Effective mass	m_1	451-800-1000	[kN/g]
Elastic stiffness	k_1	7.9-14-24	[kN/mm]
Adim. yielding force	η	0.85	[-]
Target displacement			
Inter-story drift target	θ	0.30-0.50-0.75	[%]

Table 5: Inputs of the non-linear 2 SDOF system used in case 3.

- θ=0.30 %

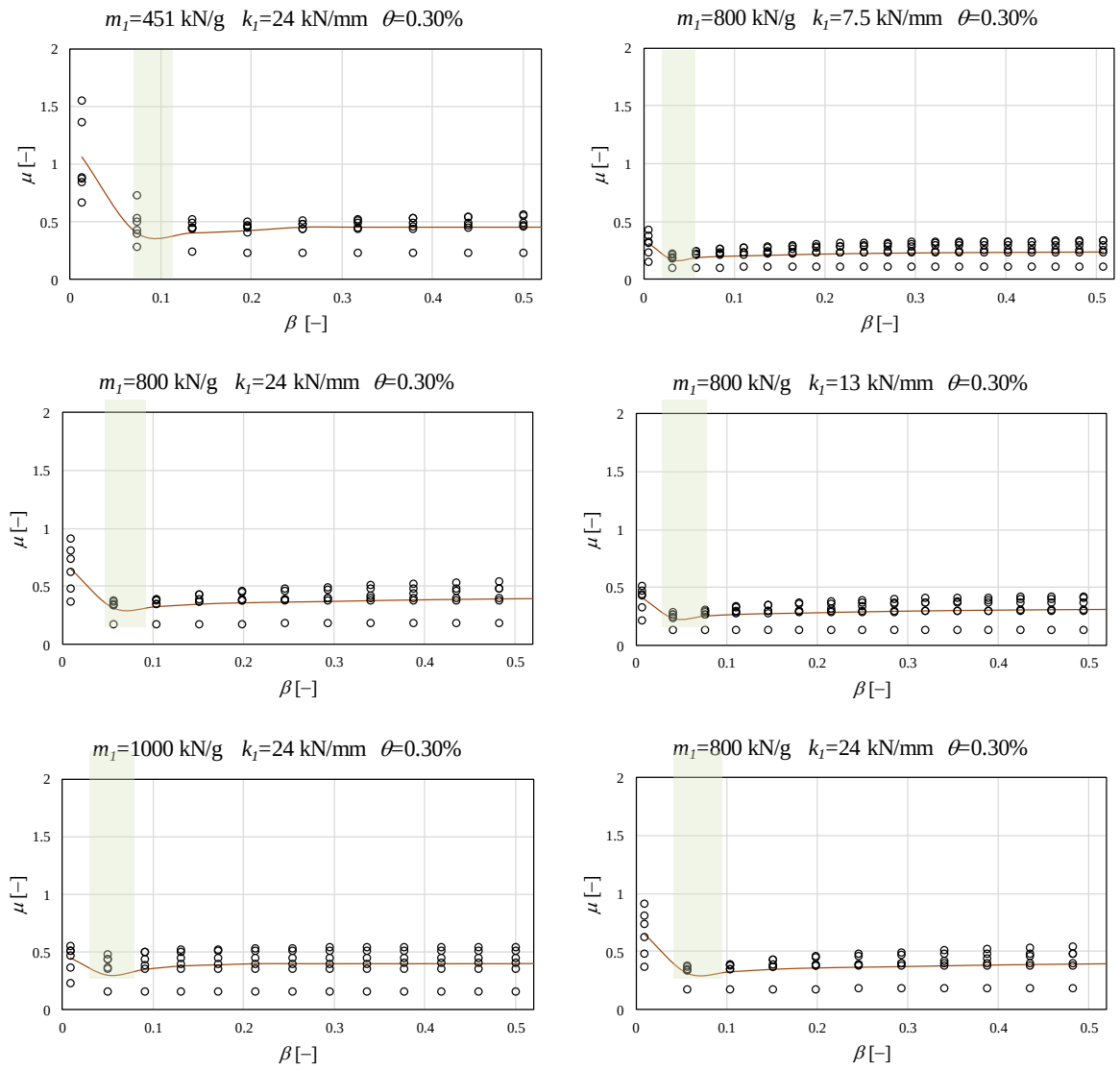

Figure 43: Ductility demand (μ) on the existing building (DOF1) as a function of yielding displacement of the non-linear connections (β) in the case of θ=0.30% considering the average response of 7 accelerograms. The response is evaluated increasing m_1 (*left*) and increasing k_1 (*right*).

- θ=0.50 %

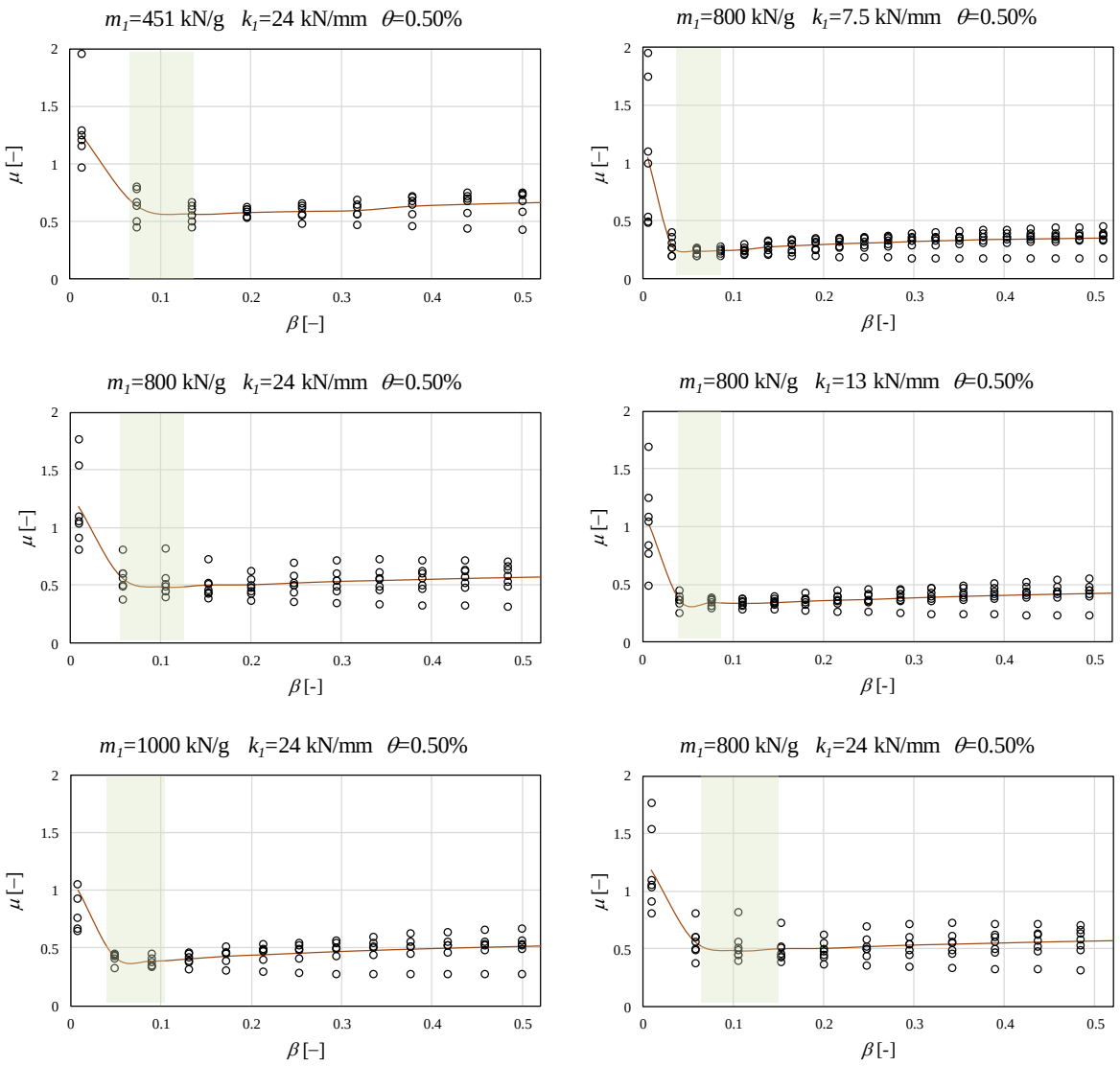

Figure 44: Ductility demand (μ) on the existing building (DOF1) as a function of yielding displacement of the non-linear connections (β) in the case of θ=0.50% considering the average response of 7 accelerograms. The response is evaluated increasing m_1 (*left*) and increasing k_1 (*right*).

- θ=0.75 %

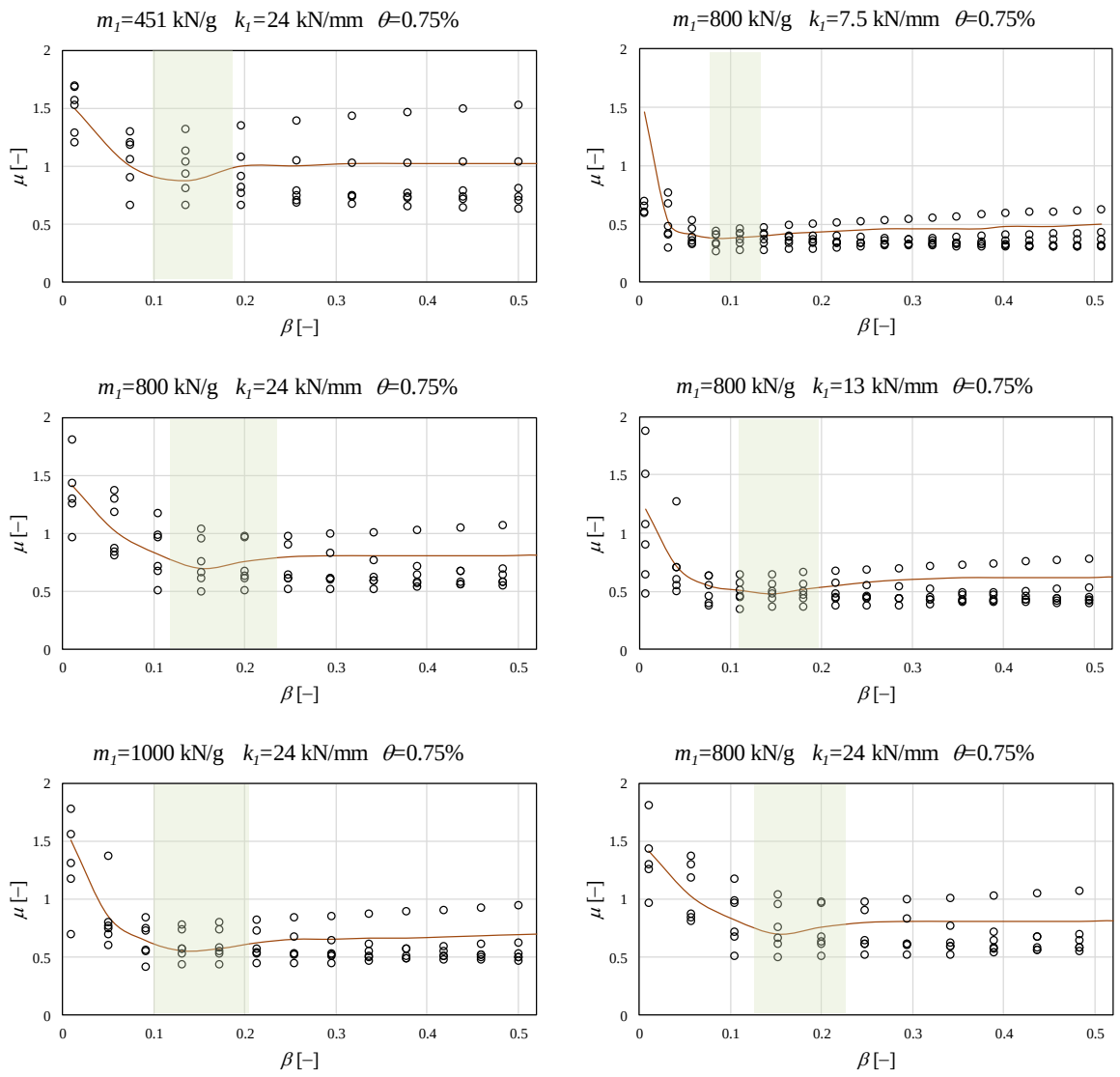

Figure 45: Ductility demand (μ) on the existing building (DOF1) as a function of yielding displacement of the non-linear connections (β) in the case of θ=0.85% considering the average response of 7 accelerograms. The response is evaluated increasing m_1 (*left*) and increasing k_1 (*right*).

From the results in Figures 43-45, it can be observed that, as already highlighted in the previous cases, by increasing the mass of the existing building (m_1) the optimal range slightly shift to the left, while increasing the stiffness of the existing building (k_1) the optimal range shift to the right. Therefore, for higher fundamental period of the existing building (T_1), the connection must yield earlier than for lower T_1. However, while the mass (m_1) and the stiffness (k_1) do not affect significantly the response, the inter-story drift target is proved to affect quite significantly the optimal value of β. From the previous plots in Figure 43÷Figure 45 one can derive that for η equal to 0.85 and θ equal to 0.30%, the optimal β ranges between 0.01÷0.10 while, as concern the optimal values for θ equal to 0.50% and 0.75%, the optimal β can be localized in the ranges 0.05÷0.15, and 0.10÷0.25, respectively.

Considering an arbitrary value of β included in these optimal ranges, the ductility demand (μ) does not significantly differ from the ductility demand obtained considering the optimal value of β for each single case. In Figure 46, the top displacement obtained solving the equations of motion with the optimal value of β for each accelerogram (minimum point of each accelerogram), is compared with the top displacement obtained by introducing in the equations of motion a reference value of β for each inter-story drift (θ); the comparison is developed in terms of the ductility demand (μ) of the DOF1.

Defining μ_{Ref} as the ductility demand obtained from the equations of motion considering a reference value of β, in Figure 46, μ_{Ref} (x-axis) is compared with μ_{opt} (y-axis) which represents the ductility demand (μ) obtained introducing in the equations of motion the optimal value for each accelerogram.

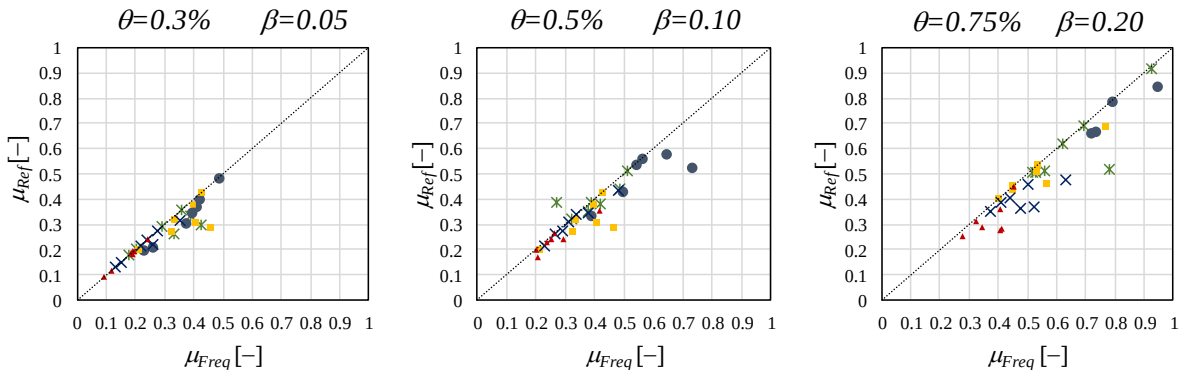

Figure 46: Comparison between the u1 obtained with the optimal value of each accelerogram and u1 obtained with the most frequent value of β.

The results show that:

(a) μ_{freq} is slightly different with respect to μ_{opt}; however, this result can be considered acceptable for preliminary consideration about the retrofit structure;

(b) As expected, for θ=0.75% the results are more scattered than for θ=0.3-0.5% since for an inter-story drift target (θ) equal to 0.75% the optimal range was larger than for lower values of inter-story drifts (θ).

To summarize: it has been demonstrated that, by plotting the ductility demand (μ) by varying the yielding displacement ratio (β) of the connection, a stationary minimum point in the curves can be identified. Parametric analyses were carried out to investigate the influence of several parameters, and it was observed that while the mass and the stiffness of the existing building do not affect significantly the results, the inter-story drift plays a more significant role. Accordingly, optimal ranges of β (useful for preliminary considerations and proportioning the retrofit structure) were identified as a function of the inter-story drift target and for an adimensionalized yielding force (η) equal to 0.85; in particular, were defined the following optimal ranges and reference values:

- β = 0.01 - 0.10 for θ = 0.30%
- β = 0.05 - 0.15 for θ = 0.50%
- β = 0.10 - 0.25 for θ = 0.75%

The same analyses were carried out by varying the adimensionalized yielding force (η). In Figure 47 the optimal ranges of the parameter β are plotted for every value of η and inter-story drift target (θ) thus highlighting how these two parameters affect the global response of the system. In particular, for each value of η and θ, a bubble chart is used to represent the distribution of the optimal values of β (x-axis); the frequency of the optimal values is represented by the size of the bubbles. Considering that, as shown in Figure 40 and Figure 41, the mass (m_1) and the stiffness (k_1) of the existing building do not significantly affect the response of the system, the results do not consider how these two parameters affect the response.

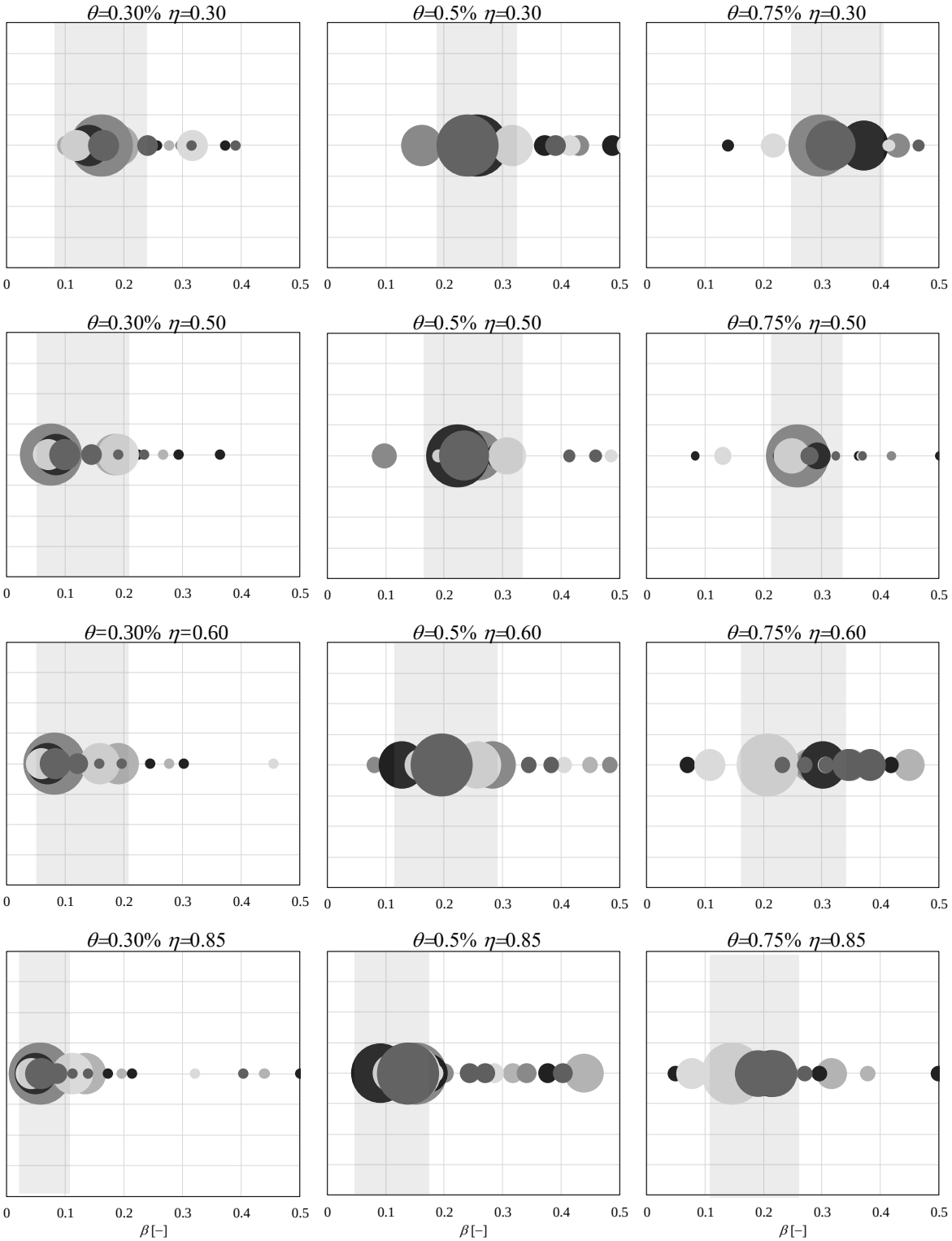

Figure 47: Distribution of the optimal values of β by varying the inter-story drift target (θ) and the adimensionalized yielding force (η).

From the results one can observe that, as expected, increasing the inter-story drift target (θ) the optimal range of β values increase; moreover, it can be observed that, increasing the value of η, the optimal range significantly shift to the left.

Provided that the response is mainly affected by the inter-story drift ratio (θ) and by the adimensionalized yielding force (η), in Figure 48, design spectra for varying periods of the existing building (T_1) are introduced to consider both these parameters in the design procedure of the diagrid connections.

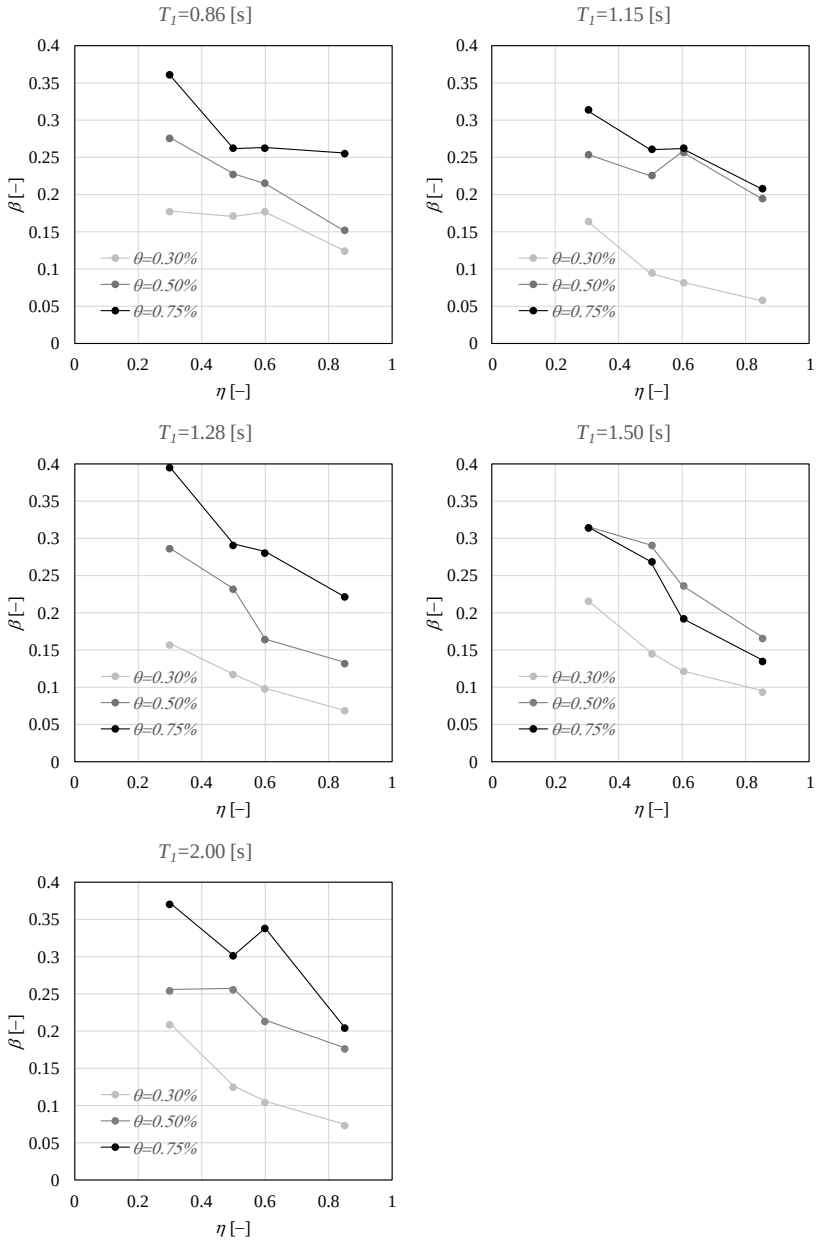

Figure 48: Design spectra for the determination of the optimal yielding ration of the connection (β) as a function of the adimensionalized yielding force (η) and of the inter-story drift target (θ).

3.5 From SDOF system to MDOF system

The equivalent stiffness obtained by the 2DOF (k_{12}) must be translated for a MDOF system (k_i).

According to Ciampi et al. (1995) the stiffness is distributed considering a linear deformed shape with constant drift. Figure 49 shows the existing building (solid black line) and the retrofit structure (solid red line) and the linear distribution of the relative displacement between the two structures. In particular, Δ represents the relative top displacement, ρ the angle obtained from the arctan of the ratio between Δ and H, k_i the connection stiffness at the *i-th* floor, and Δi the connection displacement at the *i-th* floor.

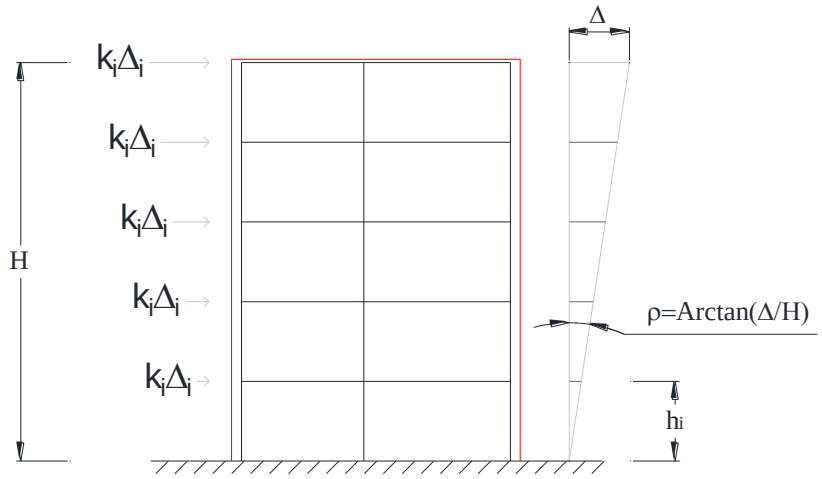

Figure 49: Simplified deformed shape of the first vibrational mode.

Accordingly, the total force in the connections (F_{12}) can be defined as:

$$F_{12} = \sum k_i \Delta_i = \sum k_i \rho H = k_i \rho \sum h_i = k_i \rho h_i \sum N = k_i \rho h_i \frac{N+1}{2}$$ **Equation 49**

where N is the number of the floors. Considering:

$$k_{12} = \frac{F_{12}}{\Delta}$$ **Equation 50**

the stiffness k_{12} can be obtained:

$$k_{12} = \frac{k_i \rho h_i \frac{N+1}{2}}{\rho h_i N} = k_i \frac{n+1}{2}$$ **Equation 51**

For each floor in the MDOF system the stiffness is:

$$k_i = k_{12}\frac{2}{N+1}$$ **Equation 52**

It is worth noting that, considering $k_i = \frac{k_{12}}{N}$, the stiffness of the *i-th* link would be under-estimated by 39%. Such under-estimation of the connections would lead to an equivalent retrofit stiffness ($\tilde{k}$) lower than the required to meet the target displacement imposed thus resulting in damage to the existing building during a seismic event.

Chapter 4: Application of the diagrid for the strengthening of a reference building

4.1 General overview

The reference structure is a post-World War II reinforced concrete building located in Chiesanuova district in Brescia (Italy) and owned by ALER (regional enterprise for social housing). The main structure was built in 1975 according to the regulation codes and the construction techniques of the time. The structure, identified with the letter H in Figure 50, was built in a residential district composed of 10 RC buildings. Main features and structural details were derived by the original structural and architectural construction documents[1] of the whole complex and by recent researches carried on the structure (Antonini, et al., 2017; Zanchi & Vassalli, 2016).

Figure 50: Location of the reference building (H) within Chiesanuova social housing district (IDES 2008).

[1] See Appendix 3

Figure 51: Views of the reference building. South-east façade (*left*), ground floor (*right*) (IDES 2008).

4.1.1 Architectural and structural features of the reference building

The reference building is composed of two constructions that are separated by a thermal joint. Since the aim of this Section is to apply a diagrid structure for the strengthening of a reference building representing ordinary WWII RC buildings, supposing that each building structurally behaves independently, only the East part is considered (Figure 52).

The reference structure is an 8-story building with a ground plan of 27.10x13.45 [m], thus covering an area of about 265m^2 out each floor (Figure 53). The garages and the entrance are located on the ground floor, while in the upper floors large residential apartments can be found.

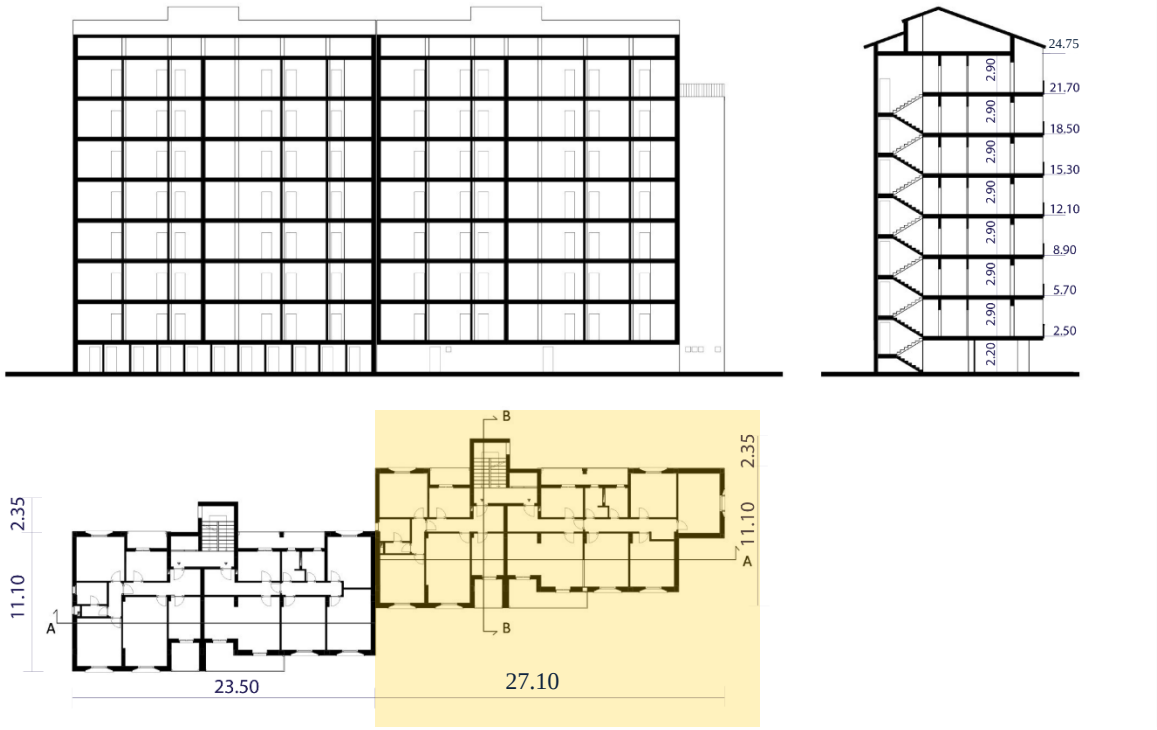

Figure 52: Longitudinal (*left*) and transversal (*right*) sections. Plan of a reference floor (*bottom*) (IDES 2008).

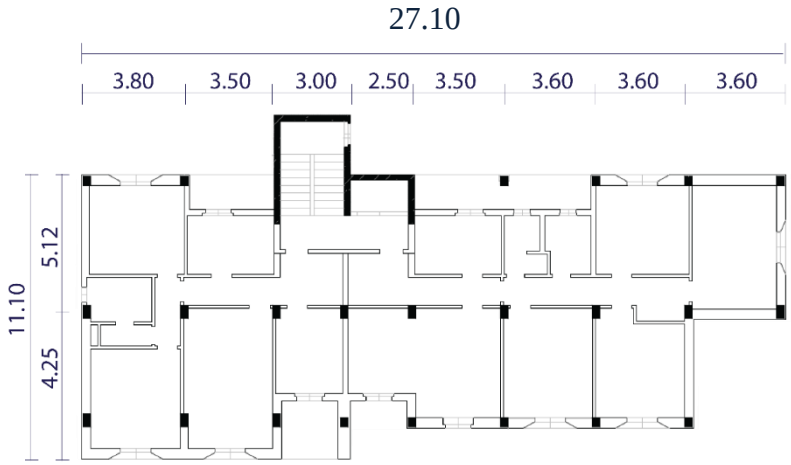

Figure 53:Plan of the East building (IDES 2008).

As concern the structural aspects, in 2007, according to O.P.C.M 3274/2003 and S.M.I., technical inspection and the structural assessment of the seismic safety level were conducted

by IDES (engineering company specialized in diagnostic investigations), and the structural details and the materials of the bearing structure were investigated[2].

The bearing structure features three one-way longitudinal frames and two infilled lateral frames. The inter-story height (h_i) is 2.50 [m] at the ground floor and 3.15 [m] at the upper floors for a total height (H) of 24.75 [m]; the span dimensions are variable: longitudinal frame beams have spans ranging between 2.5 [m] and 3.6 [m] whereas floor spans range between 4.15 [m] and 5.12 [m]. Beams and columns were designed for vertical loads only; the steel rebars in these elements were investigated through indirect tests. Based on the results of magnetometric tests on 54 columns and 2 beams, the accuracy of the original construction documents was verified.

Floors are made of a composite RC beam and clay block system featuring a 2.5 [cm] RC overlay for a total thickness of 24 [cm].

The staircase core is a reinforced concrete C-shaped shell; however, since the structural detailings were not designed to ensure a global behavior among the three walls, they should be considered as three independent walls. The thickness of the stairwell walls varies between 20 [cm] and 25 [cm].

The structure laid on direct piled foundations and additional reinforced concrete shear walls introduced during a retrofit intervention on the foundation system carried by the engineer Pietro Gelfi in the 1983s. Contemporarily, also the columns at the ground floor were consolidated because of the inability of those elements to withstand the static loads (Figure 54).

As far as the non-structural components, infills are made of one layer of hollow bricks and two lateral layers plaster (IDES, 2008).

[2] In Appendix 3 are reported the original structural documents of the reference case and detailed information about the bearing structure.

Figure 54: Pictures of the intervention on the columns and the foundation system.

The material features derived by means compressive tests on the concrete and tensile tests of the steel rebars conducted by IDES (2008), are reported in Table 6 and Table 7.

Concrete	
Floor	**$R_{ck,eff}$ [MPa]**
Ground	13.6
1st	24.5
2nd	22.1
3rd	42.1
4th	59.8
Average	32.4

Table 6: Measured concrete properties: test on 16 elements. $R_{ck,eff}$ is the measured concrete cube compressive strength.

Steel		
Floor	**f_y [MPa]**	**f_u [MPa]**
Ground	442.7	639.5
2nd	477.8	715.0
3rd	468.3	680.7

Table 7: Steel measured properties: test on 6 elements. f_y and fu are the yielding force and the ultimate strength, respectively.

4.1.2 Qualitative preliminary structural considerations

The analysis of the technical documentation highlighted how the reference building was designed to withstand only the vertical loads; consequently, in the context of the structural safety of the structures, some structural deficiencies can be identified.

1. Vertical irregularities: the inter-story height of the ground floor is lower than the inter-story height of the upper floors. This aspect, in addition to the absence of the infill panels at the ground floor, may result in severe damage and stress concentration in the columns of this floor leading to a possible soft-story mechanism. Sudden discontinuity in the lateral strength and stiffness along the height of the building can result in severe damage concentration.
2. In-plan irregularities: when the reference building is subjected to lateral loads, floors translate or rotate around their shear center. In the case of high eccentricity of the shear center from the center of gravity, a significant rotational contribution may occur thus increasing the displacements in a localized part of the structure. In the reference case, the staircase core plays a fundamental role in the definition of the shear center; therefore, given the asymmetry of the stairwell, some torsional mode shapes are expected from the modal analysis.
3. Different behaviors in the transversal and the longitudinal directions: the presence of the infill panels only in the *y*-direction (transversal direction), leads to different behavior in the two directions of the existing building in case of horizontal loads. The existing building acts as a RC frame along *x,* while as an infilled frame along *y*.
4. Floor diaphragm: event if they are not designed as in-plane diaphragms, based on previous studies, it has been assumed that floors can withstand horizontal loads (i.e. they behave like floor diaphragms) by developing an in-plane tied-arch resistant mechanism up to their ultimate capacity (Feroldi, 2014). However, since they were not designed to withstand the horizontal loads, specific evaluations are mandatory. If the previous assumption would not be verified, a strengthening of the existing floors, such as external diaphragms, may be required.

4.2 Numerical analysis of the structural response

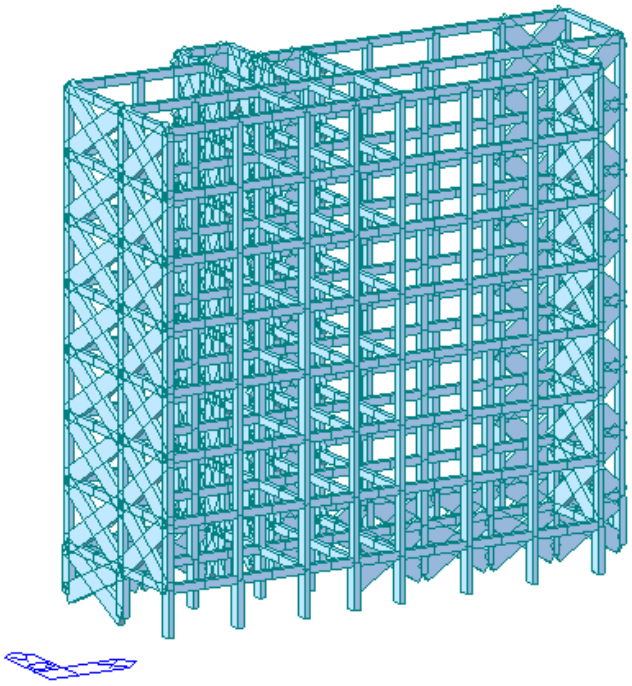

Figure 55: Finite Element Model of the reference building.

The building was modelled as a tridimensional structure with the software MidasGEN v.2018 (MidasGEN, 2018) (Figure 55). The frame components were modelled as beam elements and the inelastic behavior was accounted for by means of lumped plastic hinges in which the flexural and shear resistance of the frame elements were modelled with the degrading Takeda constitutive law (Otani, 1974) shown in Figure 56.

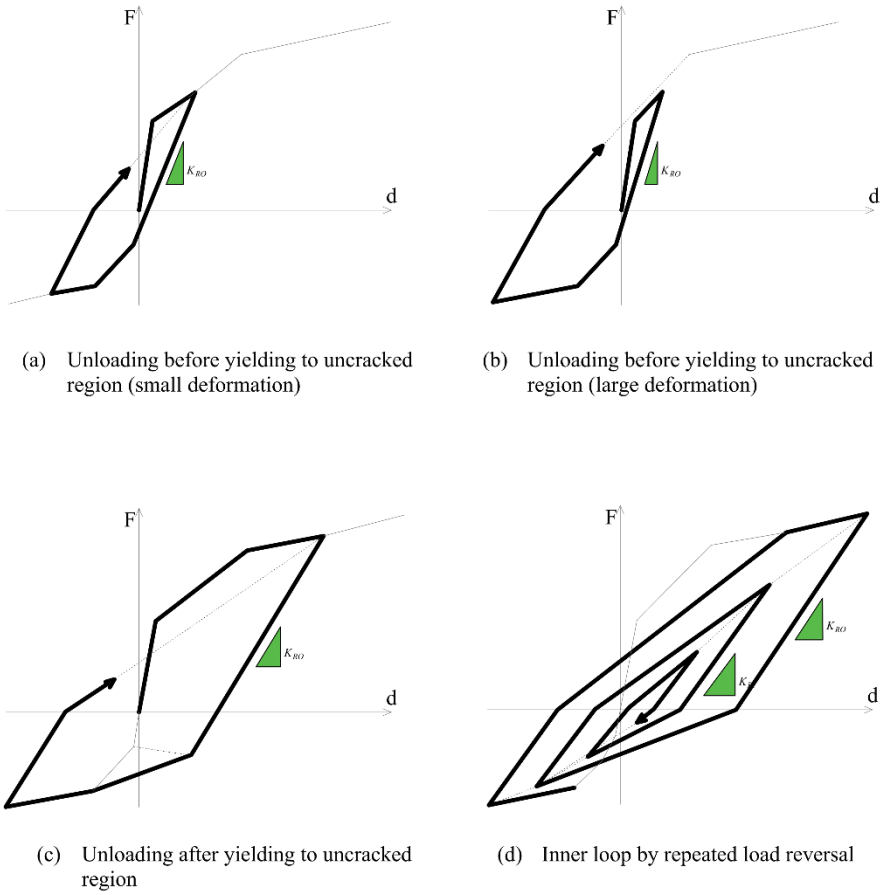

Figure 56: Takeda type hysteresis model implemented in the program MidasGEN (from: MidasGEN 2018).

The flexural plastic hinge is a trilinear curve followed by a degrading branch (Figure 57a), while the shear plastic hinge has a linear behavior up to the ultimate capacity; beyond that limit, the curve decays very quickly thus exhibiting a sudden brittle failure (Figure 57b). It is worth noting that from the initial models it was observed that the shear failure of the beam elements did not happen. Subsequently, to reduce the computational costs of the analyses, in the beams, only the flexural plastic hinge was considered.

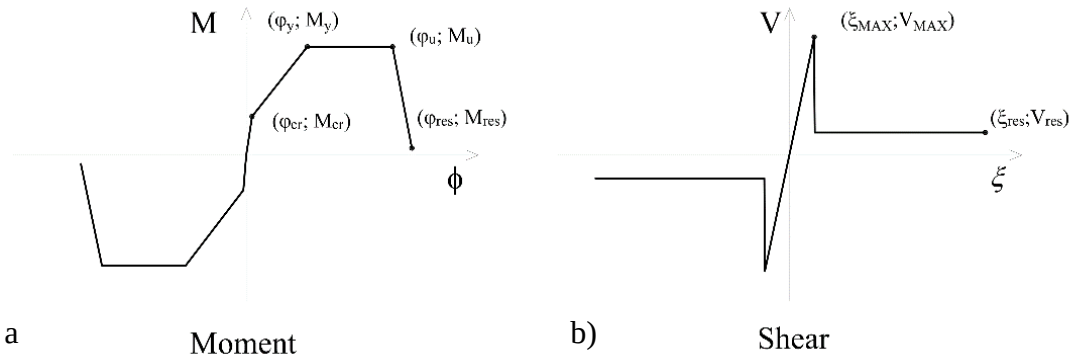

Figure 57: a) Flexural behavior; b) shear behavior.

The ultimate shear resistance (V_{Max}, ξ_{Max}), and the characteristic points of the flexural curve (cracking (M_{cr}, φ_{cr}), yielding (M_y, φ_y), ultimate (M_u, φ_u), and residual (M_{res}, φ_{res})) were calculated based on the formulations suggested from the Italian (NTC, 2018) and European (EC8, CEN 2005) codes. Some consideration on the calculation of the characteristic values of the frame elements are reported in Appendix 4.

As far the building floors are concerned, on the basis of previous studies, it was assumed that they can withstand horizontal loads (i.e. they behave like floor diaphragms) by developing an in-plane tied-arch resistant mechanism up to their ultimate capacity (Feroldi, 2014; Feroldi, et al., 2019); therefore, they were modelled as rigid diaphragms. However, specific and targeted considerations on the finite element model results have to be made. For example, the inter-story shear has to be compared with the limit story shear allowed by the existing floor.

The infill panels were modelled by means of two compression-only diagonal struts (Decanini, et al., 1993) converging in the beam-column joints. The non-linear behavior of the infills panels was accounted for by means of lumped plastic hinges. The axial plastic hinge of the infills is a trilinear curve described by a cracking (F_{cr}, θ_{cr}) and a peak (F_P, θ_P) points. The cracking force (F_{cr}) and the peak force (F_P) were evaluated according to Decanini et al. (1993), while the cracking drift (θ_{cr}) and peak drift (θ_P), were introduced in accordance to the traditional values of 0.3% drift for minor cracking in the infill panels, and 0.5% drift for the infill failure (Mehrabi, et al., 1996)[3]. Figure 58 describes the trilinear curve of the axial plastic hinge plotting the normalized force (F/F_P) as a function of the inter-story drift (θ).

[3] The reason of this assumption is due to the very low values of cracking and peak displacements obtained with the Decanini's law that do not represent well the real behavior of ordinary European infills panels.

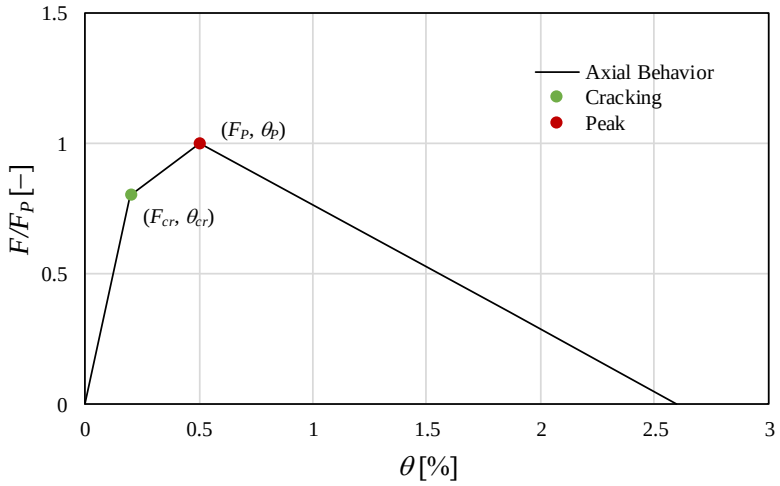

Figure 58: Axial plastic hinge of the compression-only diagonal struts.

As far as the input used in the Decanini's model, the data reported in Table 8 were considered.

f_{wh} [MPa]	f_{wv} [MPa]	f_{wu} [MPa]	f_{ws} [MPa]	E_{wh} [MPa]	E_{wv} [MPa]	G [MPa]	W [kN/m^3]
1.11	1.50	0.25	0.31	991	1873	1089	6.87

Table 8: Properties of masonry for the considered infill typology (Hak, et al., 2013), where f_{wh} and f_{wv} represent the values of compression strength for the horizontal and vertical direction, respectively. f_{wu} stands for the sliding shear resistance of the mortar joints, f_{ws} for the shear resistance under diagonal compression, E_{wh} and E_{wv} represent the secant modulus of elasticity for the horizontal and vertical direction, G is the shear modulus, and W is the unit weight of the infills.

Since the staircase walls were not designed to withstand the horizontal loads, in the Finite Element Model, the non-linear behavior of staircase walls was modeled following the same consideration introduced for the infill panels.

4.2.1 Non-linear static Pushover analyses and seismic vulnerability assessment of the reference building

Pushover analyses were performed considering both the longitudinal (x) and the transversal (y) directions of the Finite Element Model (Figure 55). The capacity curves are reported in Figure 59(*top*) and Figure 60(*top*) highlighting the significant points of each curve. For each point, the evolution of the story displacement and the inter-story drift are plotted (Figure 59 *(bottom)* and Figure 60 *(bottom)*) over the building height.

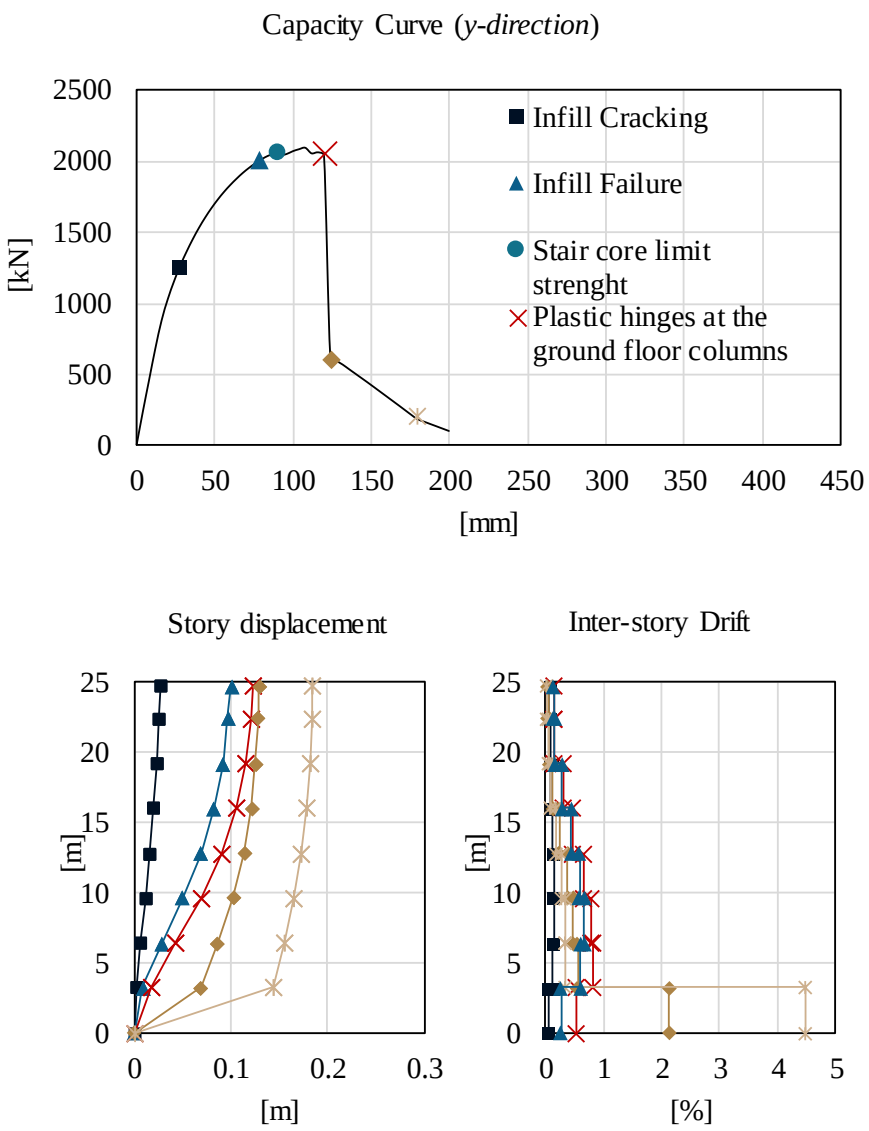

Figure 59: Capacity curve in y-direction (*top*), evolution of story-displacement (*left*) and inter-story drift (*right*) for significant points of the capacity curve.

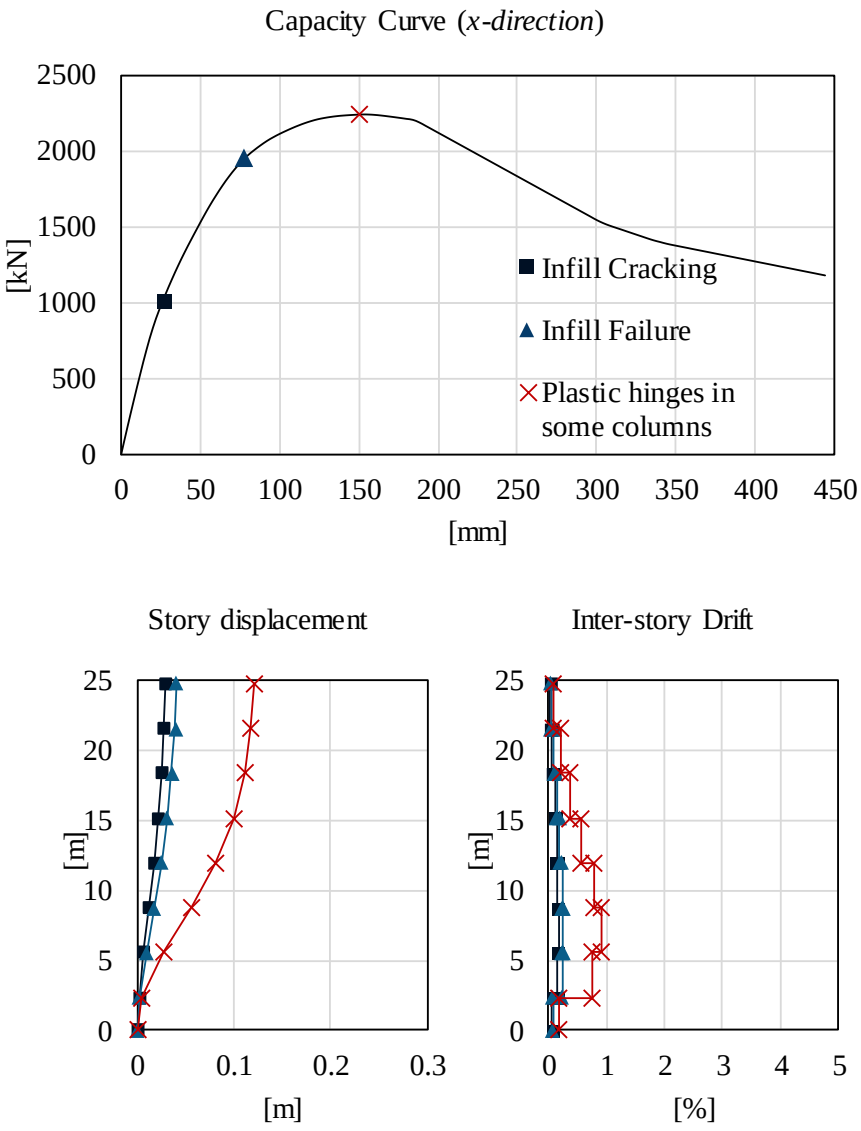

Figure 60: Capacity curve in x-direction (*top*), evolution of story-displacement (*left*) and inter-story drift (*right*) for significant points of the capacity curve

The two capacity curves feature two different behaviors at collapse; in the *y*-direction, a soft-story mechanism at the ground floor characterizes a brittle collapse of the existing building while, in the *x*-direction, the structure exhibit a more ductile behavior. In the *y*-direction, as expected, the existing building behaves mostly like an infilled frame, while in the *x*-direction it behaves like a RC bare frame.

Considering the reference building located in Brescia, on a flat surface made of deposit of sand or medium-dense sand gravel or stiff grave (soil category C and T1 topography) (NTC, 2018), according to the *N2* method (Fajfar, 2000; NTC, 2018), vulnerability analyses of the existing building were conducted. The capacity curves of the existing building were normalized through the participation factor (Γ) (NTC, 2018; EC8, CEN 2005) of the first mode in order to derive

the equivalent SDOF capacity curve. The SDOF capacity curves were then bi-linearized following the principle of the equal energy, and the displacement demands of the SDOF system were derived by means of the considered elastic response spectrum following the equal displacement principle. The results were reconverted into a MDOF system. The main parameters of the *N2* method are reported in Table 9 and Table 10 for the *y* and *x*-direction, respectively.

Parameter	**Symbol**	**Values**	
Participation factor	Γ	1.36	[-]
Yielding force of the bi-linear curve	F_{y1}	1434.2	[kN]
Yielding displacement of the bi-linear curve	δ_{y1}	0.031	[m]
Fundamental period of the equivalent SODF system	T_1	1.15	[s]
Mass of the equivalent SODF system	m_1	1567.9	[kN/g]
Stiffness of the equivalent SDOF system	k_1	45450	[kN/m]
Displacement Demand for the SODF system at the Life Safety Limit State (LSLS)	S_d^{LSLS}	0.07	[m]
Displacement Demand for the SODF system at the Collapse Limit State (CLS)	S_d^{CLS}	0.09	[m]

Table 9: *N2* method: Main parameters for the *y*-direction.

Parameter	**Symbol**	**Values**	
Participation factor	Γ	1.3	[-]
Yielding force of the bi-linear curve	F_{y1}	1529.98	[kN]
Yielding displacement of the bi-linear curve	δ_{y1}	0.044	[m]
Fundamental period of the equivalent SODF system	T_1	1.51	[s]
Mass of the equivalent SODF system	m_1	1666.13	[kN/g]
Stiffness of the equivalent SDOF system	k_1	34330	[kN/m]
Displacement Demand for the SODF system at the Life Safety Limit State (LSLS)	S_d^{LSLS}	0.08	[m]
Displacement Demand for the SODF system at the Collapse Limit State (CLS)	S_d^{CLS}	0.10	[m]

Table 10: *N2* method: Main parameters for the *x*-direction.

The bi-linearized capacity curves, the Acceleration Displacement Response Spectrums (ADRS) at the Life Safety Limit State (LSLS) and Collapse Limit State (CLS), and the displacement demand at the LSLS (S_d^{LSLS}) and CLS (S_d^{CLS}) are plotted in Figure 61 and Figure 62. It is worth noting that, from the Figure 61 and Figure 62, the adimensionalized yielding force (η) can also be derived being (η) the ratio between the yielding force of the existing building

(F_{y1}) and the associated elastic seismic demand (m_1*$Sa(T_1)$). From the ADRS (Figure 61 and Figure 62) it can be observed that in the reference building, η is equal to 0.50 and 0.55 for the *y*-direction and *x*-direction, respectively.

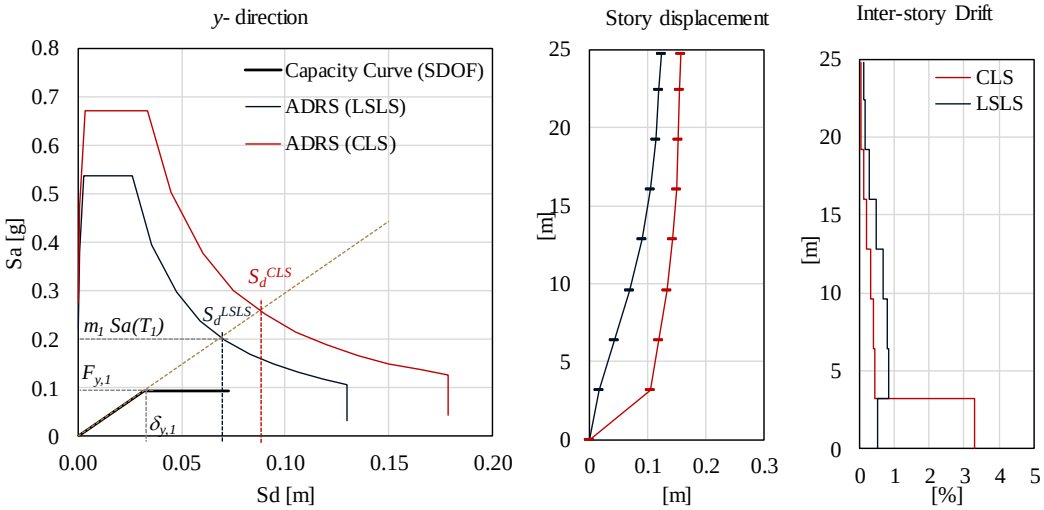

Figure 61: *y*-direction: ADRS and displacement demands at LSLS and CLS (*left*), story-displacement (*middle*), and inter-story drift (*right*) at the considered Limit States.

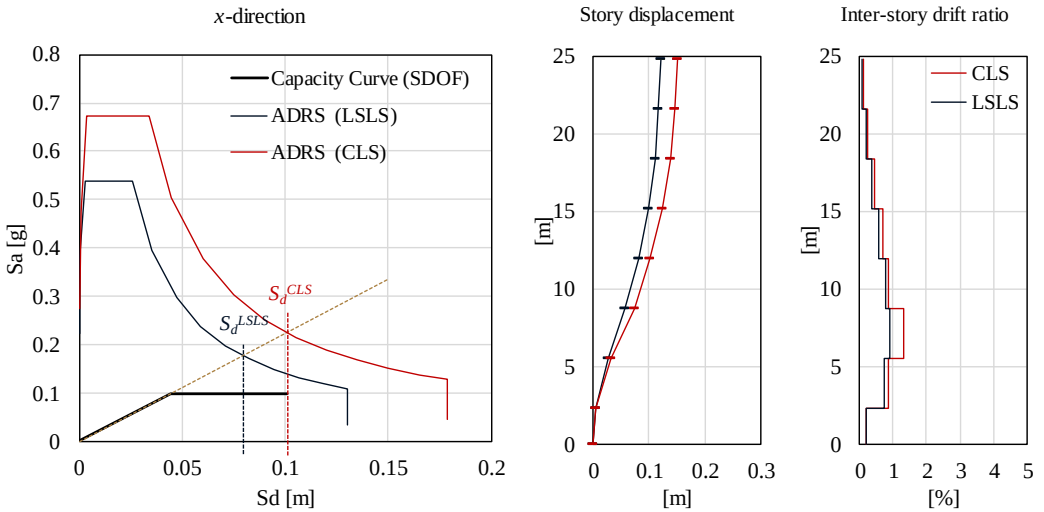

Figure 62: *x*-direction: ADRS and displacement demands at LSLS and CLS (*left*), story-displacement (*middle*), and inter-story drift (*right*) at the considered Limit States.

To critically evaluate the results, some consideration must be drawn; in this case, only the *y* - direction is considered[4]: (a) from the results in the ADR Spectra, the displacement demand at the LSLS lies in close proximity to the capacity curve failure point, meaning that a sudden

[4] Similar consideration can be drawn for the *x*-direction.

failure of the existing building may occur for a seismic event slightly higher than that expected in the design spectra; (b) the Finite Element Model is characterized by several uncertainties that may affect the response of the existing building. Some uncertainties on the building characteristics may lead to erroneous analysis models with structural responses very far from the expected targets. Ignoring these main issues may result in an erroneous expectation of the building capacity. Many uncertainties are connected to the existing materials and the structural detailing (such as the structural nodes). In many cases, it is difficult to find the original construction drawings, furthermore, variations to the plans were frequently decided on the construction site without updating the project documentation. Moreover, other uncertainties are connected to the element building modelling such as the plastic hinges of the infill panels and the staircase core, (Passoni, 2016). Many studies were developed over the years; however, the literature review has highlighted that, despite the great efforts spent in this research topic, fully satisfactory models are still not available (Passoni, 2016); (c) an inter-story drift equal to 1.0% at the LSLS, means the failure of the infills panels and severe and extended damages on the existing building, thus requiring high repairing costs and the building downtime in case of earthquake; (d) also the stairwell core, that represents the egress path of the building, results, in the As-Is condition, severely damaged at the LSLS demand. For these reasons and considering that the existing building does not satisfy the Collapse LS displacement demands (NTC, 2018), the renovation of the existing building is required.

With this aim, a diagrid structure as a strengthening solution was introduced. The structural aspects of the retrofitting diagrid were designed considering the weakest direction of the existing building (*y*-direction).

4.3 Diagrid structure design

4.3.1 Structural design of the retrofit solution

To achieve the new performance objectives (Section 2.2.2), specific design targets were set. A maximum inter-story drift (θ) equal to 0.3% (to avoid excessive damage of the non-structural components) and a maximum base shear flow equal to 200 kN/m (guaranteeing feasibility of the foundation systems) were considered. Moreover, considering that the seismic actions must be transferred across the diaphragm of the existing building, and that, in the retrofitted configuration, the span of the resisting arch is increased from the frame single-bay span (in the As-Is condition) to the span between the two webs of the diagrid (Figure 16), a target maximum

inter-story shear action was introduced to avoid retrofit of the existing floors (beyond this limit, either the retrofit of the existing floors or the adoption of external diaphragms are needed). Being this value evaluated based on the in-plane capacity of the floors and on the span of the resisting arch, it can be calculated after the diagrid geometry (in particular the longitudinal dimension) has been set[5].

4.3.1.1 Architectural aspects

The diagrid was conceived to be in close proximity to the existing building in the *y*-direction, while as an enlargement in the *x*-direction. This enables the addition of new living spaces in the longitudinal direction thereby increasing the potential economic value of the retrofitted building. The result is a rectangular diagrid structure of 27.70x15.90 m, with about 120 m^2 additional living space along the north façade, and about 40 m^2 along the south façade[6] (Figure 63).

Considering the optimal reference angle for shear buildings equal to 35° (Moon, et al., 2007; Moon, 2008) while, also accounting for the geometry and the characteristics of the reference building, an inclination angle of the diagonal elements (ψ) equal to 38.9° and a diagrid module height (h) equal to the inter-story height of the existing building (h_i) and were set.

The diagrid structure was assumed to be made of S275 tubular profiles and the profile dimension was considered equal in both directions of the exoskeleton.

[5] For the reference case a maximum inter-story shear of 628 kN was calculated (Feroldi 2014).

[6] With the diagrid, the surface of each floor increases by 80% respect to the existing one.

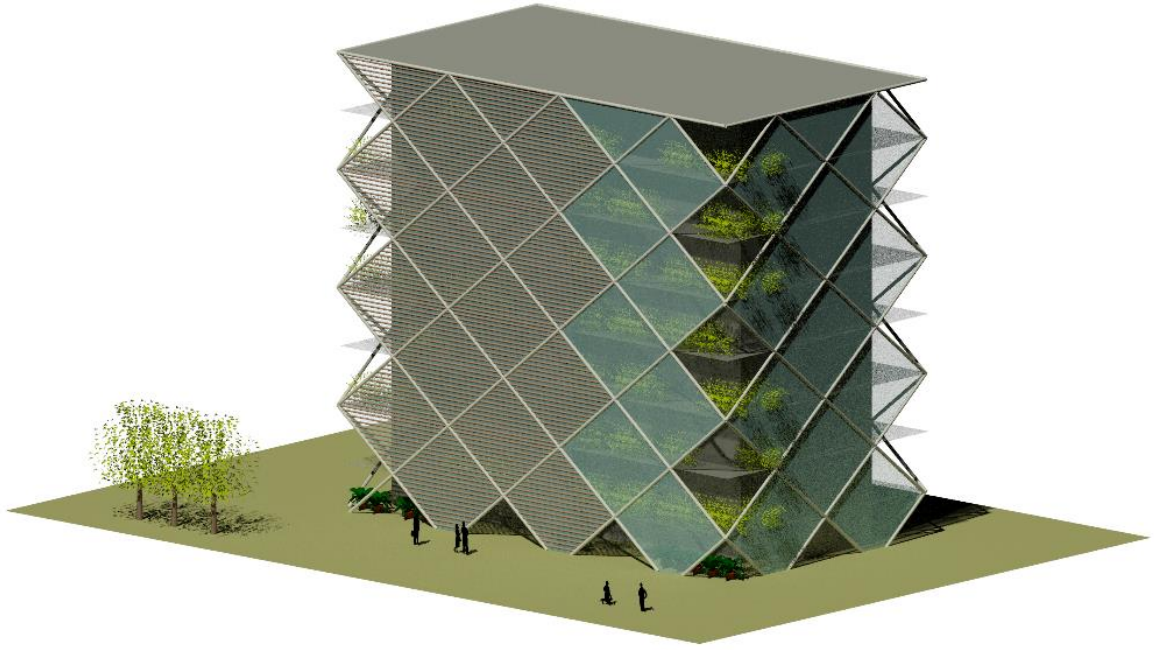

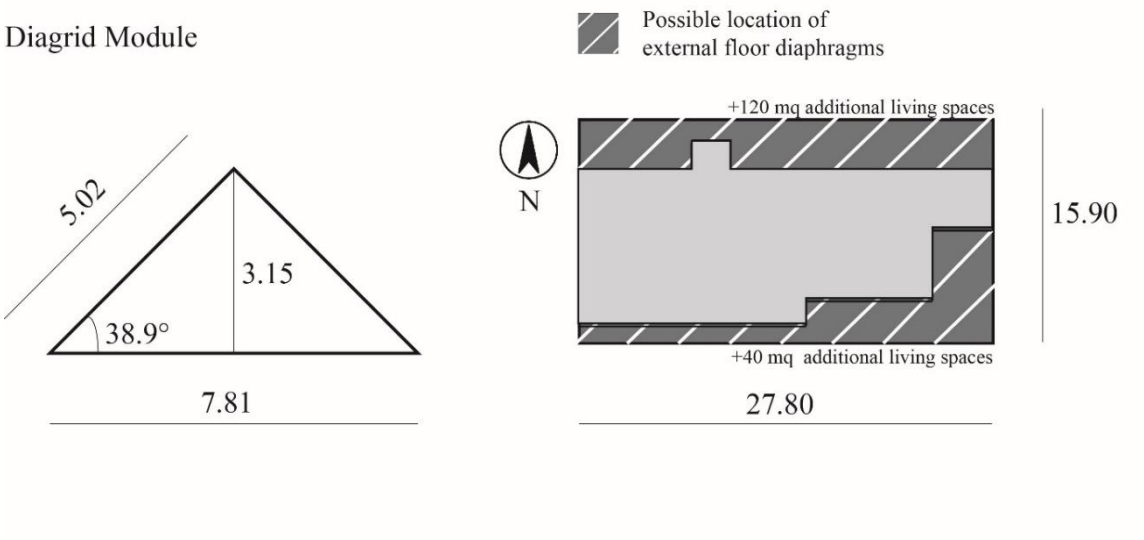

Figure 63: Architectural and formal aspects of the retrofit solution.

4.3.1.2 Preliminary proportioning of the exoskeleton: stiffness constraint and equivalent minimum stiffness

Supposing that the system behaves like a Timoshenko beam subjected to a distributed triangular load (p), the maximum top displacement of the retrofitted structure was calculated as indicated in Equation 23 considering the discrete nature of the diagrid structure (Equation **12**). It yields:

$$y(0) = \frac{8pH^2}{24A_sGk} + \frac{11pH^4}{120EI}$$

$$\begin{cases} A_s = 2n_W A_{d,W} \cos(\psi) \\ I = n_f A_{d,f} \sin(\psi) l^2 \end{cases}$$

where for the reference structure:

$$\begin{cases} p = 2 \cdot V / H \\ H = 24.75[m] \\ \psi = 38.9° \\ n_W = 4 \\ n_f = 8 \\ l = 15.90[m] \\ A_{d,W} = A_{d,f} \end{cases}$$

in which (V) is the total base shear of the retrofitted building and was expressed as:

$$V = m_1 \cdot Sa^D \cdot \Gamma_{FIN}$$

where (m_1) is the existing building mass[7], (Γ_{FIN}) is the participation factor of the retrofitted building, and (S_a^D) is the design spectrum acceleration derived as a function of the target design spectrum displacement (S_d^D) (Figure 64). More precisely, defining the target displacement of the existing building (d_{TOP}) as the product between the inter-story target (θ) and the existing building height (H), the design spectrum displacement (S_d^D) can be obtained dividing d_{TOP} by the participation factor of the retrofitted building (Γ_{FIN}); consequently, the design spectrum acceleration (S_a^D) can be derived.

[7] The mass of the diagrid was considered negligible

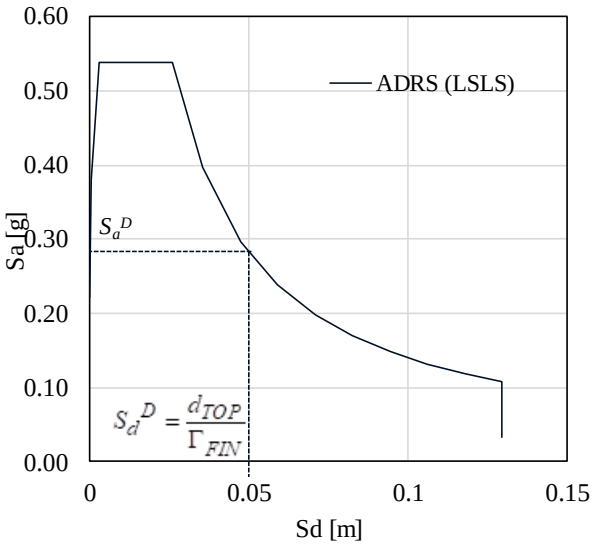

Figure 64: Representation on the ADR Spectrum at the LSLS the design parameters.

By combining Equation 23 and Equation 12, and by enforcing *y(0)* equal to the target displacement (d_{TOP}),

$$d_{TOP} = \frac{8pH^2}{24(2n_W A_d \cos(\psi))Gk} + \frac{11pH^4}{120E(n_f A_d \sin(\psi) l^2)}$$

the cross-section area of the diagonal elements (A_d) was calculated.

By imposing a tubular thickness (s_1) of 10 mm, the equivalent element diameter of the diagonal element (Φ_1) was determined. Therefore, the enforcement of the stiffness constraint results in:

$$\begin{cases} \Phi_1 = 107.0 \ \ mm \\ s_1 = 10.0 \ \ mm \end{cases}$$

which leads to an equivalent stiffness of the retrofit structure equal to 60.63 [kN/mm].

Representing the retrofitted building as a Timoshenko beam, the connections between the diagrid and the existing building are not considered. Consequently, the result of the stiffness constraint can be compared to the minimum equivalent stiffness ($\tilde{k}$) obtained by the equivalent SDOF system in Section 3.3.

By enforcing the maximum displacement experienced by the DOF1 in case of a seismic event (δ_{MAX}), as equal to the target displacement of the existing building (d_{TOP}) divided by the participation factor of the retrofitted building[8] (Γ_{FIN}), the target ductility demand for the reference case (μ^R) can be calculated (Equation 53).

$$\mu^R = \frac{\delta_{MAX}}{\delta_{y,1}} = \frac{d_{TOP}}{\Gamma_{FIN}} \cdot \frac{1}{\delta_{y,1}} = 1.5 \qquad \textbf{Equation 53}$$

From the Figure 34 in correspondence of a ductility factor (μ) equal to 1.5 (μ^R), the ratio ($\tilde{\lambda}$), between the equivalent stiffness of retrofit structure ($\tilde{k}$) and the stiffness of the existing building (k_1), results to be equal to 1.3 and agrees with the result of the stiffness constraint. More precisely, the ratio between the equivalent stiffness of the retrofit structure obtained from the stiffness constraint (equal to 60.63 [kN/mm]) and the elastic stiffness of the existing building (k_1=45.45 [kN/mm]) leads to the same value of $\tilde{\lambda}$ derived in Figure 34.

The result is confirmed also in the second graph (Figure 36) in which for an existing building period (T_1) equal to 1.15 [s] the same ductility demand (μ^R) is given by a retrofit stiffness ($\tilde{k}$) equal to about 1.3 times the stiffness of the existing building (k_1).

4.3.1.3 Strength constraint

To avoid buckling of the diagonal elements and to meet the strength limit constraint, the second minimum profile features (Φ_2, s_2) were determined by combining the maximum axial force of the diagonals (N_k) and the maximum capacity of the commercial profiles (N_k^{LIM}).

The axial forces in each diagonal element of the diagrid were calculated according to the Eq. **18**. In the reference case, the dead loads related to the diagrid weight were neglected because their magnitude was negligible[9] (Equation 54).

[8] MDOF to SDOF system conversion

[9] It would entail a ±1% axial force

$$N_k = N_{M,k} + N_{V,k} = \frac{M_m d_k}{\sum_{i=1}^{n_k} d_i^2} \cdot \frac{\sin(\psi)}{2} \pm \frac{V_m \cos(\alpha)_k}{\sum_{i=1}^{n_k} \cos(\alpha)_i} \cdot \frac{\cos(\psi)}{2}$$ **Equation 54**

The maximum capacity of the commercial profiles, instead, depends on their cross-section area, on the boundary conditions of the diagonal elements, and the diagrid material (Figure 65).

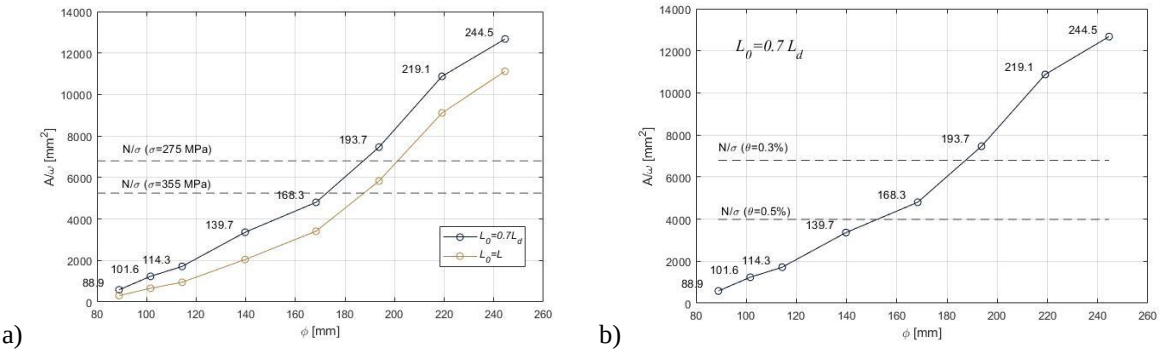

Figure 65: Evaluation of the commercial profile capacity as a function of the technological aspects related to the diagrid structure and the imposed target. a) by varying the boundary condition of the diagonal elements, and the material properties; b) by changing the drift target setting the boundary condition.

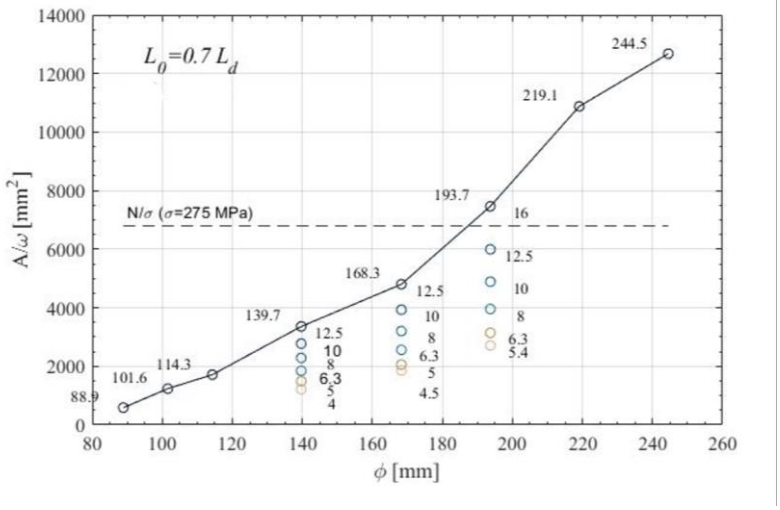

Figure 66: The maximum axial force of the elements and the maximum capacity of the commercial profiles in the reference case. Individuation of the minimum profile that satisfies the strength constraint.

In the reference case, considering a diagrid structure made of S275 steel with diagonal elements fixed at each end ($L_0=0.7L_d$), the required minimum profile is (Figure 66):

$$\begin{cases}\Phi_2 = 193.7 \ \ mm \\ s_2 = 16.0 \ \ mm\end{cases}$$

which leads to a retrofit stiffness equal to 179.21 [kN/mm]. The results of the stiffness and strength constraints are reported in Table 11.

	1st constraint	**2nd constraint**	
Diameter (Φ)	107.0	193.7	[mm]
Thickness (s)	10.0	16.0	[mm]
Stiffness (k)	60.6	179.2	[kN/mm]

Table 11: Results of the 1st and 2nd constraints.

The design profile diameter (Φ_{FIN}, s_{FIN}) was derived as the maximum between Φ_1 and Φ_2.

$$\begin{cases}\Phi_{Fin} = 193.7 \ \ mm \\ s_{Fin} = 16.0 \ \ mm\end{cases}$$

In the reference case, the strength constraint governs the design procedure of the diagrid exoskeleton defining the diagrid exoskeleton features (Φ_2, s_2, k_2), while, from the stiffness constraint the equivalent stiffness of the retrofit solution (diagrid and connections) ($\tilde{k}$) was obtained.

4.3.1.4 Evaluation of the connection properties

Once the equivalent stiffness of the retrofit solution ($\tilde{k}$) and the stiffness of the diagrid exoskeleton (k_2) were defined, the properties of connections (k_{12}, k_i, δ_{y1}) were derived.

The elastic stiffness of the connection (2DOF systems) was derived by means Equation 46:

$$k_{12} = \frac{\tilde{k} \cdot k_2}{k_2 - \tilde{k}}$$

that leads to a connection stiffness (k_{12}) equal to 91.63 [kN/mm].

According to Equation 52, the stiffness of the connection (k_i) at each floor of the reference building was derived as follow:

$$k_i = k_{12} \frac{2}{N+1}$$

Considering the number of floors of the reference building (N) equal to 8, the resulting connection stiffness at each floor (k_i) was equal to 20.36 [kN/mm].

In the case of non-linear connections between the existing building and the diagrid exoskeleton, the non-linear parameters were derived based on the design spectra shown in Figure 48.

Considering an inter-story drift target (θ) equal to 0.3%, for an adimensionalized yielding force (η) of 0.5, the resulting optimal yielding ratio of the connection (β) is 0.1. By multiplying β for the yielding displacement of the reference building (δ_{y1}), the yielding displacement of the connection (δ_{y12}) was derived.

4.3.2 Non-linear analyses and result discussion

The results of the structural design (Section 4.1.1), were validated through non-linear analyses on the FE Model.

4.3.2.1 Non-linear static Pushover analysis of the retrofitted building

The capacity curve of the retrofitted building is plotted in Figure 67 (Blue). The crosses and the rhombus indicate the bucking and the yielding of the diagonal elements, respectively. The numbers indicate the significant points of the existing building capacity curve (brown). More precisely: (1) Infill Cracking (Mid-point), (2) Infill Failure, (3) Stair core limit strength, (4) Plastic hinges in the lateral columns, (5) Plastic hinges at the base of all columns. The black dotted line represents the displacement demands at the Life Safety Limit State (LSLS). The Story displacement and inter-story drift at the LSLS displacement demand are reported.

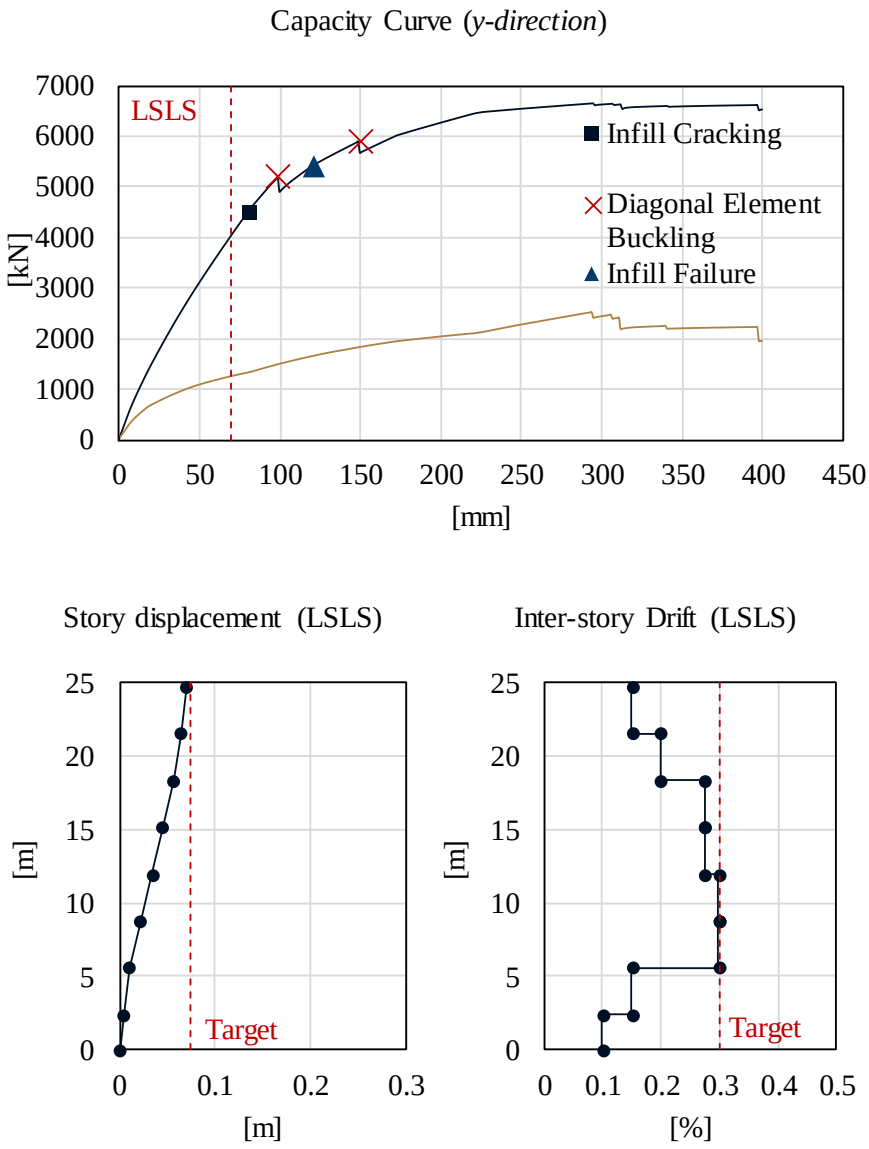

Figure 67: Capacity curve of the retrofitted structure. Capacity curve of the whole system (*black*), and of the existing building (brown) (*Top*); Story displacement and Inter-story drift ratio at the LSLS (*Bottom*).

The Life Safety Limit State target is satisfied, and the buckling of the diagonal elements is avoided. The deformed shape of the retrofitted building at the LSLS displacement demand could be considered as linear and the inter-story drift satisfies the imposed limit target (Figure 67*bottom*). In correspondence with the displacement demand (LSLS) the existing building is still in the elastic range with a few minor cracks developing in the infills.

4.3.2.2 Non-linear Time History analyses

Non-linear Time History analyses were carried out considering (a) the elastic retrofit solution (ES) in which the inelastic behavior of the sole existing building is considered, and (b) the retrofit with dissipative connections (NLS).

Seven accelerograms compatible with the code spectrum of Brescia (soil category C and topography T1) (NTC, 2018) were determined by adopting the software Rexel 2.2beta[10] (Iervolino, et al., 2010). A maximum scale factor equal to 2 and upper and lower tolerances equal to 10%, were imposed (Figure 68).

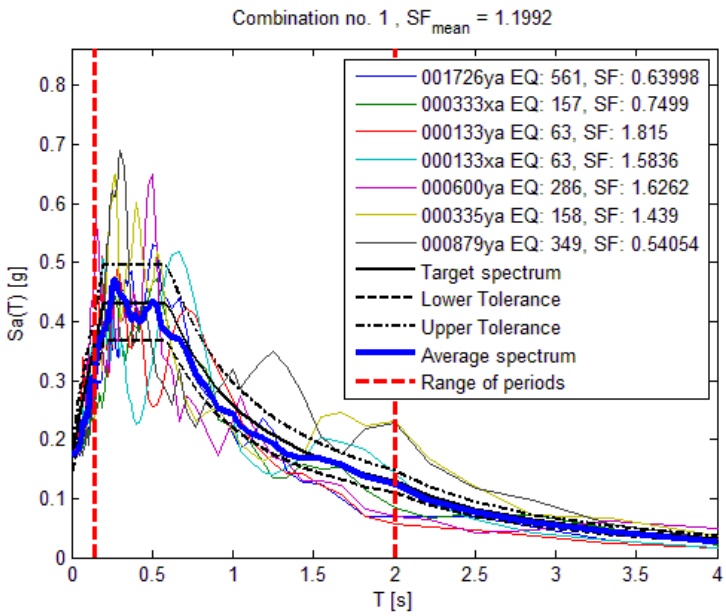

Figure 68: A selected combination of compatible accelerograms used for the time history analyses (Iervolino et al. 2010).

(a) Time History analyses considering the elastic retrofit solution (ES). Comparison with the analytical method.

Time History results of the elastic retrofit solution (ES), expressed in terms of maximum total base shear (V_{MAX}), base shear at the base of the diagrid (V'_{MAX}), maximum base shear on the existing building (V''_{MAX}), maximum axial force on the diagonal elements ($N_{k,MAX}$), top displacement of the existing building (d_{TOP}), and total drift of the existing building (θ_{TOP}), are reported in Table 12.

[10] All the 7 accelerograms are reported in Appendix 5

Accelerograms	V_{MAX}[kN]	V'_{MAX}[kN]	V''_{MAX}[kN]	$N_{k,MAX}$[kN]	d_{TOP}[m]	θ_{TOP} [%]
000133_xa	4506.3	2450.3	1251.9	1961.5	0.060	0.24
000133_ya	4762.1	3509.7	1275.0	2283.3	0.072	0.29
000333_xa	3995.3	2661.7	1319.7	1820.6	0.063	0.25
000335_ya	4428.9	2739.4	1757.3	1855.0	0.065	0.26
000600_ya	5079.5	3628.5	1546.0	2706.5	0.084	0.33
000879_ya	5965.6	4378.8	1594.2	3135.5	0.098	0.39
001726_ya	4800.8	3156.7	1410.5	2178.5	0.063	0.25
Average	**4791.2**	**3217.8**	**1450.7**	**2277.2**	**0.073**	**0.29**
Max	**+24%**	**+36%**	**+21%**	**+18%**	**+34%**	**+34%**

Table 12: Time history analyses results. Elastic retrofit solution (ES).

Results show that both the limit top displacement target of 0.074 (m) and the maximum inter-story drift target are met (Table 12 and Figure 69). The average maximum force in the diagonal elements satisfies the commercial profile limit ($N_{k,LIM}$ was equal to 2456 kN at the ground floor and 2052 kN at the upper floors). It is worth noting that, also if the average values satisfy the imposed target, the absolute maximum results do not satisfy the limit imposed. These results can be justified considering that the values of the pseudo-acceleration of the respective accelerograms (000879_ya) in correspondence of the retrofitted building period (0.40 s) are significantly higher than the target spectrum (until 1.30 times).

In Table 13, the analytic predictions evaluated in accordance with the design procedure described in section 4.1.1, are compared with the average Finite Element Model results demonstrating the accuracy of the design method.

	V_{MAX}[kN]	V'_{MAX}[kN]	V''_{MAX}[kN]	$N_{k,MAX}$[kN]	d_{TOP}[m]	θ_{TOP}[%]
Avg. FEM (ES)	4791.2	3217.8	1450.7	2277.2	0.073	0.29
Analytic Method	5311.6	3976.3	1335.3	2226.3	0.070	0.28
Percentage error	+10%	+20%	-8%	-3%	-3%	-3%

Table 13: Comparison between the analytic method and the FEM results.

The total base shear of the diagrid (V') of 4791.2 kN corresponds to a base shear flow of 150 kN/m thus resulting acceptable for the imposed limit value. As concerns the inter-story shear, the adopted limit value of 628 kN (Antonini, et al., 2017) is exceeded in the floors 6, 7, and 8 and, therefore external diaphragms, bridging the span between the exoskeleton and the existing building, should be introduced in those floors, as shown in Figure 69a.

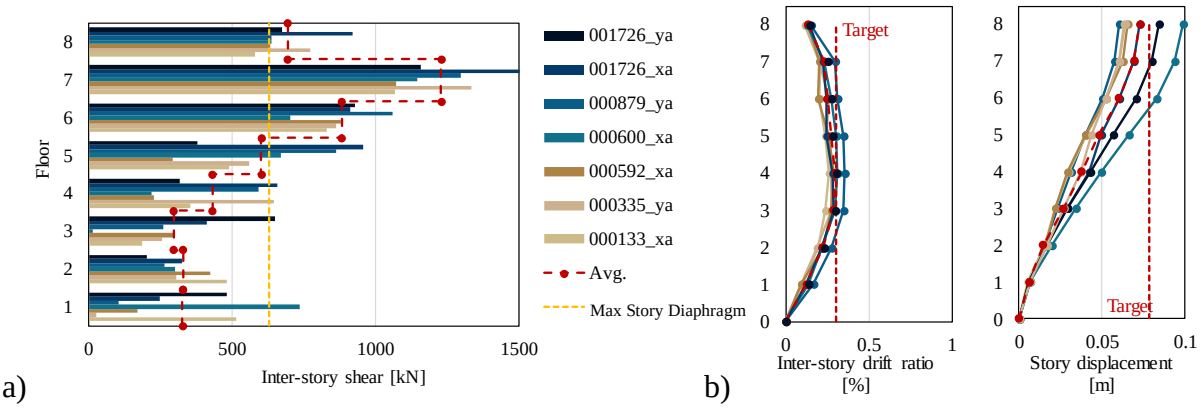

Figure 69: a) Floor shear along the building's height for different accelerograms, b) inter-story drift, and story displacement.

In Figure 70 through a floor by floor evaluation of the maximum forces in the diagonal elements, a comparison between the forces obtained in the numerical FEM analyses and the analytical method shows that the results obtained with the simplified method slightly overestimate the axial forces in the diagonal elements and that the average stress rate of the diagonal elements is always smaller than the buckling limit, particularly at the upper floors.

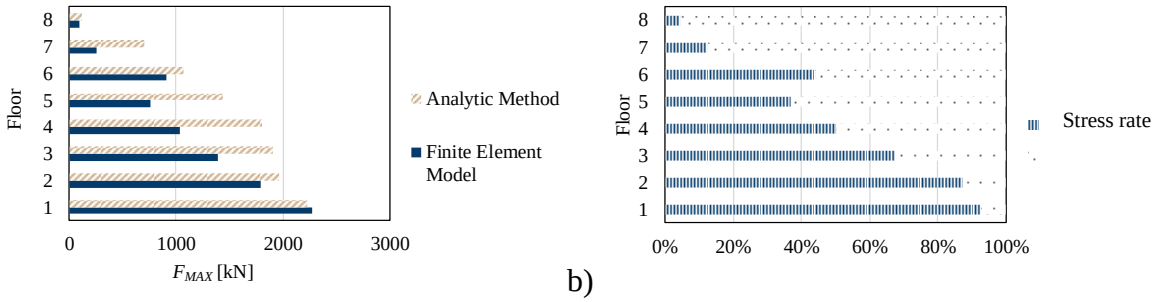

Figure 70: a) Comparison between the forces obtained with the hand calculation method and the finite element model, b) Stress rate of the most solicited diagonal elements at each floor expressed as $N_{k,MAX}/N_{k,LIM}$

Based on these results, a possible way to optimize the elastic diagrid design could be by reducing the cross-section area of the diagonal elements as a function of the relative stress rate and the floor. Interestingly, the optimized diagrid leads to a weight reduction of the structural components equal to 21% increasing the sustainability of the solution.

(b) Time History analyses considering non-linear connections (NLS)

The non-linear connections were modeled by introducing hysteretic links between the existing building and the diagrid exoskeleton on each floor. In Figure 71 the general link and the

parameters introduced to describe the non-linear behavior are shown. In the reference case, the same parameters used in the Bouc-Wen hysteretic model (Section 3.4) were considered.

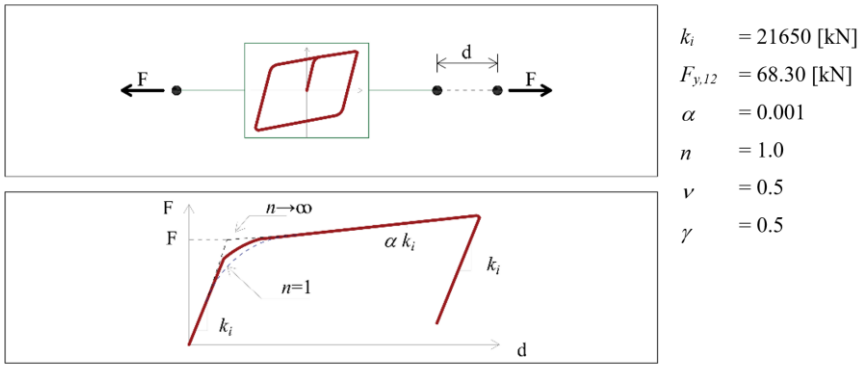

Figure 71: General link introduced in the FEM to model the non-linear behavior of the connections.

Time History results of the non-linear retrofit solution (NLS), expressed in terms of maximum total base shear (V_{MAX}), base shear at the base of the diagrid (V'_{MAX}), maximum base shear on the existing building (V''_{MAX}), maximum axial force on the diagonal elements ($N_{k,MAX}$), top displacement of the existing building (d_{TOP}), and total drift of the existing building (θ_{TOP}), are reported in Table 14.

Accelerograms	V_{MAX}**[kN]**	V'_{MAX}**[kN]**	V''_{MAX}**[kN]**	$N_{k,MAX}$**[kN]**	d_{TOP}**[m]**	θ_{TOP} **[%]**
000133_xa	2774.3	1437.4	1308.1	989.9	0.058	0.23
000133_ya	2645.8	1411.8	1229.9	984.1	0.058	0.23
000333_xa	2355.4	1353.9	1153.2	958.0	0.060	0.24
000335_ya	2994.9	1492.7	1589.5	981.5	0.056	0.23
000600_ya	2522.9	1274.4	1129.5	952.0	0.057	0.23
000878_ya	3413.4	1645.4	1468.5	1132.1	0.074	0.29
001726_ya	2483.6	1359.8	1125.4	961.8	0.046	0.18
Average	**2741.5**	**1425.1**	**1286.4**	**994.2**	0.059	**0.24**
Max	**+24%**	**+15%**	**+14%**	**+14%**	**+21%**	**+21%**

Table 14: Time history analyses results. Non-Linear retrofit solution (NLS).

Here again, the target displacement (d_{TOP}) and inter-story drift (θ), the target shear flow at the base, and the target axial force in the diagonal element ($N_{k,MAX}$) are met. The spread between the average and the maximum values on the non-linear retrofit (NLS) is more controlled than with the elastic retrofit solution (ES). Results in Figure 72, show that, by introducing a non-linear connection between the diagrid and the existing building, the inter-story shear target is

satisfied. The adopted limit value (628 kN) is not exceeded and, therefore, external diaphragms are not needed, as shown in Figure 72a.

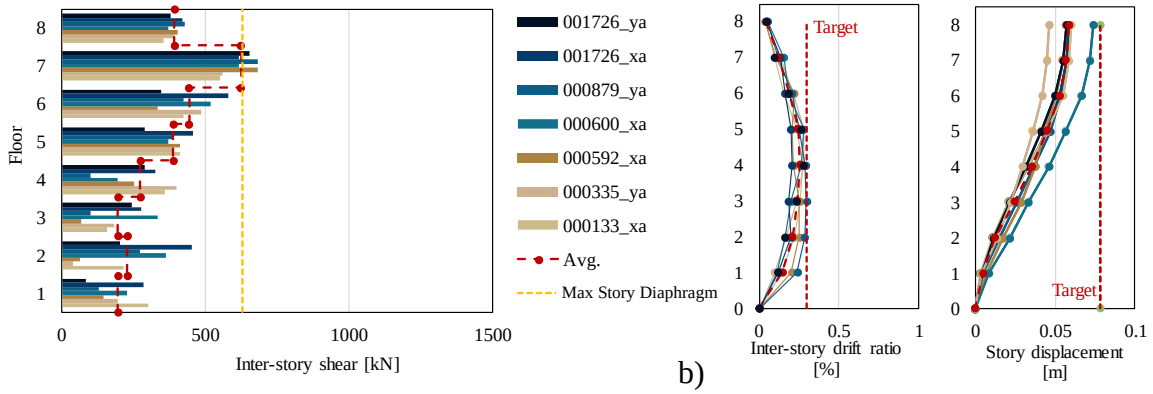

a) b)

Figure 72: a) Floor shear along the building's height for different accelerograms, b) inter-story drift and story displacement.

The results obtained considering non-linear connections (NLS) between the existing building and the diagrid are here compared with the results of the elastic retrofit solution (ES).

	V_{MAX}[kN]	V'_{MAX}[kN]	V''_{MAX}[kN]	$N_{k,MAX}$[kN]	d_{TOP}[m]	θ_{TOP}[%]
FEM (ES)	4791.2	3217.8	1450.7	2277.2	0.073	0.29
FEM (NLS)	2741.5	1425.1	1286.4	994.2	0.059	0.24
Percentage Variation	-43%	-56%	-11%	-56%	-18%	-18%

Table 15: Comparison between the analytic prediction and the numerical FEM results.

The results in Table 15, show a top displacement (d_{TOP}) reduction of 18% and a significant reduction of the seismic action on the retrofitted building when non-linear connections between the existing building and the diagrid (NLS) were introduced. More precisely, a 43% reduction of total base shear (V_{MAX}), and a 56% reduction of diagrid base shear (V'_{MAX}) were obtained. Consequently, the forces in the diagonal elements ($N_{k,MAX}$) (-56% axial force) were substantially reduced. Reducing the axial stress in the diagonal elements, the cross-section area of the diagonals can be re-evaluated. Considering a maximum axial force in the diagonal element ($N_{k,MAX}$) equal to 994.2 kN, the resulting required profile in the case of non-linear retrofit solution would be:

$$\begin{cases} \Phi_{NLS} = 168.3 \ mm \\ s_{NLS} = 12.5 \ mm \end{cases}$$

That lead to a stiffness of the diagrid (k_2) equal to 122.75 kN/mm. Consequently, the stiffness of the connection (k_{12}) was 119.80 kN/mm; which lead to a stiffness of the connection at each floor (k_i) equal to 26.62 kN/mm. It is worth noting that the minimum equivalent stiffness ($\tilde{k}$) of the retrofit solution did not change; therefore, the global response of the retrofitted building was the same as the previous profile.

The reduction of the diagonal cross-section leads to a weight reduction of the structural components equal to 31.5 % (with respect to the constant profile configuration) further increasing the sustainability of the solution.

4.3.3 Adaptive-Responsive Diagrid

A comparison between the proposed solutions and the passive-responsive diagrid is here conducted. Responsive structures, in the reference case, are designed to act as stiff systems for the Damage Limit State, and as dissipative systems for the Life Safety Limit State, therefore avoiding the damage for low-intensity earthquakes and reducing the loads transferred to the floor diaphragms and to the foundations in case of strong earthquakes. The diagonal elements are designed as hinged at the base; for high-intensity earthquakes, beyond a target base shear, the base restraint will downgrade into special non-linear supports allowing for the controlled sliding of the diagrid. Activation of these supports significantly reduces the stiffness of the structure, thus increasing its fundamental period. As a result, seismic loads decrease, and building displacements increase. An excessive horizontal displacement and possible second-order effects are avoided by limiting the maximum displacement of the supports with a bumper at the end of the gap which introduces a $k_2^{III}>0$.

The new supports are designed to be initially rigid ($k_2^{I} \uparrow\uparrow$) and to behave as an elastoplastic system beyond a base shear flow (V_b) of 45 [kN/m]. In addition, an elastic bumper is provided to limit the diagrid displacements at the ground level; the bumper is activated for base displacements greater than 15 [mm]. The hysteresis shape of the diagrid base restraints is shown in Figure 73.

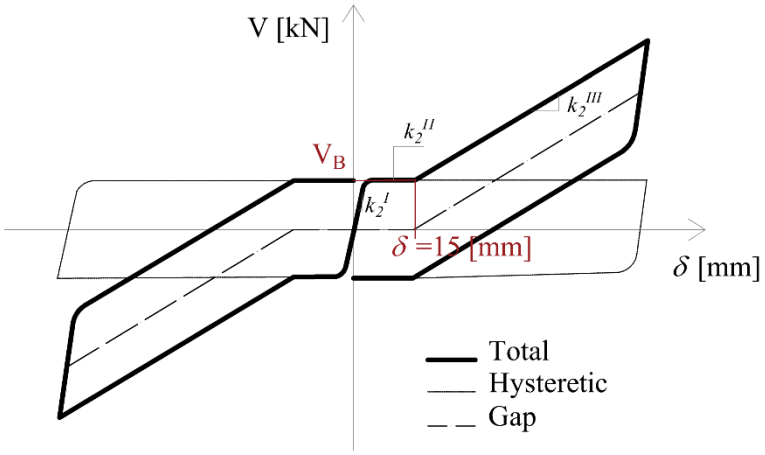

Figure 73: Hysteretic cycle of the sliding support as the sum of elastoplastic support (*dashed line*) and a gap system (*dotted line*).

As a preliminary intervention, the stiff elements are disengaged from the existing RC frame at the ground floor to avoid interference with the lateral displacements. In particular, vertical sliding joints are inserted in the masonry infills and in the RC walls of the staircase wells with a technique similar to what was proposed by Preti et al. (2012). Moreover, to ensure the required ductility, the shear capacity, and the end rotation capacity of the columns are increased by means of fiber-reinforced polymer wrapping. A maximum target inter-story drift of the ground floor equal to 1.0% is here considered. Also in this case non-linear Time Histories were carried out by adopting 7 spectrum-compatible accelerograms.

In Figure 74, the Time History results of the passive-responsive diagrid (*SLIDING*), expressed in terms of maximum total base shear (V_{MAX}), base shear at the base of the diagrid (V'_{MAX}), maximum base shear on the existing building (V''_{MAX}), maximum axial force on the diagonal elements ($N_{k,MAX}$) and top displacement of the existing building (d_{TOP}), are compared with the elastic diagrid (ES) and non-linear diagrid (NLS) results.

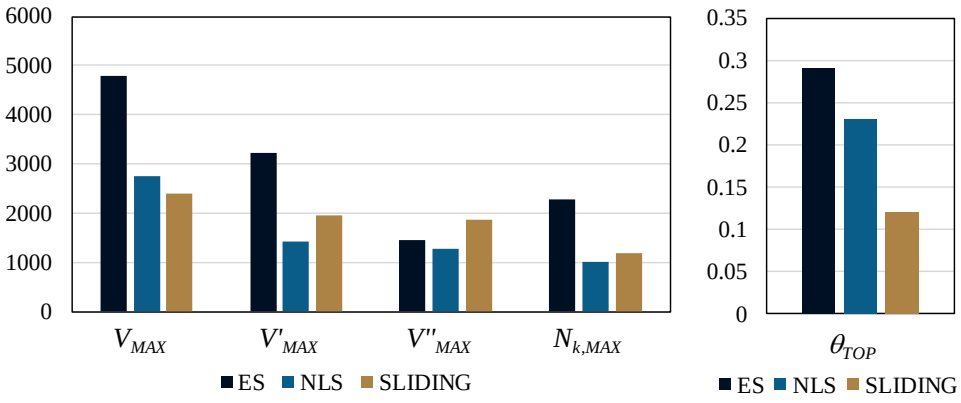

Figure 74: Time history analyses results. Comparison between the results obtained with the elastic diagrid (*ES*), the non-linear diagrid (*NLS*), and the passive-responsive diagrid (*SLIDING*).

Finally, the floor drift and floor shear obtained with the sliding diagrid are reported in Figure 75. The drift distribution shows how the building shifts to a controlled soft story mechanism in the adaptive sliding solution at the Life Safety Limit State (LSLS).

Although the floor loads are reduced with the sliding diagrid solution with respect to a traditional stiff solution, the retrofit of the existing floor diaphragms is still required.

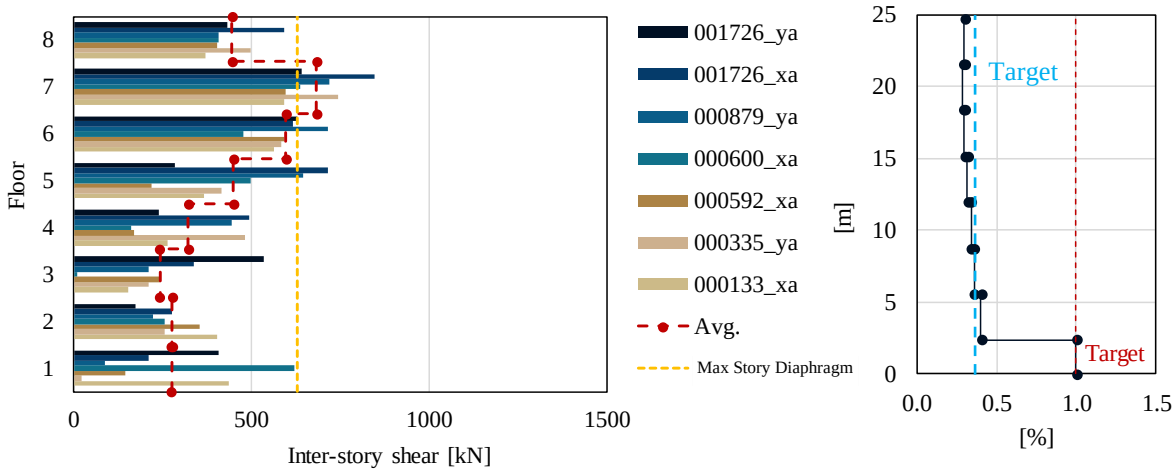

Figure 75: a) Floor shear along the building's height for different accelerograms, b) inter-story drift, and story displacement. The red target (1%) refers to the ground floor; the light blue target (0.3%) refers to the upper floors.

Concluding remarks

To date, despite this urgent need for the renovation of the existing building heritage, the renovation rate in the construction sector is equal to 1.5% because of the major barriers[1], and drawbacks[2] of the current renovation strategies.

To overcome the major barriers and drawbacks to the renovation, a holistic approach tackling all the deficiencies of the existing buildings with an intervention carried out from outside (was introduced to avoid the inhabitant relocation). A new Life-Cycle Perspective was addressed for the conceptual design of the renovation action (Passoni, et al., 2018; Marini, et al., 2018). Introducing a LC Perspective will trigger a paradigm shift in how we deal with existing building performances and needs, with relevant consequences in terms of operative choices, innovative solution sets, and societal challenges and demands. It will lead to a new holistic approach to renovation that will look at the building as a system of interacting subsystems (structural, energy, functional) that evolve with time and need to be maintained and improved to extend its life. That, in turn, requires strong multidisciplinary competences and the synergistic work of researchers from different area and a new LCT-based design framework, conjugating the principles of sustainability, safety and resilience to replace the sectorial codes and traditional design methods should be replaced by a new LCT-based design framework, conjugating the principles of sustainability, safety, and resilience.

The adoption of life cycle thinking principles would completely change the conception of building renovation, redefining qualitative and quantitative performance objectives, design targets, and principles, thereby re-directing research in the construction sector and boosting the design of new integrated retrofitting techniques. Besides the use of eco-compatible materials and renewable resources, additional criteria would define the retrofit design. Reparability, ease of maintenance, adaptability, selective dismantling, demountability, recyclability, and reuse at the end of life would become mandatory features of the retrofit solution. This new perspective would also affect the decision-making process. Minimum environmental footprint and cost

[1] inhabitant' relocation, building disruption, high costs

[2] structural retrofit carried out according to modern codes, that result in retrofitted buildings that are safe and resilient but rather unsustainable and still energy intensive; while energy efficiency measures carried out disregarding structural vulnerability that result in unsafe building, thus resulting both unsustainable and non-resilient

over the life cycle, minimum building downtime, no need for the relocation of the inhabitants, reduction of the duration of the works, and demolition waste management would serve as guiding criteria when selecting the most appropriate strengthening solution.

In this work, following the principles and the guidelines of this new approach to the renovation diagrid exoskeletons were introduced as an innovative strengthening solution of Reinforced Concrete building. Diagrid structures can be carried out from outside and can be complemented with energy efficiency and architectural improvement measures; they comply with the LCT principles and given the high adaptability and flexibility of diagrids compared with other solutions, these structures can be easily adapted in an incremental rehabilitation plan when the initial cost of the retrofit is too demanding or to minimize the existing building disruption.

A proportioning method for elastic diagrid was derived. This method is based on the optimization of the structural performances of the retrofitted building and on the adoption of Life Cycle Thinking principles. The main parameter for the preliminary design of the diagrid are: 1) the geometry of the diagrid module, which depends on the layout of the existing building and on the optimization of the diagonals' inclination angle; 2) the optimization of the diagrid stiffness, which must entail the reduction of the total and inter-story drift of the existing building, as to reduce the possible damage induced by an earthquake; 3) the optimization of the diagonal element cross-section as to avoid the buckling of the elements. Diagrid structures were also conceived to be dissipative and passive -responsive (able to adapt their properties as a function of the seismic event).

Moreover, to evaluate how different diagrid features affect the global response of the retrofitted system and to derive the design diagrid parameters, a sensitivity analysis was carried out considering a simplified 2DOF system representative of ordinary post World War II RC building (DOF1) and the strengthening exoskeleton carried out from outside (DOF2); the 2DOF were connected by a general link. In the sensitivity analyses the connection between the 2ODF was considered both as elastic (ES) and as non-linear (NLS). As far as the non-linear retrofit is concerned, a hysteretic connection was considered; it represents those sacrificial elements that enable localizing damage in the case of an earthquake, thereby reducing the repairing costs and construction time after the seismic event.

From the sensitivity analyses, design spectra were derived. These spectra provide any insight on the parameters that govern the retrofitted structure response, and their optimal setting values (minimum required elastic stiffness (k_{12}), and optimal yielding displacement of the non-linear connection ($\delta_{y,12}$)).

The proportioning method for elastic diagrid and the design spectra results were applied to a reference building representative of ordinary RC post World War II European buildings. Through non-linear analyses, the effectiveness of the design method and the accuracy of the design spectra were proved.

Appendices

Appendix 1

When the retrofit intervention is too much demanding from an economical point of view, incremental rehabilitation strategies can be addressed consistently with a LC approach.

Incremental rehabilitation is an innovative approach to the seismic renovation of the existing building that integrates an ordered series of discrete rehabilitation actions into ongoing facility maintenance and capital improvement activities over an extended period of time. The process involves a series of projects that are planned around regularity scheduled building maintenance, repairs, or renovations, and are timed to coincide with periods of reduced occupancy or use thus reducing the impact on the building activities and reducing the initial costs of the project. This innovative approach has already been developed in the United States through cooperation between researchers and the Federal Emergency Management Agency (FEMA) and in this context, a guideline for the application of incremental strategies to the existing building stock has been made. The main document in this context is the (FEMA P-420, 2009) that has introduced the incremental rehabilitation as an effective alternative to the ordinary options for the renovation of the existing buildings that are:

1. Do nothing: No capital investment is made in improving structural or non-structural performance. This option can include the purchase of earthquake insurance or plan to self-insure for capital losses.
2. Replace: Demolition and reconstruction are carried out in accordance with current building codes. This alternative is generally associated with the greatest cost and lowest overall risk. Financial constraints, historic preservation concerns, and zoning restrictions can make replacement difficult or infeasible. Moreover, this solution has a great impact on the environment and, even more, on the building activities. Very often, the need of relocating all building activities may be the strongest barrier to its renovation.
3. Rehabilitate: Also referred to as “retrofit” of “strengthening”, rehabilitation involves capital investment to improve the structural performance, non-structural performance, or both. A rehabilitation project could be realized in a single stage (as usual) or by adopting incremental strategies.
    a. Single-stage rehabilitation: Pursues all seismic performance objectives in a single step, by incurring all costs and disruption of occupancy and use at once.
    b. Incremental rehabilitation: At the end meets all seismic performance objectives by implementing an ordered series of actions over an extended period of time.

These actions could be integrated into ongoing facility maintenance and capital improvement operations.

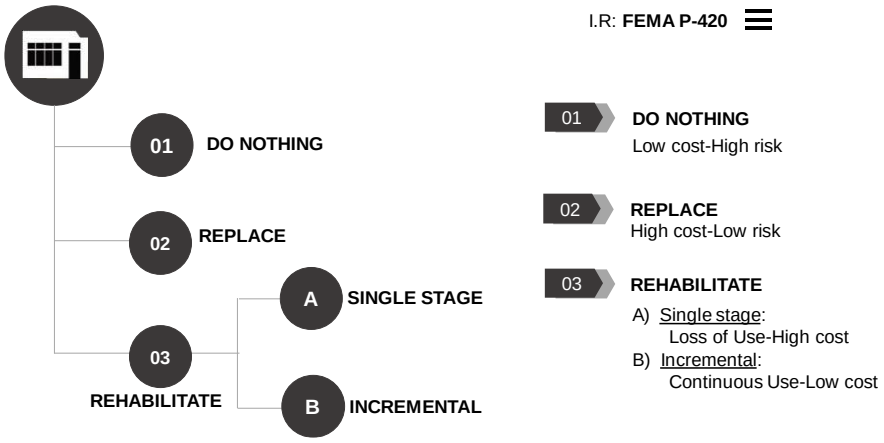

Figure 76: Alternative strategies for the renovation of the existing building proposed by FEMA P-420 (Adapted from. FEMA P-420).

Focusing on the two alternatives of the rehabilitation, FEMA P-420 reported how the benefits of incremental and single-stage seismic rehabilitation were compared. In Figure 77 the incremental rehabilitation strategy is compared to a single-stage rehabilitation project by developing a life-cycle cost/benefit analysis that compares in which, benefits, are expressed as a percentage of the benefits achieved by a full seismic rehabilitation conducted in year zero.

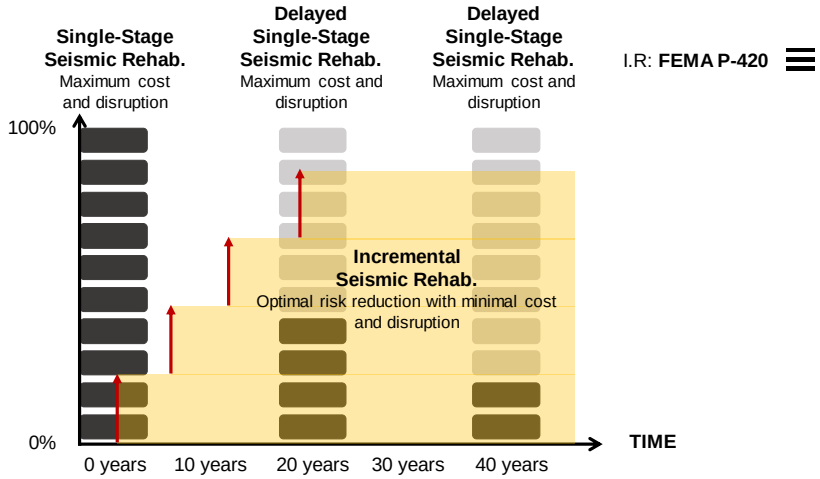

Figure 77:Life-cycle cost/benefit analysis of an incremental rehabilitation project and of single-stage retrofit solutions over an extended period of time. Benefits of the same single-stage rehabilitation project occurring at different years (*dark grey*). Incremental rehabilitation plan benefits (*yellow*).

The results in Figure 77 shows that a series of seismic rehabilitation increments conducted over a defined period of time can produce nearly as many benefits as a single-stage rehabilitation project conducted in year zero. It is worth noting that the relative benefits of a single-stage rehabilitation project occurring in the later years are only a fraction of the benefits of the rehabilitation project at the year zero. Therefore, incremental rehabilitation allows spreading the investment over time, while disruption is less invasive because associated with planned maintenance works. In this way, but anyway achieving, in some steps, the same benefits of a single stage rehabilitation project.

Since rehabilitation work will be staged over an extended period of time, some rehabilitation measures will be implemented sooner and others later: this is the "worst first" approach. Rehabilitation measures can be prioritized based on (FEMA P-420, 2009):

- Structural priority: is influenced by a relative impact on overall seismic performance. Deficiencies that will result in damage with a high consequence of casualties, property loss, or loss of use should be mitigated first. Similarly, rehabilitation measures with a large impact on reducing potential damage (and consequences resulting from that damage) should be implemented first.
- Use priority: is influenced by the importance of current building use and occupancy. Considering an inventory of buildings, building with higher occupant loads, critical functions, high-value equipment or property should be rehabilitated first. Instead, consider a single building, important portions of a structure such as assembly areas and elements of the egress system (e.g., corridors, stairs, lobbies), should be rehabilitated before other less critical areas (FEMA P-420, 2009).

- Integration priority: implies doing first rehabilitation measures associated with ongoing building maintenance or capital improvement activities. This reduces the cost of the seismic rehabilitation activities by taking advantage of construction mobilization, access to the area of work, and disruption of occupancy and use that would have occurred anyway.

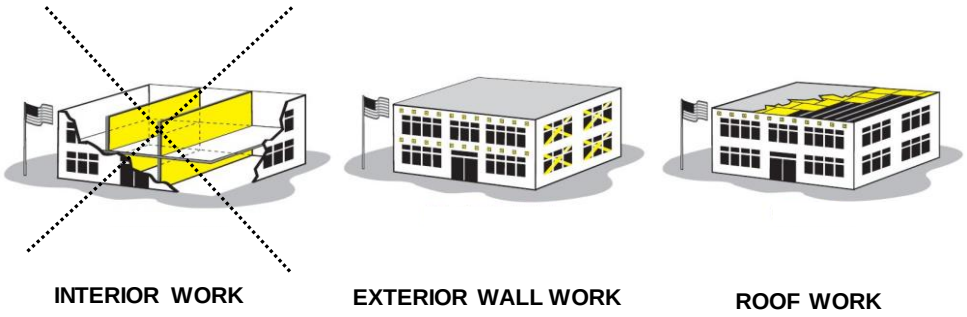

Figure 78: Example of integration priority (From FEMA P-420). Since the retrofit solutions proposed are carried out from outside, the interior works are not considered.

In recent researches (Labò, et al., 2018), structural priority earns higher relevance following the principle that first retrofit actions should be those that have a high impact on the safety of inhabitants and prevent heavy losses. A new concept to be combined with incremental rehabilitation is thus introduced, that is, the definition of minimum intervention (Figure 79). In fact, the order of retrofit actions should be planned according to the definition of some level of safety and performance to be guaranteed, especially for the first step of the process.

The minimum intervention can be defined as such intervention that completely removes the main critical aspects and so the heavy potential casualties, as building collapse and risks for inhabitants. To define a minimum intervention, it is necessary to investigate the seismic vulnerabilities of the building and identify those repair actions that solve the main ones. Those actions cannot be defined a priori for any building, but they would depend on the kind of structure and on its level of safety.

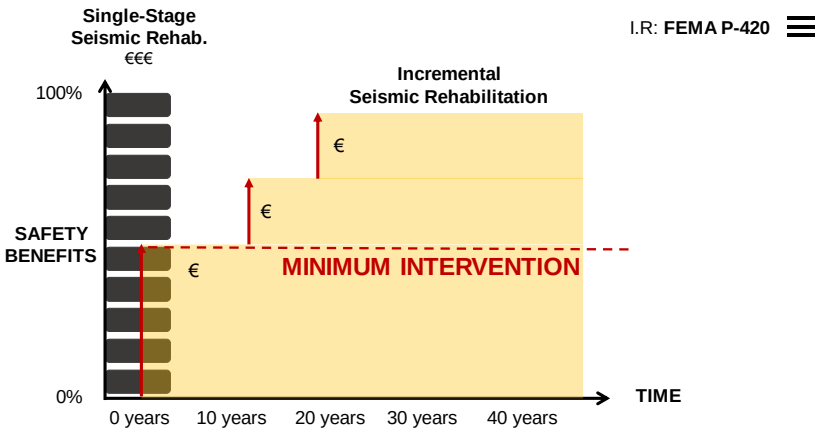

Figure 79: Life-cycle cost/benefit analysis of an incremental rehabilitation project and of single-stage retrofit solutions over an extended period of time introducing the innovative concept of minimum intervention (*red dotted line*).

Building typology for the seismic incremental rehabilitation

Given these premises on the incremental rehabilitation, adopting an incremental rehabilitation strategy is particularly suited for every situation in which a one-step rehabilitation project can result difficult to sustain in terms of costs and execution time. Moreover, the adoption of an incremental rehabilitation strategy gives the possibility to exploit the inactivity or low-use periods of the existing building thus significantly reducing the impact in the building activities. Basing on these premises FEMA outline a series of building type particularly adapted for the adoption of an incremental rehabilitation strategy. These are:

- Hotels and tourist establishment, where intervention can be planned during low season periods;
- Hospitals: for which is not possible consider periods with reduced use, but each incremental step can be localized in some specific area, to reduce consumer disruption.
- Office buildings: inactivity summer periods can be exploited to plan the incremental steps;
- Industrial buildings: few specific minimal actions can be planned to reduce seismic risk, safeguarding workers lives;
- Schools: which undoubtedly offers the opportunity to adopt an incremental rehabilitation strategy by exploiting the inactivity summer and winter that are quite long and regular in time. FEMA 395 (2003) provides guidelines for the design of seismic incremental rehabilitation strategies on school buildings.

It is worth noting that FEMA does not introduce the residential sector as a suitable case for the adoption of an incremental rehabilitation strategy; however, incremental rehabilitation strategy is a good option also for residential buildings to reduce the initial costs of the retrofit solution and significantly increase the feasibility of the renovation. As already said, one of the major barriers to the renovation is the high cost of the retrofit solution.

Appendix 2

Seven accelerograms compatible with the code spectrum were determined by adopting the software Rexel 2.2beta (Iervolino, et al., 2010). The records are real earthquakes (Figure 81) scaled to fit L'Aquila Response Spectrum at the Life Safety Limit State (LSLS) considering a flat surface made of deposit of sand or medium-dense sand gravel or stiff grave (soil category C and T1 topography) (NTC, 2018). A maximum scale factor equal to 2 and upper and lower tolerance equal to 10% and 15%, were imposed (Figure 80).

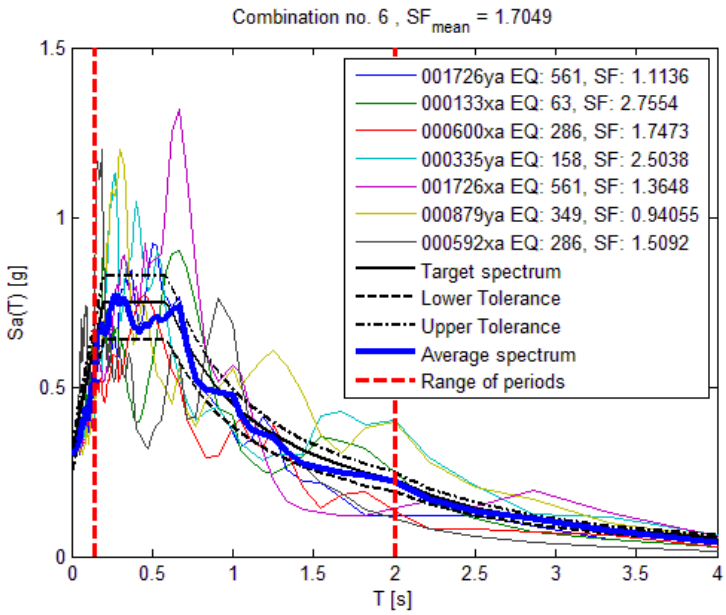

Figure 80: Selected combination of compatible accelerograms used for the time history analyses (Iervolino et al. 2010).

Earthquake Name	Date	Mw	Fault Mechanism	Epicentral Distance	PGA_X [m/s^2]	PGA_Y [m/s^2]	PGV_X [m/s]	PGV_Y [m/s]
Adana	27/06/1998	6.30	strike slip	30.00	2.16	2.64	0.28	0.20
Friuli (aftershock)	15/09/1976	6.00	thrust	9.00	1.07	0.93	0.11	0.11
Umbria Marche	26/09/1997	6.00	normal	22.00	1.69	1.04	0.14	0.12
Alkion	25/02/1981	6.30	normal	25.00	1.14	1.18	0.11	0.15
Adana	27/06/1998	6.30	strike slip	30.00	2.16	2.64	0.28	0.20
Dinar	01/10/1995	6.40	normal	8.00	2.67	3.13	0.29	0.41
Umbria Marche	26/09/1997	6.00	normal	5.00	1.95	2.18	0.17	0.14

Table 16: Real earthquake considered. From the European strong-motion database.

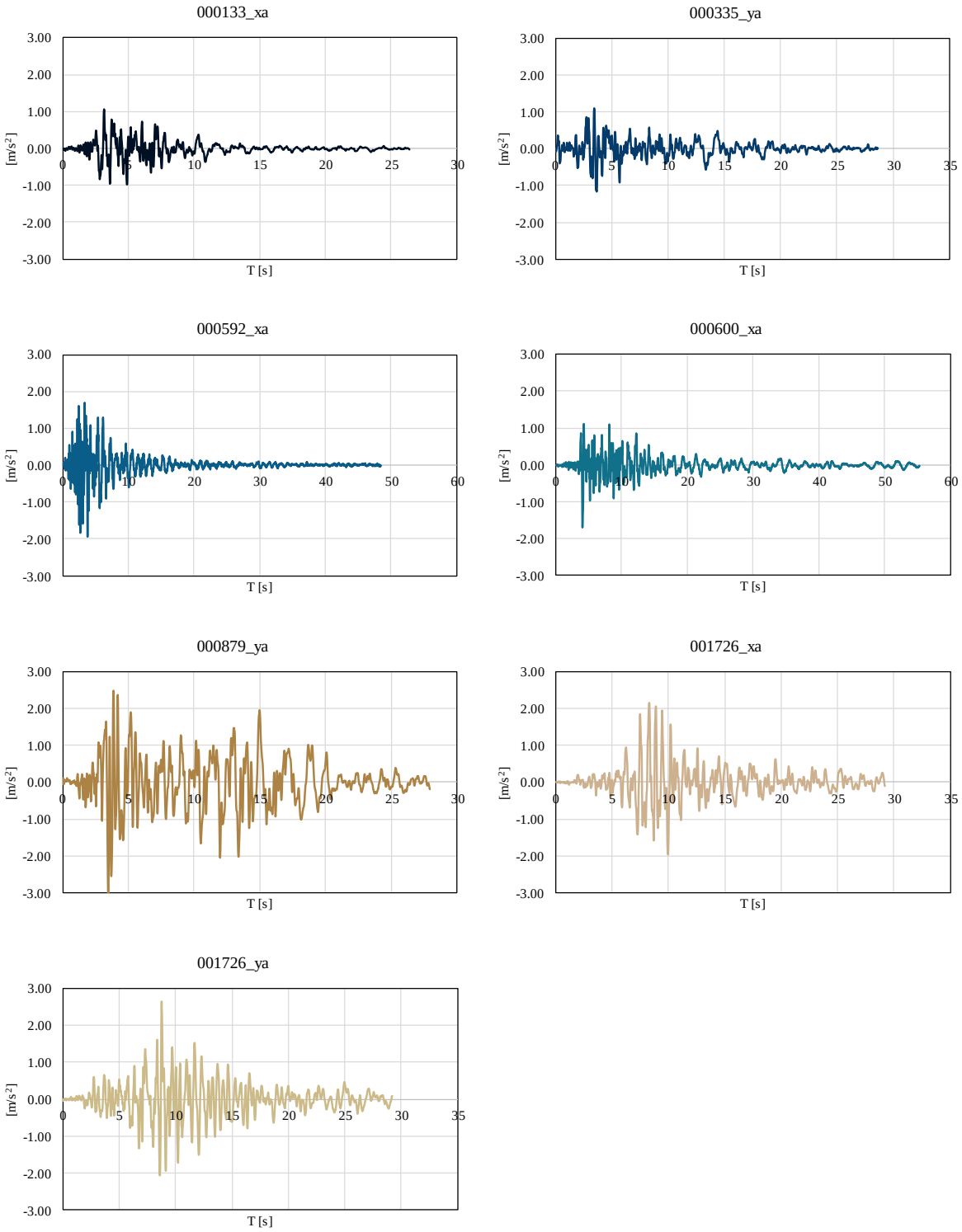

Figure 81: Seven accelerograms considered (Iervolino et al. 2010).

Appendix 3

The original structural documents are here reported. For each component of the reference building, the load analysis is reported.

Three stratigraphies for three typologies of inter-story floor were considered: 1) for the floors from 1 to 7; 2) for the attic floor; 3) for the roof. The thickness of the inter-story is variable. In the Load analysis, the thicker inter-story floor was considered for each typology.

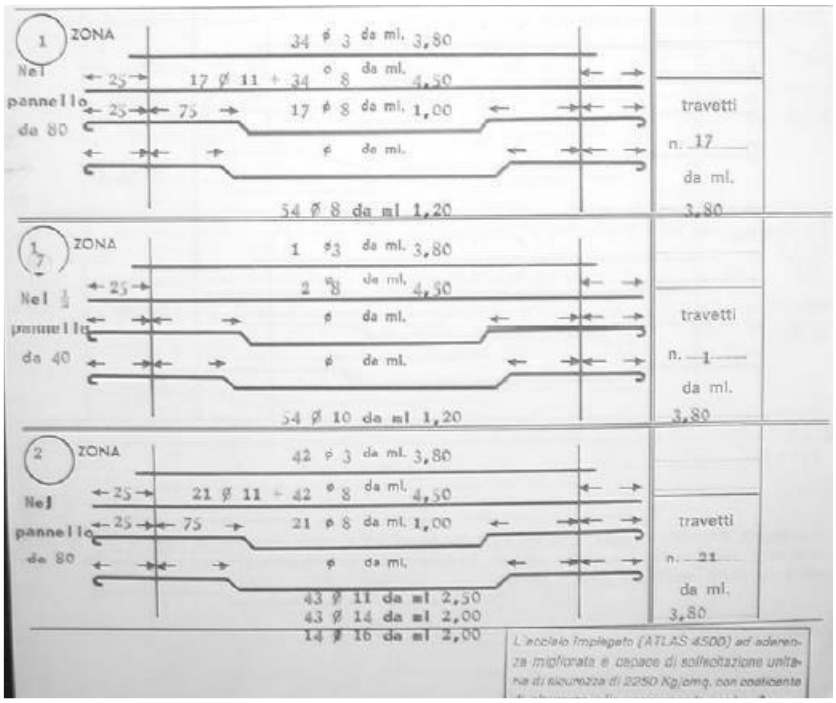

Figure 82: Inter-story floor steel rebars. (IDES, 2008).

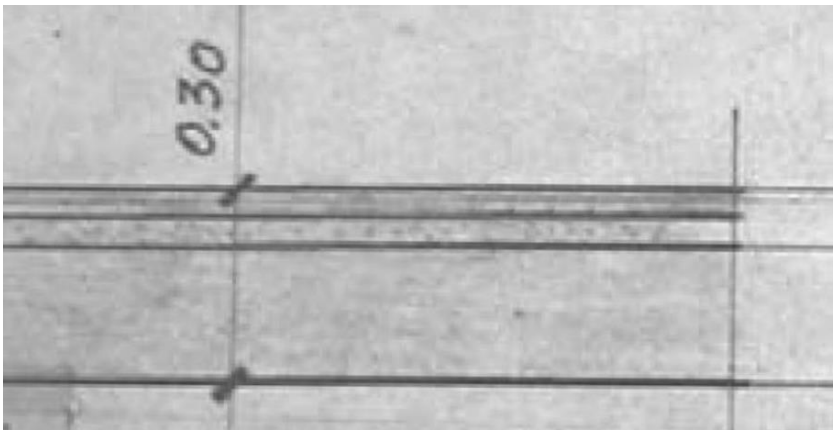

Figure 83: Section of the inter-story floor (1st typology) (IDES, 2008).

1) Floors from 1 to 7	Load [kN/m^2]

Self-weight (20+4 cm)	2.50
Floor finishing	0.34
Mortar slab (4 cm)	0.76
Plaster	0.30
Internal partitions	0.80
Dead and live loads	4.70
Variable loads	2.00
Total	**6.70**
2) Attic Floor	
Self-weight (20+2 cm)	2.30
Plaster	0.30
Dead and live loads	2.60
Variable loads	0.50
Total	**3.30**
3) Roof	
Self-weight (20 cm)	2.30
Waterproof case and tiles	0.95
Dead and live loads	3.25
Variable loads	0.50+1.50
Total	**5.25**

Table 17:Load analysis: three typologies of inter-story floor.

Another stratigraphy was considered for the balconies (Figure 84).

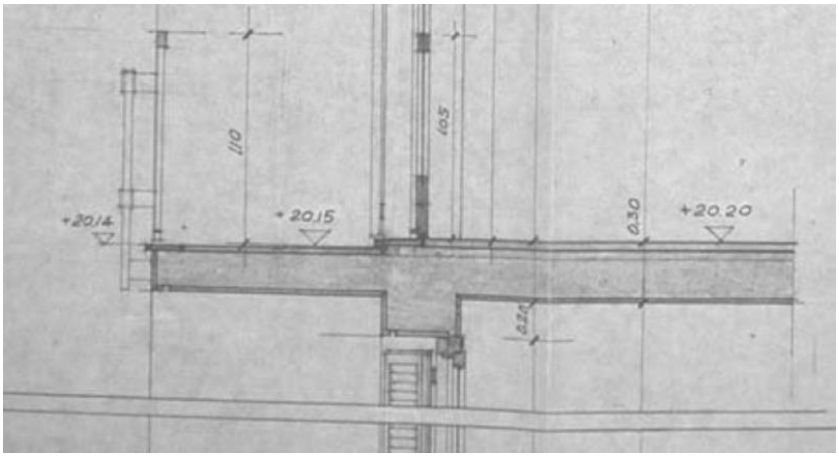

Figure 84: Balcony (IDES 2008).

Balconies	

Self-weight (20+2 cm)	2.5
Finishing	0.61
Mortar slab (4 cm)	0.44
Dead and live loads	3.90
Variable loads	4.00
Total	**7.90**

Table 18: Load analysis: balcony of the reference case.

As far as the internal partitions 0.80 kN/m^2 are considered while the external infills are made of Hollow bricks (35cm). The staircase is made of reinforced walls of thickness included between 20 and 25 [cm] (Figure 85), and the load analysis is reported in Table 19.

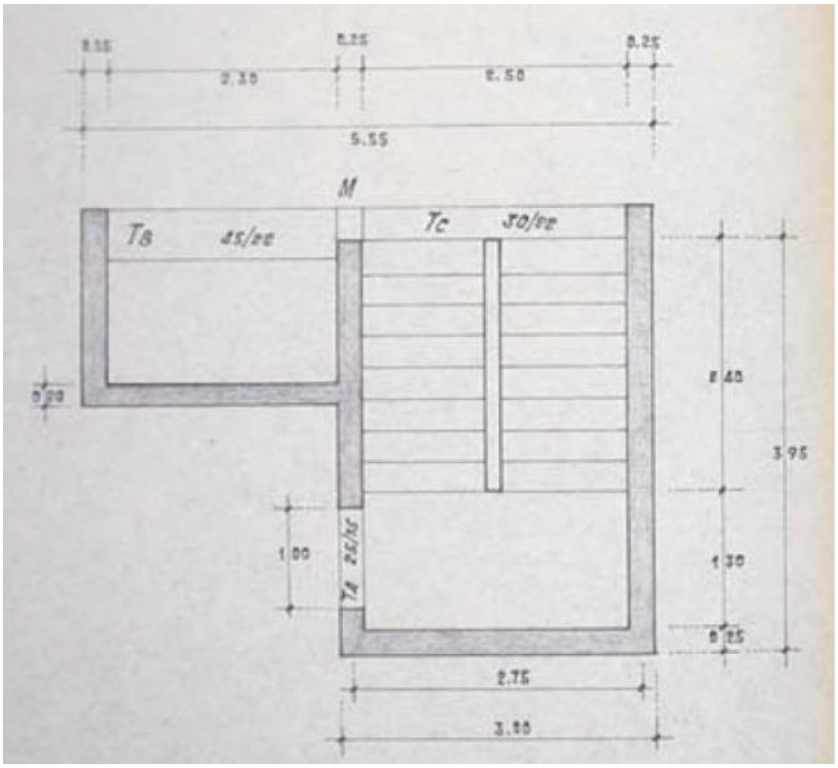

Figure 85: Staircase and elevator cores (IDES 2008).

External infills	**Load [kN/m^2]**
Hollow bricks (35cm) + double layer plaster	**13.40**
Staircase core	**Load [kN/m^2]**
Wall 20+4	
Plaster	**0.30**
RC Wall (20 cm)	**0.50**
Plaster	**0.30**
Total	**5.60**
Wall 25+4	
Plaster	**0.30**
RC Wall (25 cm)	**6.25**
Plaster	**0.30**
Total	**6.85**

Table 19: Load analysis:External infills and staircase core.

As far as the bearing frame of the reference building, the main features of columns and beams are reported in Figure 87÷Figure 95 (IDES, 2008). The Column number is reported in Figure 86, while the beams are indicated by means the numbers of the two supports (columns).

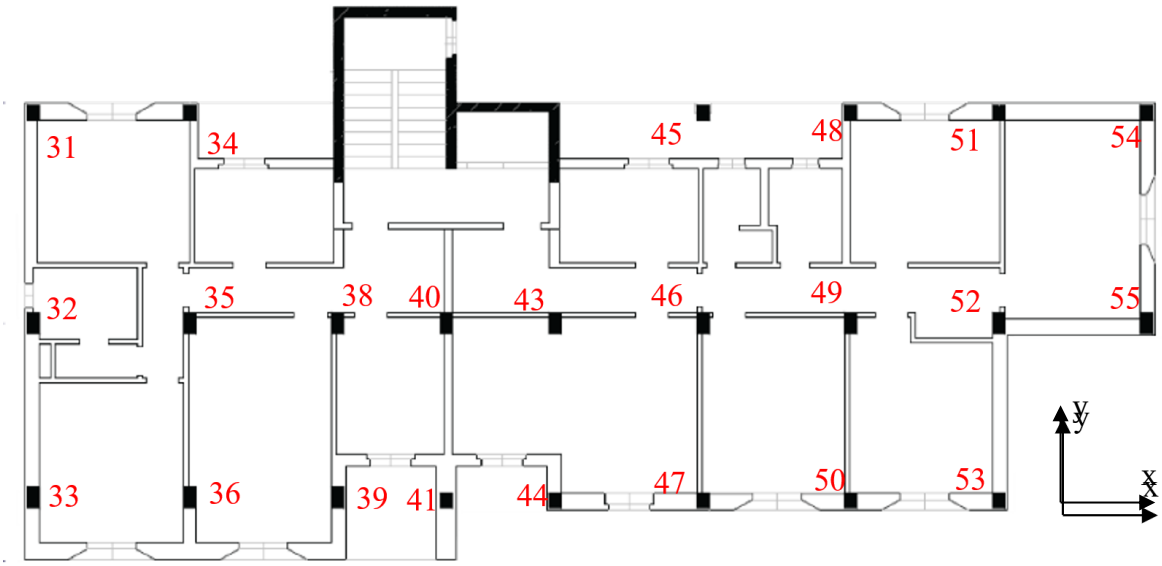

Figure 86: Plan of the East building with indicated the number of the columns (IDES 2008).

Ground Floor

Column	Lx [cm]	Ly [cm]	Steel rebars	Stirrup
31	30	40	4Φ14+2Φ12	Φ6/20
32	30	60	6Φ16	Φ6/20
33	30	50	6Φ14	Φ6/20
34	45	30	6Φ14	Φ6/20
35	30	60	6Φ16	Φ6/20
36	30	60	6Φ16	Φ6/20
38	30	50	6Φ14	Φ6/20
39	30	50	6Φ14	Φ6/20
40	30	50	6Φ14	Φ6/20
41	30	60	6Φ16	Φ6/20
43	30	50	6Φ14	Φ6/20
44	30	50	6Φ14	Φ6/20
45	30	50	6Φ14	Φ6/20
46	30	60	6Φ16	Φ6/20
47	45	30	6Φ14	Φ6/20
48	45	30	6Φ14	Φ6/20
49	30	60	6Φ16	Φ6/20
50	45	30	6Φ14	Φ6/20
51	45	30	6Φ14	Φ6/20
52	30	60	6Φ16	Φ6/20
53	30	50	6Φ14	Φ6/20
54	30	35	4Φ14+2Φ10	Φ6/20
55	30	35	4Φ14+2Φ10	Φ6/20

Figure 87: Ground floor column structural details (IDES 2008).

First Floor

Column	Lx [cm]	Ly [cm]	Steel rebars	Stirrup
31	30	35	4Φ14+2Φ10	Φ6/20
32	30	50	6Φ14	Φ6/20
33	30	40	4Φ14+2Φ12	Φ6/20
34	40	30	4Φ14+2Φ12	Φ6/20
35	30	50	6Φ14	Φ6/20
36	30	50	6Φ14	Φ6/20
38	30	40	4Φ14+2Φ12	Φ6/20
39	30	40	4Φ14+2Φ12	Φ6/20
40	30	40	4Φ14+2Φ12	Φ6/20
41	30	50	6Φ14	Φ6/20
43	30	40	4Φ14+2Φ12	Φ6/20
44	30	40	4Φ14+2Φ12	Φ6/20
45	30	40	4Φ14+2Φ12	Φ6/20
46	30	50	6Φ14	Φ6/20
47	40	30	4Φ14+2Φ12	Φ6/20
48	40	30	4Φ14+2Φ12	Φ6/20
49	30	50	6Φ14	Φ6/20
50	40	30	4Φ14+2Φ12	Φ6/20
51	40	30	4Φ14+2Φ12	Φ6/20
52	30	50	6Φ14	Φ6/20
53	30	40	4Φ14+2Φ12	Φ6/20
54	30	30	4Φ14	Φ6/20
55	30	30	4Φ14	Φ6/20

Figure 88: First-floor column structural details (IDES 2008).

Second Floor

Column	Lx [cm]	Ly [cm]	Steel rebars	Stirrup
31	30	30	4Φ14	Φ6/20
32	30	40	4Φ14+2Φ12	Φ6/20
33	30	35	4Φ14+2Φ10	Φ6/20
34	35	30	4Φ14+2Φ10	Φ6/20
35	30	40	4Φ14+2Φ12	Φ6/20
36	30	40	4Φ14+2Φ12	Φ6/20
38	30	35	4Φ14+2Φ10	Φ6/20
39	30	35	4Φ14+2Φ10	Φ6/20
40	30	35	4Φ14+2Φ10	Φ6/20
41	30	40	4Φ14+2Φ12	Φ6/20
43	30	35	4Φ14+2Φ10	Φ6/20
44	30	35	4Φ14+2Φ10	Φ6/20
45	30	35	4Φ14+2Φ10	Φ6/20
46	30	40	4Φ14+2Φ12	Φ6/20
47	35	30	4Φ14+2Φ10	Φ6/20
48	35	30	4Φ14+2Φ10	Φ6/20
49	30	40	4Φ14+2Φ12	Φ6/20
50	35	30	4Φ14+2Φ10	Φ6/20
51	35	30	4Φ14+2Φ10	Φ6/20
52	30	40	4Φ14+2Φ12	Φ6/20
53	30	35	4Φ14+2Φ10	Φ6/20
54	30	30	4Φ14	Φ6/20
55	30	30	4Φ14	Φ6/20

Figure 89: Second-floor column structural details (IDES 2008).

Third Floor

Column	Lx [cm]	Ly [cm]	Steel rebars	Stirrup
31	30	30	4Φ14	Φ6/20
32	30	35	4Φ14+2Φ10	Φ6/20
33	30	30	4Φ14	Φ6/20
34	30	30	4Φ14	Φ6/20
35	30	35	4Φ14+2Φ10	Φ6/20
36	30	35	4Φ14+2Φ10	Φ6/20
38	30	30	4Φ14	Φ6/20
39	30	30	4Φ14	Φ6/20
40	30	30	4Φ14	Φ6/20
41	30	35	4Φ14+2Φ10	Φ6/20
43	30	30	4Φ14	Φ6/20
44	30	30	4Φ14	Φ6/20
45	30	30	4Φ14	Φ6/20
46	30	35	4Φ14+2Φ10	Φ6/20
47	30	30	4Φ14	Φ6/20
48	30	30	4Φ14	Φ6/20
49	30	35	4Φ14+2Φ10	Φ6/20
50	30	30	4Φ14	Φ6/20
51	30	30	4Φ14	Φ6/20
52	30	35	4Φ14+2Φ10	Φ6/20
53	30	30	4Φ14	Φ6/20
54	30	30	4Φ14	Φ6/20
55	30	30	4Φ14	Φ6/20

Figure 90: Third-floor column structural details (IDES 2008).

Fourth-Fifth-Sixth Floor

Column	Lx [cm]	Ly [cm]	Steel rebars	Stirrup
31	30	30	4Φ14	Φ6/20
32	30	30	4Φ14	Φ6/20
33	30	30	4Φ14	Φ6/20
34	30	30	4Φ14	Φ6/20
35	30	30	4Φ14	Φ6/20
36	30	30	4Φ14	Φ6/20
38	30	30	4Φ14	Φ6/20
39	30	30	4Φ14	Φ6/20
40	30	30	4Φ14	Φ6/20
41	30	30	4Φ14	Φ6/20
43	30	30	4Φ14	Φ6/20
44	30	30	4Φ14	Φ6/20
45	30	30	4Φ14	Φ6/20
46	30	30	4Φ14	Φ6/20
47	30	30	4Φ14	Φ6/20
48	30	30	4Φ14	Φ6/20
49	30	30	4Φ14	Φ6/20
50	30	30	4Φ14	Φ6/20
51	30	30	4Φ14	Φ6/20
52	30	30	4Φ14	Φ6/20
53	30	30	4Φ14	Φ6/20
54	30	30	4Φ14	Φ6/20
55	30	30	4Φ14	Φ6/20

Figure 91: Fourth-Fifth-Sixth floor column structural details (IDES 2008).

Seventh-Eighth Floor

Column	Lx [cm]	Ly [cm]	Steel rebars	Stirrup
31	30	30	4Φ14	Φ6/20
32	30	30	4Φ14	Φ6/20
33	30	30	4Φ14	Φ6/20
34	30	30	4Φ14	Φ6/20
35	30	30	4Φ14	Φ6/20
36	30	30	4Φ14	Φ6/20
38	30	30	4Φ14	Φ6/20
39	30	30	4Φ14	Φ6/20
40	30	30	4Φ14	Φ6/20
41	30	30	4Φ14	Φ6/20
43	30	30	4Φ14	Φ6/20
44	30	30	4Φ14	Φ6/20
45	30	30	4Φ14	Φ6/20
46	30	30	4Φ14	Φ6/20
47	30	30	4Φ14	Φ6/20
48	30	30	4Φ14	Φ6/20
49	30	30	4Φ14	Φ6/20
50	30	30	4Φ14	Φ6/20
51	30	30	4Φ14	Φ6/20
52	30	30	4Φ14	Φ6/20
53	30	30	4Φ14	Φ6/20

Figure 92: Seventh-Eighth floor column structural details (IDES 2008).

Floors from 1 to 7				Middle		Support	
Columns	[cm]	[cm]	Srirrup	Steel rebars (Top)	(Bottom)	(Top)	Steel rebars (Bottom)
53-50	30	42	Φ6/20	4Φ12	2Φ10	2Φ12	2Φ10+2Φ12
54-51	30	42	Φ6/20	4Φ12	2Φ10	2Φ12	2Φ10+2Φ12
45-48	30	42	Φ6/20	2Φ10+2Φ12	2Φ10	2Φ12	4Φ10
50-47	30	42	Φ6/20	2Φ10+2Φ12	2Φ10	2Φ12	4Φ10
51-48	30	42	Φ6/20	2Φ10+2Φ12	2Φ10	2Φ12	4Φ10
47-44	30	42	Φ6/20	2Φ12+2Φ14	2Φ10	2Φ12	2Φ10+2Φ14
44-41	30	42	Φ6/20	3Φ12	2Φ10	2Φ12	2Φ10+1Φ12
41-39	30	42	Φ6/20	2Φ14	2Φ14	2Φ14	2Φ14
52-53	30	42	Φ6/20	4Φ10	2Φ10	2Φ10	4Φ10
52-55	30	42	Φ6/20	4Φ12	2Φ10	2Φ12	2Φ10+2Φ12
54-55	30	42	Φ6/20	2Φ10+2Φ12	2Φ10	2Φ10	2Φ10+2Φ12
45-Wall	30	42	Φ6/20	4Φ12	2Φ10	2Φ12	2Φ10+2Φ12
Wall-34	30	42	Φ6/20	4Φ12	2Φ10	2Φ12	2Φ10+2Φ12
34-31	30	42	Φ6/20	2Φ12+2Φ14	2Φ10	2Φ12	2Φ10+2Φ14
31-32	30	42	Φ6/20	2Φ10+2Φ12	2Φ10	2Φ10	2Φ10+2Φ12
32-33	30	42	Φ6/20	4Φ10	2Φ10	2Φ10	4Φ10
35-38	70	22	Φ8/20	7Φ12	3Φ10	3Φ12	4Φ12+3Φ10
46-43	70	22	Φ8/20	7Φ12	3Φ10	3Φ12	4Φ12+3Φ10
38-40	70	22	Φ8/20	4Φ12	3Φ10	3Φ12	3Φ10+1Φ12
43-40	70	22	Φ8/20	4Φ12	3Φ10	3Φ12	3Φ10+1Φ12
52-49	80	22	2Φ8/20	2Φ10+6Φ12+2Φ14	4Φ10	2Φ10+4Φ12	4Φ10+2Φ12+2Φ14
49-46	80	22	2Φ8/20	8Φ12+2Φ10	4Φ10	4Φ10+2Φ12	4Φ10+4Φ12
35-35	90	22	2Φ8/20	4Φ12+4Φ14	4Φ10	4Φ10+4Φ14	4Φ12
39-36	90	22	2Φ8/20	8Φ12	4Φ10	4Φ10+4Φ12	4Φ12
36-33	90	22	2Φ8/20	4Φ12+4Φ14	4Φ10	4Φ12	4Φ10+4Φ14

Figure 93: Beam structural details (floors from 1 to 7) (IDES 2008).

Attic floor				Middle		Support	
Columns	[cm]	[cm]	Srirrup	Steel rebars (Top)	(Bottom)	(Top)	Steel rebars (Bottom)
31-34	30	42	Φ6/20	2Φ12	2Φ12	2Φ12	2Φ12
34-Wall	30	42	Φ6/20	2Φ12	2Φ12	2Φ12	2Φ12
48-51	30	42	Φ6/20	2Φ12	2Φ12	2Φ12	2Φ12
53-50	30	42	Φ6/20	2Φ12	2Φ12	2Φ12	2Φ12
41-44	30	42	Φ6/20	2Φ12	2Φ12	2Φ12	2Φ12
31-32	30	42	Φ6/20	2Φ12	2Φ12	2Φ12	2Φ12
32-33	30	42	Φ6/20	2Φ12	2Φ12	2Φ12	2Φ12
51-52	30	42	Φ6/20	2Φ12	2Φ12	2Φ12	2Φ12
52-53	30	42	Φ6/20	2Φ12	2Φ12	2Φ12	2Φ12
47-50	30	42	Φ6/20	2Φ12+2Φ14	2Φ12	2Φ12	2Φ12+2Φ14
44-47	30	42	Φ6/20	2Φ12+2Φ14	2Φ12	2Φ12	2Φ12+2Φ14
49-52	50	22	Φ6/15	3Φ12+2Φ14	3Φ10	3Φ12	3Φ10+2Φ14
46-49	50	22	Φ6/15	3Φ12+2Φ14	3Φ10	3Φ12	3Φ10+2Φ14
43-46	50	22	Φ6/15	3Φ12+2Φ14	3Φ10	3Φ12	3Φ10+2Φ14
40-43	50	22	Φ6/15	3Φ12	3Φ10	3Φ12	3Φ10
38-40	50	22	Φ6/15	2Φ12+1Φ14	3Φ10	2Φ12+1Φ14	3Φ10
32-35	50	22	Φ6/15	2Φ12+3Φ14	3Φ10	2Φ12+1Φ14	3Φ10+2Φ14
35-38	50	22	Φ6/15	4Φ12+1Φ14	3Φ10	2Φ12+1Φ14	3Φ10+2Φ12
Wall-45	30	30	Φ6/20	2Φ10	2Φ10	2Φ10	2Φ10
45-48	30	30	Φ6/20	2Φ10	2Φ10	2Φ10	2Φ10
33-36	40	22	Φ6/15	2Φ12+2Φ14	2Φ12	2Φ12	2Φ12+2Φ14
36-39	40	22	Φ6/15	4Φ12	2Φ12	2Φ12	4Φ12
39-41	40	22	Φ6/15	2Φ12	2Φ12	2Φ12	2Φ12

Figure 94: Beam structural details (attic floor) (IDES 2008).

Roof				Middle		Support	
Columns	Base [cm]	Height [cm]	Srirrup	Steel rebars (Top)	Steel rebars (Bottom)	Steel rebars (Top)	Steel rebars (Bottom)
32-35	30	35-40	Φ8/20	4Φ12	3Φ10	2Φ12	3Φ10+2Φ12
35-38	30	35-40	Φ8/20	2Φ10+2Φ12	3Φ10	2Φ12	5Φ10
38-40	30	35-40	Φ8/20	2Φ12	2Φ10	2Φ12	2Φ10
40-43	30	35-40	Φ8/20	2Φ12	2Φ10	2Φ12	2Φ10
43-46	30	35-40	Φ8/20	4Φ10	3Φ8	2Φ10	3Φ8+2Φ10
46-49	30	35-40	Φ8/20	4Φ10	3Φ8	2Φ10	3Φ8+2Φ10
49-52	30	35-40	Φ8/20	2Φ10+2Φ8	3Φ8	2Φ10	5Φ8
33-36	30	40-51	Φ8/20	2Φ10+2Φ12	2Φ10	2Φ10	2Φ10+2Φ12
36-39	30	40-51	Φ8/20	4Φ10	2Φ10	2Φ10	4Φ10
39-41	30	40-51	Φ8/20	2Φ10	2Φ10	2Φ10	2Φ10
41-44	30	40-51	Φ8/20	2Φ10+2Φ14	2Φ10	2Φ12	2Φ10+2Φ14
31-34	30	30-41	Φ8/20	2Φ12+2Φ14	2Φ10	2Φ12	2Φ10+2Φ14
34-Wall	30	30-41	Φ8/20	4Φ12	2Φ10	2Φ12	2Φ10+2Φ12
48-51	30	30-41	Φ8/20	4Φ12	2Φ10	2Φ12	2Φ10+2Φ12
Wall-45	40	20	Φ8/20	2Φ12+2Φ14	2Φ12	2Φ12	2Φ12+2Φ14
45-48	40	20	Φ8/20	2Φ12+2Φ14	2Φ12	2Φ12	2Φ12+2Φ14
31-32	30	20	Φ6/25	2Φ10	3Φ8	2Φ10	3Φ8
32-33	30	20	Φ6/25	2Φ10	3Φ8	2Φ10	3Φ8
51-52	30	20	Φ6/25	2Φ10	3Φ8	2Φ10	3Φ8
52-53	20	50	Φ6/20	2Φ10+2Φ14	2Φ10	2Φ14	4Φ10
46-47	20	50	Φ6/20	2Φ10+2Φ14	2Φ10	2Φ14	4Φ10
49-50	20	50	Φ6/20	2Φ10+2Φ14	2Φ10	2Φ14	4Φ10
43-44	20	50	Φ6/20	2Φ10+2Φ14	2Φ10	2Φ14	4Φ10

Figure 95: Beam structural details (Roof) (IDES 2008).

Appendix 4

The characteristic values (Figure 57) of the plastic hinges evaluated by addressing the formulation of the Italian (NTC, 2018) and the European codes (EC8, CEN 2005), are calculated considering the three typologies of columns reported in Figure 96 (Zanchi & Vassalli, 2016).

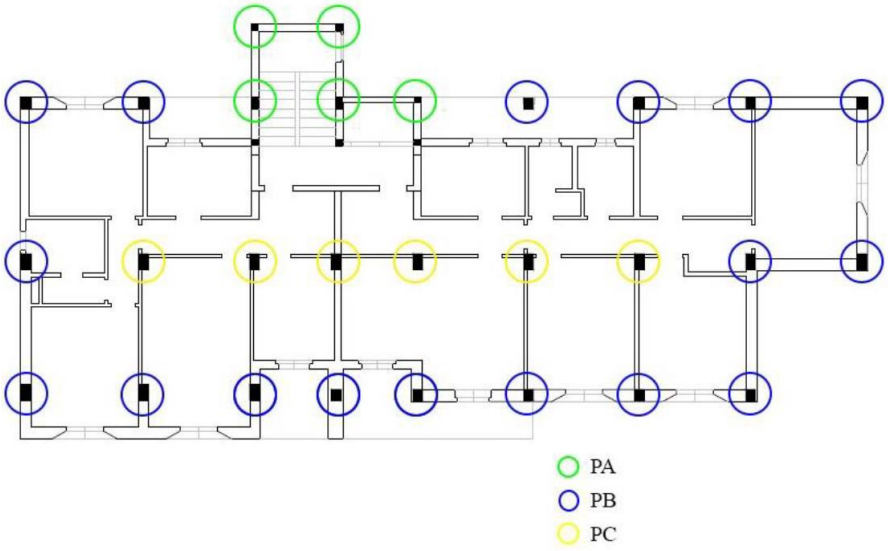

Figure 96: Individuation of the three column typologies on the plan of the East building.

Appendix 5

Seven accelerograms compatible with the code spectrum were determined by adopting the software Rexel 2.2beta (Iervolino, et al., 2010). The records are real earthquakes (Figure 98) scaled to fit Brescia (Italy) Response Spectrum at the Life Safety Limit State (LSLS) considering a flat surface made of deposit of sand or medium-dense sand gravel or stiff grave (soil category C and T1 topography) (NTC, 2018). A maximum scale factor equal to 2 and upper and lower tolerance equal to 10%, was imposed (Figure 97).

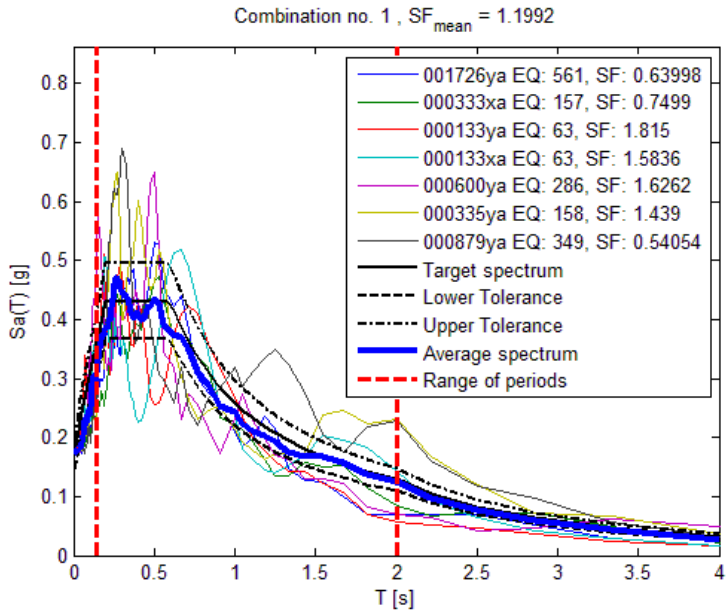

Figure 97: Selected combination of compatible accelerograms used for the time history analyses (Iervolino, et al., 2010).

Earthquake Name	Date	Mw	Fault Mechanism	Epicentral Distance [km]	PGA_X [m/s^2]	PGA_Y [m/s^2]	PGV_X [m/s]	PGV_Y [m/s]
Adana	27/06/1998	6.30	strike slip	30.00	2.16	2.64	0.28	0.20
Alkion	24/02/1981	6.60	normal	20.00	2.26	3.04	0.22	0.23
Friuli (aftershock)	15/09/1976	6.00	thrust	9.00	1.07	0.93	0.11	0.11
Friuli (aftershock)	15/09/1976	6.00	thrust	9.00	1.07	0.93	0.11	0.11
Umbria Marche	26/09/1997	6.00	normal	22.00	1.69	1.04	0.14	0.12
Alkion	25/02/1981	6.30	normal	25.00	1.14	1.18	0.11	0.15
Dinar	01/10/1995	6.40	normal	8.00	2.67	3.13	0.29	0.41

Table 20: Real earthquake considered. From the European strong-motion database

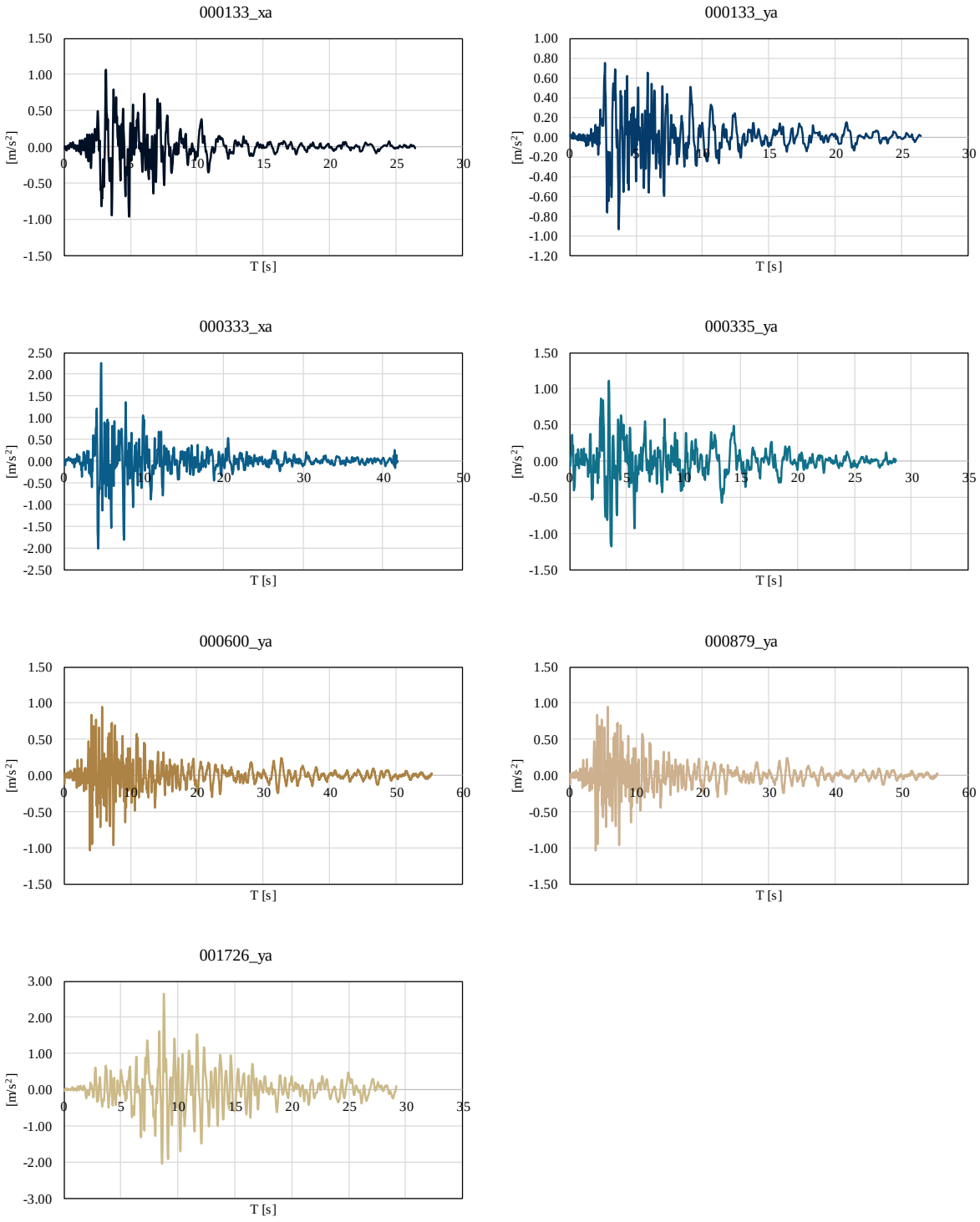

Figure 98: Seven accelerograms considered (Iervolino, et al., 2010).

Appendix 6

Analysis of the expected annual loss emphasizes the additional benefit of increasing the structural stiffness. Through a simplified procedure, the expected annual losses (PAM) of the reference case in the As-Is condition and after the strengthening intervention were evaluated (NTC, 2018), and risk classes of both the configurations were derived. The expected annual loss (PAM) is based on the economic losses related to structural and non-structural components and is expressed as a percentage of the re-construction cost (CR) of the existing building. The risk class, instead, is derived as a function of the economic parameter PAM and the safety index (IS-V). The safety index (IS-V) of the structure is defined as the ratio between the pick ground acceleration (PGA_C) at the Life Safety Limit State (LSLS) and the pick ground acceleration of the reference site (PGA_D). Plotting the direct loss as a function of the average annual frequency of exceedance (λ) (the inverse of the earthquake return period T_R), the PAM can be evaluated as the area enclosed by this curve (Figure 99). With reference to Figure 99: point (1) represents the condition of no damage on the non-structural components (SLID), point (2) the Operativity Limit State (SLO), point (3) the Damage Limit State (SLD), point (4) the Life Safety Limit State (LSLS), point (5) the Collapse Limit State (CLS), and point (6) the situation in which the demolition and reconstruction of the existing building became mandatory (SLR). In Figure 99 the curves obtained by considering the As-Is condition and by considering the retrofitted building are reported. The smaller is the enclosed area, the lower is the annual expected losses. From Figure 99 the reduction of the expected annual loss obtained by introducing a diagrid retrofit exoskeleton is significant and the benefit of increasing the structural stiffness of the reference building is highlighted.

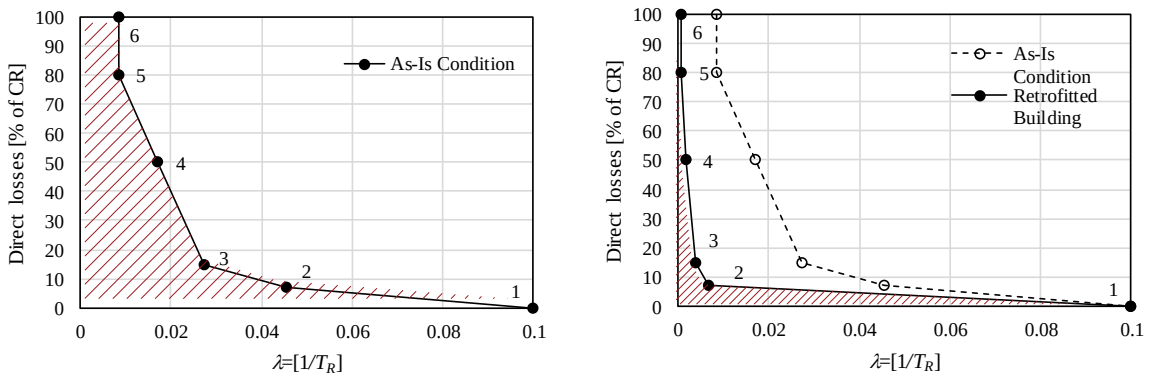

Figure 99: PAM curve considering the reference case before the retrofit solution (*left*), and after the retrofit solution (*right*).

The risk class is identified as the worst class between the PAM Class and the IS-V Class (NTC, 2018). In the case study, the As-Is condition was classified as a D Risk Class (the worst class being G), while, after the strengthening solution, the retrofitted building was classified as an A+ Risk Class.

Appendix 7

The LCA methodology is implemented in the reference case to compare the environmental impact of materials and processes related to other different retrofit options. With a cradle-to-gate system boundary, the analysis allows a partial assessment that takes into account environmental impacts from the resource extraction to the installation phase (Di Bari, 2018).

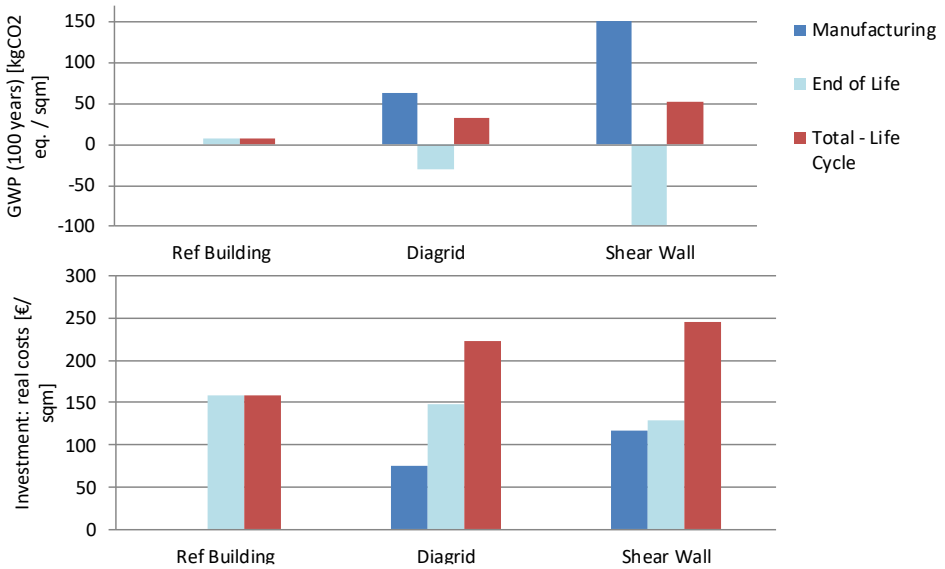

Figure 100: Life Cycle Assessment of 3 different solutions.

The Diagrid solution has a lower impact on the environment in terms of waste and natural resources during the whole life cycle.

References

Antonini, A., Labò, S., Passoni, C. & Marini, A., 2017. *Responsive structures: seismic retrofit of existing RC buildings. (Degree thesis).* University of Brescia: s.n.

Antonopoulos, C. P. & Triantafillou, T., 2003. Experimental investigation of FRP-strengthened RC beam-column joints. *Journal of Composites for Construction,* p. 39–49.

Baker, W. F., 2013. *Structural possibilities. In: Parker D, Wood A (eds.) The tall buildings reference book.* London: Routledge Taylor & Francis Group.

Belleri, A. & Marini, A., 2016. Does seismic risk affect the environmental impact of existing buildings?. *Energy and Buildings,* Volume 110, pp. 149-158.

BPIE, 2011. *Europe's buildings under the microscope: A country-by-country review of the energy performance of the buildings.* Brussel: s.n.

Casprini, E. et al., 2018. *Critical analysis of the models for the residual life evaluation of RC buildings.* Lecco, Proceedings of Italian Concrete Days.

Cavalli, C. et al., 2017. *Vulnerabilità sismica degli edifici esistenti in c.a.: il ruolo del vano scale.*, Technical Report n.9, Dipartimento di Ingegneria, Architettura, Territorio, Ambiente e Matematica dell'Università degli Studi di Brescia.: s.n.

Ciampi, V., De Angelis, M. & Paolacci, F., 1995. Design of yielding or friction-based dissipative bracings for seismic protection of buildings. *Engineering Structures,* 17(5), pp. 381-391.

COM, 2011. *Communication from the commission to the European Parliament, the Council, the European Economic and Social Committee and the Committee of the Regions. A Roadmap for moving to a competitive low carbon economy in 2050.* Brussels: European Commission.

Decanini, L. D., Mollaioli, F. & Mura, A., 2001. Equivalent SDOF systems for the estimation of seismic response of multistory frame structures. *Advances in Earthquake Engineering,* Volume 9, p. 101–110.

Decanini, L., Gavarini, C. & Bertoldi, S., 1993. *Telai tamponati soggetti ad azioni sismiche, un modello semplificato: confronto sperimentale e numerico.* Perugia, s.n.

Deierlein, G. et al., 2011. Earthquake resilient steel braced frames with controlled rocking and energy dissipating fuses. *Steel Construction,* 4(3), p. 171–175.

Di Bari, R., 2018. *Seismic, environmental and Life Cycle Cost analyses of renovation works on existing building,* s.l.: University of Bergamo.

EC8, CEN 2005. *Design of structures for earthquake resistance.* Brussels, Belgium: European Committee for Standardization.

Fajfar, P., 2000. A Nonlinear Analysis Method for Performance-Based Seismic Design. *Earthquake Spectra,* 16(3), pp. 573-592.

Fardis, M. N. & Panagiotakos, ., 1997. Seismic design and response of bare and masonry-infilled reinforced concrete buildings. Part II: Infilled structures. *Journal of Earthquake Engineering,* Volume 1, p. 219–256.

FEMA 395, F. E. M. A., 2003. *Incremental Seismic Rehabilitation of School Buildings.* USA: s.n.

FEMA P-420, F. E. M. A., 2009. *Engineering Guideline for Incremental Seismic Rehabilitation.* USA: s.n.

Feroldi, F., 2014. *Sustainable renewal of the post WWII building stock through engineered double skin, allowing fro structural retrofit, energy efficiency upgrade, architectural restyling and urban regeneration. (PhD Thesis).* University of Brescia: s.n.

Feroldi, F. et al., 2019. *Il ruolo critico dei diaframmi di piano negli in-terventi di adeguamento sismico condotti dall'esterno*. Ascoli Piceno, s.n.

Gioiella, L. et al., 2016. *An innovative seismic protection system for existing buildings: External Dissipative Towers.* Santiago Chile, s.n.

Giuriani, E. P. & Marini, A., 2008. Wooden roof box structure for the anti-seismic strengthening of historical buildings. *International Journal of Architectural Heritage,* Volume 2, pp. 226-246.

Giuriani, E. P., Marini, A. & Preti, M., 2015. Thin folded shell for the renewal of existing wooden roofs. *Journal of Architectural Heritage,* pp. 797-816.

Hak, S., Morandi, P. & Magenes, G., 2013. *Damage control of masonry infills in seismic desing. Research report.,* Pavia: Istituto Universitario di Studi Superiori (IUSS).

IDES, 2008. *Verifiche tecniche dei livelli di sicurezza sismica ai sensi dell'O.P.C.M. N.3274/2003 e S.M.I. dell'edificio "H" del quartiere Chiesanuova di proprietà dell'ALER - Azienda Lombarda per l'Edilizia Residenziale di Brescia,* Brescia: s.n.

Iervolino, I., Galasso, C. & Cosenza, E., 2008. *REXEL 2.2 beta: uno strumento per la selezione di accelerogrammi naturali per le NTC e l'Eurocodice 8.* Rome, XVII Congresso CTE.

Iervolino, I., Galasso, C. & Cosenza, E., 2010. REXEL: computer aided record selection for code-based seismic structural analysis. *Bulletin of Earthquake Engineering,* Volume 8, pp. 339-362.

Klingner, R. E. & Bertero, V. V., 1978. Earthquake resistance of infilled frames. *Journal of the Structural Division,* Volume 104, p. 973–989.

Krimgold, F., Hattis, D. & Green, M., 2004. *Incremental seismic rehabilitation of multifamily apartment buildings: providing protection to people and buildings.* Washington, D.C.: U.S. Dept. of Homeland Security, FEMA.

Kuramoto, H. et al., 2000. *Predicting the earthquake response of buildings using equivalent single degree of freedom system.* Auckland, New Zeland, 12th World Conference on Earthquake Engineering (WCEE).

La Greca, P. & Margani, G., 2018. Seismic and Energy Renovation Measures for Sustainable Cities: A Critical Analysis of the Italian Scenario. *Sustainability,* 10(1), p. 254.

Labò, S. et al., 2017. *Approccio "Life Cycle Thinking" applicato alla riparazione di una scuola danneggiata dal terremoto dell'Italia Centrale.* Pistoia, s.n.

Labò, S. et al., 2018. *Design of the Seismic Retrofit of a School in Accordance To a Life Cycle Thinking Approach.* Thessaloniki, s.n.

Labò, S. et al., 2018. *Application of low-invasive techniques and incremental seismic rehabilitation to increase the feasibility and cost-effectiveness of seismic interventions.* Florence, s.n.

Labò, S. et al., 2016. *Diagrid solutions for a sustainable seismic, energy, and architectural upgrade of European RC buildings.* Porto, s.n.

Labò, S. et al., 2017. *Prefabricated responsive diagrids for holistic renovatin of existing mid-rise RC buildings.* Rhodes, s.n.

Mansour, N., Christopoulos, C. & Tremblay, R., 2011. Experimental Validation of Replaceable Shear Links for Eccentrically Braced Steel Frames. *Journal of Structural Engineering,* 137(10), p. 1141–1152.

Maqhareh, M. R., 2014. The Evolutionary Process of Diagrid Structure Towards Architectural, Structural and Sustainability Concepts: Reviewing Case Studies. *Journal of Architectural Engineering Technology,* 3(2).

Marini, A., Passoni, C. & Belleri, A., 2018. *Life cycle perspective in RC building integrated renovation.* Florence, s.n.

Marini, A. et al., 2017. Combining seismic retrofit with energy refurbishment for the sustainable renovation of RC buildings: a proof of concept. *European Journal of Environmental and Civil Engineering,* pp. 1-21.

Marini, A. et al., 2014. *Technology option for earthquake resistant, eco-efficient buildings in Europe: Research needs.* s.l.:Publications Office of the European Union.

Mehrabi, A. B., Shing, B. P.-S., Schuller, M. P. & Noland, J. L., 1996. Experimental evaluation of masonry-infilled RC frames. *Journal of Structural Engineering,* 122(3), pp. 228-237.

Mehrabi, A. B. & Shing, P.-S. B., 2003. Seismic analysis of masonry infilled reinforced concrete frames. *The Maonsry Society Journal,* 21(1), p. 81–94.

Mele, E., Fraldi, M., Montuori, G. M. & Perrella, G., 2016. *Non-conventional Structural Patterns for Tall Buildings: from Diagrid to Hexagrid and Beyond.* Rome, s.n.

Mele, E., Toreno, M., Brandonisio, G. & De Luca, A., 2012. Diagrid structures for tall buildings: case studies and design considerations. *The Structural Design of Tall and Special Buildings,* 23(2), pp. 124-145.

MidasGEN, 2018. *Analysis Manual for Midas GEN.* s.l.:s.n.

Misawa, Y. et al., 2015. Diagonally arranged louvers in integrated facade systems - effects on the interior lighting environment. *Journal of Facade Design and Engineering,* 2(3-4), pp. 163-182.

Montuori, G. M., Fadda, M., Perrella, G. & Mele, E., 2015. Hexagrid - hexagonal tube structures for tall buildings: patterns, modeling, and design. *The Structural Design of Tall and Special Buildings,* 24(15), pp. 912-949.

Montuori, G. M., Mele, E., Brandonisio, G. & De Luca, A., 2013. Design criteria for diagrid tall buildings: Stiffness versus strength. *The Structural Design of Tall and Special Buildings,* 23(17), pp. 1294-1314.

Moon, K.-S., 2008. Practical Design Guidelines for Steel Diagrid Structures. *Aei 2008.*

Moon, K.-S., Connor, J. J. & Fernandez, J. E., 2007. Diagrid structural systems for tall buildings: characteristics and methodology for preliminary design. *The Structural Design of Tall and Special Buildings,* 16(2), pp. 205-230.

Morales-Beltran, M. & Teuffel, P., 2013. Towards smart building structures: adaptive structures in earthquake and wind loading control response – a review. *Intelligent Buildings International,* 5(2), p. 83–100.

NTC, 2018. *Norme Tecniche per le Costruzioni (NTC 2018).* Gazzetta Ufficiale del 20/02/2018, Supplemento ordinario n.42: s.n.

Otani, S., 1974. *SAKE: A Computer Program for Inelastic Response of R/C Frames to Earthquakes.* s.l.:s.n.

Passoni, C., 2016. *Holistic renovation of existing RC buildings: a framework for possible integrated structural interventions. (PhD thesis).* University of Brescia: s.n.

Passoni, C. et al., 2018. *Renovating the existing building sotck: a life cycle thinking desing approach.* Thessaloniki, s.n.

Preti, M. & Bettini, N. P. G., 2012. Infill Walls with Sliding Joints to Limit Infill-Frame Seismic Interaction: Large-Scale Experimental Test. *Journal of Earthquake Engineering,* Volume 16(1).

Qu, Z. et al., 2012. Pin-supported walls for enhancing the seismic performance of building structures. *Earthquake Engineering & Structural Dynamics,* Volume 41, p. 2075–2091.

Riva, P., Perani, M. & Belleri, A., 2011. *External R.C. Structural Walls for the Repair of Earthquake Damaged Buildings.* Rome, s.n.

Shing, P.-S. B. & Mehrabi, A. B., 2002. Behaviour and analysis of masonry-infilled frames. *Progress in Structural Engineering and Materials,* 4(3), p. 320–331.

Takeuchi, T., Yasuda, K. & Iwata, M., 2009. *Seismic Retrofitting using Energy Dissipation Façades.* San Francisco, Proceedings of ATC & SEI Conference on Improving the Seismic Performance of Existing Buildings and Other Structures.

The MathWorks, I., 2017. *Matlab.* s.l.:s.n.

Thormark, C., 2006. The effect of material choice on the total energy need and recycling potential of a building. *Building and Environment,* 41(8), p. 1019–1026.

Uva, G., Porco, F. & Fiore, A., 2012. Appraisal of masonry infill walls effect in the seismic response of RC framed buildings: A case study. *Engineering Structures,* Volume 34, p. 514–526.

Vitiello, U. et al., 2016. Life-Cycle Assessment of Seismic Retrofit Strategies Applied to Existing Building Structures. *Sustainability,* 8(12), p. 1275.

Wen, Y.-K., 1976. Method for Random Vibration of Hysteretic System. *Journal of the Engineering Mechanics Division,* 102(2), pp. 249-263.

Whittaker, A. & Soong, T. T., 2003. *An overview of nonstructural research at three U.S. Earthquake Engineering Research Centers.* Irvine, ATC-29-2 Seminar on the Seismic Design, Performance and Retrofit of Nonstructural Components in Critical FacilitiesAt.

Yadav, S. & Garg, V., 2015. Advantage of Steel Diagrid Building Over. *International Journal of Civil and Structural Engineering Research,* 3(1), pp. 394-406.

Zanchi, M. & Vassalli, L., 2016. *Pratiche di riqualificazione integrata: applicazione ad un edificio ALER di social housing (Degree thesis).* University of Bergamo: s.n.

List of figures

Figure 1: Existing building stock impacts on the environment (data from BPIE, 2011; Marini, et al., 2014). 4
Figure 2: Typical residential district built after the WWII in European city peripheries (from: Feroldi 2014).....4
Figure 3: Traditional uncoupled retrofit approach. Sole energy retrofit industrial warehouse after the Emilia-Romagna earthquake (2012) (*left*). Sole structural retrofit (*right*) (from http://www.studiomapi.it/).....6
Figure 4: Life Cycle Design for sustainability and resilience (Marini et al. 2017). 8
Figure 5: Retrofit solutions: (a) non-dissipative or (b) dissipative shear walls embedded in the external exoskeleton, (c) non-dissipative, or (d) dissipative shell structure with twofold use of the same encasing components (adapted from Marini et al., 2016).....10
Figure 6: Diagrid structure: definition of diagrid module, node, and horizontal and diagonal elements. 11
Figure 7: SWISS RE TOWER, Location: London, England, Architect: Foster & Partners, Engineer: Arup, Year: 2004.....13
Figure 8: HEARST MAGAZINE TOWER, Location: New York City, USA, Architect: Foster & Partners, Engineer: WSP Cantor Seniuk, Year: 2006.....14
Figure 9: GUANGZHOU WEST TOWER, Location: Guangzhou, (CHINA), Architect: Wilkinson Eyre Architects, Engineer: Arup, Year: 2010. 15
Figure 10: Comparison of different techniques under a life cycle perspective. Under a LC perspective, the differences between the traditional solution (R.C. Walls) and the Diagrid are immediately apparent.....17
Figure 11: Braced frame model (Moon et al. 2007). 20
Figure 12: Normalized shear stiffness as a function of the inclination angle (Moon et al. 2007). 21
Figure 13: 60-story diagrid with different diagonal angle (Adapted from Moon et al. 2007).22
Figure 14: Top displacement of the diagrid as a function of the diagonal angle (Moon et al. 2007). 22

Figure 15: Different configurations of the Timoshenko beam for the simplified representation of the retrofitted system (existing building-diagrid): a) distributed triangular load proportional to the first mode shape, b) nodal point load with mass proportional distribution; c) analytic simplification of the case a) with a triangular distributed load. 23
Figure 16: Internal actions in the diagrid structure due to gravity and later loads. After Montuori et al. (2013). 26
Figure 17: Internal actions in the diagonal elements due to the gravity loads in the case of module higher than one floor of the building. (Mele, et al., 2012). 27
Figure 18: Main seismic vulnerabilities in RC frames: a) Plan irregularities, and b) vertical irregularities. 29
Figure 19: Conceptual scheme of the new multi-criteria performance-based design approach (From Passoni et al. 2018). 31
Figure 20: Different possible configurations of the diagrid: a) By varying the module geometry. b) The horizontal projection of the retrofitted structure in the case of diagrid in adhesion and as an enlargement of an existing building. 34
Figure 21: Responsive structure behavior. 37
Figure 22:a) Sketch of the retrofitted building equipped with special sliding supports; b) hysteretic cycle of the innovative support, which is the sum of traditional elastoplastic support (*dashed line*) and a gap system (*dotted line*). 39
Figure 23: 2 degrees of freedom model. a) Simplified 2DOF system. u1 is the relative displacement of the existing building; u_2 is the relative displacement of the retrofitting exoskeleton; b) Response curve of the retrofitted structure with 2 degrees of freedom (2DOF) working in parallel. 40
Figure 24: Reference geometry representative of ordinary Post World War RC buildings (Ref. Marini et al. (2014), Feroldi (2014)). 41
Figure 25: Selected combination of compatible accelerograms used for the time history analyses (Iervolino et al. 2010). All the 7 accelerograms are reported in Appendix 2. 43
Figure 26: Representation of the parameter λ and μ on the response curve of the retrofitted structure with 2 degrees of freedom (2DOF) working in parallel. 43
Figure 27: Damage states of the existing building. DS1: minor cracking; DS2: moderate cracking; DS3: Severe cracking. 44
Figure 28: Free-body diagrams of the 2DOF system. 45
Figure 29: Hysteretic behavior of the connections according to Bouc-Wen law. 46

Figure 30: In-frequency response of the 2DOF system for k_2=k_1, for varying the mass (m_2) of the retrofit system. 49
Figure 31: In-frequency response of the 2DOF system for m_2=m_1, for varying the retrofit stiffness k_2. 50
Figure 32: a) Simplified SDOF system; b) Simplified SDOF system with equivalent spring and damping.....51
Figure 33: Response curve of the retrofitted structure with 2 degrees of freedom (2DOF) working in parallel. 51
Figure 34: Evaluation of the ductility demand (μ) as a function of the retrofit stiffness ratio ($\tilde{\lambda}$) for varying adimensionalized yielding force of the existing building (η). R refers to the reference case in section 4.1.1.2. Red dotted line: the constant value of the ductility demand (μ).....53
Figure 35: Evaluation of the ductility demand (μ) as a function of the retrofit stiffness ratio ($\tilde{\lambda}$) for varying adimensionalized yielding force of the existing building (η) and existing building fundamental period (T_1).....54
Figure 36: Evaluation of the ductility demand (μ) as a function of the existing building fundamental period (T_1) for varying the equivalent stiffness of the retrofit ($\boldsymbol{k}$). 55
Figure 37: Evaluation of the ductility demand (μ) as a function of the existing building period (T_1) for varying retrofit stiffness ($\boldsymbol{k}$) and adimensionalized yielding forces (η). 56
Figure 38: Evaluation of the series of pairs (k_{12}-k_2) obtained by varying the inter-story drift target of the existing building (θ). 57
Figure 39: Parametric evaluation of the pairs of (k_{12}-k_2) for the reference existing buildings described in Figure 24 by varying the inter-story drift target (θ). 58
Figure 40: Ductility demand (μ) on the existing building (DOF1) as a function of yielding displacement ratio of the non-linear connections (β) in the cases of m_1=451-800-1000 [kN/g] (k_1=24 kN/mm, η=0.85, and θ=0.5%) for specific input accelerogram. 62
Figure 41: Ductility demand (μ) on the existing building (DOF1) as a function of yielding displacement ratio of the non-linear connections (β) in the cases of k_1=7.9-14-24 [kN/mm] (m_1=800 kN/mm, η=0.85, and θ=0.5%) for specific input accelerogram. 65

Figure 42: Comparison, in terms of ductility demand (μ), between the u1 obtained with the optimal value of each accelerogram and u1 obtained with the optimal value of the average curve. 66
Figure 43: Ductility demand (μ) on the existing building (DOF1) as a function of yielding displacement of the non-linear connections (β) in the case of θ=0.30% considering the average response of 7 accelerograms. The response is evaluated increasing m_1 (left) and increasing k_1 (right). 68
Figure 44: Ductility demand (μ) on the existing building (DOF1) as a function of yielding displacement of the non-linear connections (β) in the case of θ=0.50% considering the average response of 7 accelerograms. The response is evaluated increasing m_1 (left) and increasing k_1 (right). 69
Figure 45: Ductility demand (μ) on the existing building (DOF1) as a function of yielding displacement of the non-linear connections (β) in the case of θ=0.85% considering the average response of 7 accelerograms. The response is evaluated increasing m_1 (left) and increasing k_1 (right). 70
Figure 46: Comparison between the u1 obtained with the optimal value of each accelerogram and u1 obtained with the most frequent value of β. 71
Figure 47: Distribution of the optimal values of β by varying the inter-story drift target (θ) and the adimensionalized yielding force (η). 73
Figure 48: Design spectra for the determination of the optimal yielding ration of the connection (β) as a function of the adimensionalized yielding force (η) and of the inter-story drift target (θ). 74
Figure 49: Simplified deformed shape of the first vibrational mode. 75
Figure 50: Location of the reference building (H) within Chiesanuova social housing district (IDES 2008). 77
Figure 51: Views of the reference building. South-east façade (*left*), ground floor (*right*) (IDES 2008). 78
Figure 52: Longitudinal (*left*) and transversal (*right*) sections. Plan of a reference floor (*bottom*) (IDES 2008). 79
Figure 53:Plan of the East building (IDES 2008). 79
Figure 54: Pictures of the intervention on the columns and the foundation system. 81
Figure 55: Finite Element Model of the reference building. 83

Figure 56: Takeda type hysteresis model implemented in the program MidasGEN (from: MidasGEN 2018). 84
Figure 57: a) Flexural behavior; b) shear behavior. 85
Figure 58: Axial plastic hinge of the compression-only diagonal struts. 86
Figure 59: Capacity curve in y-direction (*top*), evolution of story-displacement (*left*) and inter-story drift (*right*) for significant points of the capacity curve. 87
Figure 60: Capacity curve in x-direction (*top*), evolution of story-displacement (*left*) and inter-story drift (*right*) for significant points of the capacity curve 88
Figure 61: *y*-direction: ADRS and displacement demands at LSLS and CLS (*left*), story-displacement (*middle*), and inter-story drift (*right*) at the considered Limit States..... 90
Figure 62: *x*-direction: ADRS and displacement demands at LSLS and CLS (*left*), story-displacement (*middle*), and inter-story drift (*right*) at the considered Limit States..... 90
Figure 63: Architectural and formal aspects of the retrofit solution. 93
Figure 64: Representation on the ADR Spectrum at the LSLS the design parameters. 95
Figure 65: Evaluation of the commercial profile capacity as a function of the technological aspects related to the diagrid structure and the imposed target. a) by varying the boundary condition of the diagonal elements, and the material properties; b) by changing the drift target setting the boundary condition. 97
Figure 66: The maximum axial force of the elements and the maximum capacity of the commercial profiles in the reference case. Individuation of the minimum profile that satisfies the strength constraint. 97
Figure 67: Capacity curve of the retrofitted structure. Capacity curve of the whole system (*black*), and of the existing building (brown) (*Top*); Story displacement and Inter-story drift ratio at the LSLS (*Bottom*). 100
Figure 68: A selected combination of compatible accelerograms used for the time history analyses (Iervolino et al. 2010). 101
Figure 69: a) Floor shear along the building's height for different accelerograms, b) inter-story drift, and story displacement. 103
Figure 70: a) Comparison between the forces obtained with the hand calculation method and the finite element model, b) Stress rate of the most solicited diagonal elements at each floor expressed as $N_{k,MAX}/N_{k,LIM}$ 103
Figure 71: General link introduced in the FEM to model the non-linear behavior of the connections. 104

Figure 72: a) Floor shear along the building's height for different accelerograms, b) inter-story drift and story displacement. 105
Figure 73: Hysteretic cycle of the sliding support as the sum of elastoplastic support (*dashed line*) and a gap system (*dotted line*). 107
Figure 74: Time history analyses results. Comparison between the results obtained with the elastic diagrid (*ES*), the non-linear diagrid (*NLS*), and the passive-responsive diagrid (*SLIDING*) 108
Figure 75: a) Floor shear along the building's height for different accelerograms, b) inter-story drift, and story displacement. The red target (1%) refers to the ground floor; the light blue target (0.3%) refers to the upper floors. 108
Figure 76: Alternative strategies for the renovation of the existing building proposed by FEMA P-420 (Adapted from. FEMA P-420). 115
Figure 77:Life-cycle cost/benefit analysis of an incremental rehabilitation project and of single-stage retrofit solutions over an extended period of time. Benefits of the same single-stage rehabilitation project occurring at different years (*dark grey*). Incremental rehabilitation plan benefits (*yellow*). 115
Figure 78: Example of integration priority (From FEMA P-420). Since the retrofit solutions proposed are carried out from outside, the interior works are not considered. 117
Figure 79: Life-cycle cost/benefit analysis of an incremental rehabilitation project and of single-stage retrofit solutions over an extended period of time introducing the innovative concept of minimum intervention (*red dotted line*). 117
Figure 80: Selected combination of compatible accelerograms used for the time history analyses (Iervolino et al. 2010). 119
Figure 81: Seven accelerograms considered (Iervolino et al. 2010). 120
Figure 82: Inter-story floor steel rebars. (IDES, 2008). 121
Figure 83: Section of the inter-story floor (1st typology) (IDES, 2008). 121
Figure 84: Balcony (IDES 2008). 122
Figure 85: Staircase and elevator cores (IDES 2008). 123
Figure 86: Plan of the East building with indicated the number of the columns (IDES 2008). 124
Figure 87: Ground floor column structural details (IDES 2008). 125
Figure 88: First-floor column structural details (IDES 2008). 125
Figure 89: Second-floor column structural details (IDES 2008). 126

Figure 90: Third-floor column structural details (IDES 2008). 126
Figure 91: Fourth-Fifth-Sixth floor column structural details (IDES 2008). 127
Figure 92: Seventh-Eighth floor column structural details (IDES 2008). 127
Figure 93: Beam structural details (floors from 1 to 7) (IDES 2008). 128
Figure 94: Beam structural details (attic floor) (IDES 2008). 129
Figure 95: Beam structural details (Roof) (IDES 2008). 130
Figure 96: Individuation of the three column typologies on the plan of the East building. .. 131
Figure 97: Selected combination of compatible accelerograms used for the time history analyses (Iervolino, et al., 2010). 132
Figure 98: Seven accelerograms considered (Iervolino, et al., 2010). 133
Figure 99: PAM curve considering the reference case before the retrofit solution (*left*), and after the retrofit solution (*right*). 134
Figure 100: Life Cycle Assessment of 3 different solutions 136

List of tables

Table 1: Inputs used in the parametric evaluation of the elastic SDOF system. 52
Table 2: Input parameters and setting values adopted in the sensitivity evaluation of the non-linear 2 SDOF system. 60
Table 3: Inputs of the non-linear 2 SDOF system used in case 1. 61
Table 4: Inputs of the non-linear 2 SDOF system used in case 2. 64
Table 5: Inputs of the non-linear 2 SDOF system used in case 3. 67
Table 6: Measured concrete properties: test on 16 elements. $R_{ck,eff}$ is the measured concrete cube compressive strength. 81
Table 7: Steel measured properties: test on 6 elements. f_y and fu are the yielding force and the ultimate strength, respectively. 81
Table 8: Properties of masonry for the considered infill typology (Hak, et al., 2013), where f_{wh} and f_{wv} represent the values of compression strength for the horizontal and vertical direction, respectively. f_{wu} stands for the sliding shear resistance of the mortar joints, f_{ws} for the shear resistance under diagonal compression, E_{wh} and E_{wv} represent the secant modulus of elasticity for the horizontal and vertical direction, G is the shear modulus, and W is the unit weight of the infills. 86
Table 9: *N2* method: Main parameters for the *y*-direction. 89
Table 10: *N2* method: Main parameters for the *x*-direction. 89
Table 11: Results of the 1st and 2nd constraints. 98
Table 12: Time history analyses results. Elastic retrofit solution (ES). 102
Table 13: Comparison between the analytic method and the FEM results. 102
Table 14: Time history analyses results. Non-Linear retrofit solution (NLS). 104
Table 15: Comparison between the analytic prediction and the numerical FEM results. 105
Table 16: Real earthquake considered. From the European strong-motion database. 119
Table 17:Load analysis: three typologies of inter-story floor. 122
Table 18: Load analysis: balcony of the reference case. 123
Table 19: Load analysis:External infills and staircase core. 124
Table 20: Real earthquake considered. From the European strong-motion database 132

Glossary

ε_d	Elastic strain of the diagonal elements
$\Delta\beta$	Angle related to the elongation of the column of the braced frame model
Δ_h	Lateral displacement of the braced frame model
D_T	Shear Stiffness
φ	Beam deflection
$\tilde{k}$	Equivalent stiffness of the SDOF system
$\tilde{c}$	Equivalent damping of the SDOF system
$\hat{k}$	Total stiffness of the SDOF system
$\tilde{\lambda}$	Stiffness ratio: $\tilde{k} / k_1$
A_d	Cross-section area of the diagonal element
$A_{d,f}$	Cross-section area of the diagonal elements on the “flange”
$A_{d,w}$	Cross-section area of the diagonal elements on the “web”
$\underline{C}$	Damping matrix
c_1	Damping coefficient of the DOF1
c_{12}	Damping coefficient of the DOF2
c_2	Damping coefficient of the connection
C_i	Constant of integration
d	Distance of the *i-th* module from the whole diagrid centroid axis
d^*_y	Yielding displacement of the bi-linear curve
d_{TOP}	Target maximum top displacement of the existing building
E_d	Elastic modulus of the diagonal element
e_d	Elongation of the diagonal element
E_{wh}	Secant modulus of elasticity for horizontal direction
E_{wv}	Secant modulus of elasticity for vertical direction
F^*_y	Yielding force of the bi-linear curve
F_{12}	Total force in the connection
F_d	Axial force in the diagonal element
$F_{m,k}$	Forces in the *k-th* module due to overturning moment
$F_{p,k}$	Forces in the *k-th* module due to vertical loads
$F_{v,k}$	Forces in the *k-th* module due to shear force

f_{wh}	Compression strength for the horizontal direction
f_{ws}	Shear resistance under diagonal compression
f_{wu}	Sliding shear resistance of the mortar joints
f_{wv}	Compression strength for the vertical direction
$F_{y,1}$	Yielding force of the DOF1
f_{yk}	Maximum allowed axial stress allowed
G	Shear modulus
h	Diagrid Module height
H	Existing building height
h_i	Inter-story height
k	Timoshenko shear coefficient
$\underline{K}$	Stiffness matrix
k_1	Initial elastic stiffness of the DOF1
k_{12}	Initial elastic stiffness of the connection
k_2	Initial elastic stiffness of the DOF2
k_i	Connection stiffness at the i-th floor
l	Plan direction of the building parallel to the considered horizontal loads direction
L_d	Diagonal elements length
M	Bending Moment
m	Mass of the equivalent SODF system
$\underline{M}$	Mass matrix
m_1	Effective mass of the DOF1
m_2	Effective mass of the DOF2
N	Number of floors of the existing building
n	Smoothness of the curve in proximity of the yielding point
n_f	Number of diagonals on the “flange” façade
n_k	Total number of the modules in the whole diagrid
$N_{m,k}$	Internal actions due to overturning moment
$N_{p,k}$,	Internal actions due to vertical loads
$N_{v,k}$	Internal actions due to shear force
n_w	Number of diagonals on the “web” façade
p	Triangular distributed load

P	Nodal load
s_1, s_2	Tubular thickness obtained with the 1st and 2nd constraints
S_a^D	Design spectrum acceleration
S_d^{CLS}	Displacement Demand for the SODF system (CLS)
S_d^D	Design spectrum displacement
S_d^{LSLS}	Displacement Demand for the SODF system (LSLS)
$\underline{T}$	Transfer matrix
T^*	Period of the equivalent SODF system
T_1	Elastic period of the DOF1
T_2	Elastic period of the DOF2
u_1	Displacement of the DOF1
u_2	Displacement of the DOF2
V	Shear action
W	Unit weight of the infills
X_g	Ground acceleration
$y(x)$	Displacement of the Timoshenko beam in the variable x
$\underline{Z}$	Impedance matrix
Δ	Relative top displacement between diagrid and existing building
Φ_1, Φ_2	Diameter of the diagonal elements obtained with the 1st and 2nd constraints
Γ	Participation factor
Γ_{FIN}	Participation factor of the retrofitted building
α	Post yielding stiffness ratio
β	Yielding displacement ratio
χ	Coefficient functions of the profile slenderness
δ_{MAX}	Maximum displacement experienced by the DOF 1
$\delta_{y,1}$	Yielding displacement of the DOF1
$\delta_{y,12}$	Yielding displacement of the connection
γ	Size parameter of the hysteretic loop
γ_{M0}	Material safety factor
η	Yield force adimensionalized with respect to the mass (m_1) multiplied by the ground acceleration ($Sa(T_1)$)
η	Adimensionalized yield strength of the DOF1

λ	Stiffness ratio: k_2/k_1
λ_{12}	Stiffness ratio: k_{12}/k_1
μ^R	Ductility demand for the Reference case
μ	Ductility demand
ν	Size parameter of the hysteretic loop
θ	Inter-story drift ratio target
θ_{TOP}	Total drift of the existing building
ρ	Inclination angle of the linear deformed shape of the retrofitted building
ξ	Shear deformation
ψ	Diagonal element inclination
ζ	Damping ratio